Final Report OGC funding agreement 2000-16

Acid Gas Sorption by British Columbia Coals: Implications for Permanent Disposal of Acid Gas in Deep Coal Seams and Possible Co-Production of Methane

May 2004

R.M. Bustin
Department of Earth and Ocean Sciences
The University of British Columbia
Vancouver, B.C.
V6T 1Z4
ph 604 822 6279 fax 604 822 6088
bustin@unixg.ubc.ca

TABLE OF CONTENTS

EXECUTIVE SUMMARY

Sequestration of CO_2 and H_2S into deep unminable coal seams is a very attractive option to reduce their atmospheric emission. The 'Acid Gas Sorption by Coal' research project was undertaken with an objective to provide the essential information for the design and implementation of a pilot injection project for sequestering greenhouse and acid gases into deep coal seams with a possible co-production of methane. The objectives of the research program were to determine the potential volume of acid gas that maybe sequestered in British Columbia coals of various ranks and compositions; and to investigate if and to what degree matrix swelling takes place during sequestration and what the effects such volume change will have on coal permeability and hence acid gas injection. The project was undertaken in three major phases: In phase one, the sorption capacities of representative British Columbian coals of varying rank and composition to pure hydrogen sulphide (H_2S), sulphur dioxide ($SO_{2)}$), carbon dioxide (CO_2), methane (CH_4) and nitrogen (N_2) were determined; in phase two the degree of matrix swelling of coal cores during sorption were measured and in phase 3 the results of phase one and two were integrated in a numerical simulator to predict the injectivity of acid gas into various coals. The detailed technical scientific and engineering results from the study are embodied in two parts. Here in the executive summary a less technical summation of the study is provided.

i. Potential volume of acid gas that maybe sequestered.

A wide range of British Columbian coals of varying rank and composition were analyzed for their sorption capacity to hydrogen, nitrogen, methane, carbon dioxide, hydrogen sulphide and sulphur dioxide at various pressures and temperatures. The sample suites were fully characterized for the chemical and physical properties using standard procedures. The non-toxic gas analyses were done at UBC. For the hydrogen sulphide and sulphur dioxide experiments a safe module at the Devon research facility of the Alberta Research Council was utilised. The figure below provides is an example of our results quantifying the sequestration potential of Telkwa coal. Similar data were ollected for other coals of the study and are provided in the body of this report. This figure shows that with increasing gas pressure, such as would exist in reservoirs at various depth the amount of the various gases that can be held in the sorbed state in the coal seam in cubic centimeters per gram of coal. The data clearly indicate the tremendous sorption capacity of coal to hydrogen sulphide and sulphur dioxide and the real potential for utilizing coal as sink or scrubbing for these gases. The order of adsorption is SO_2 & H_2S> CO_2> CH_4> N_2> H_2 in all the samples. Overall the sorption capacity of all gases increases with coal rank. The ratio of sorption capacity of the varying gases to CH_4 declines with coal rank-which has implications on the amount of differential matrix swelling that may occur.

Telkwa
Isotherms of H2, N2, CH4, CO2, SO2, H2S

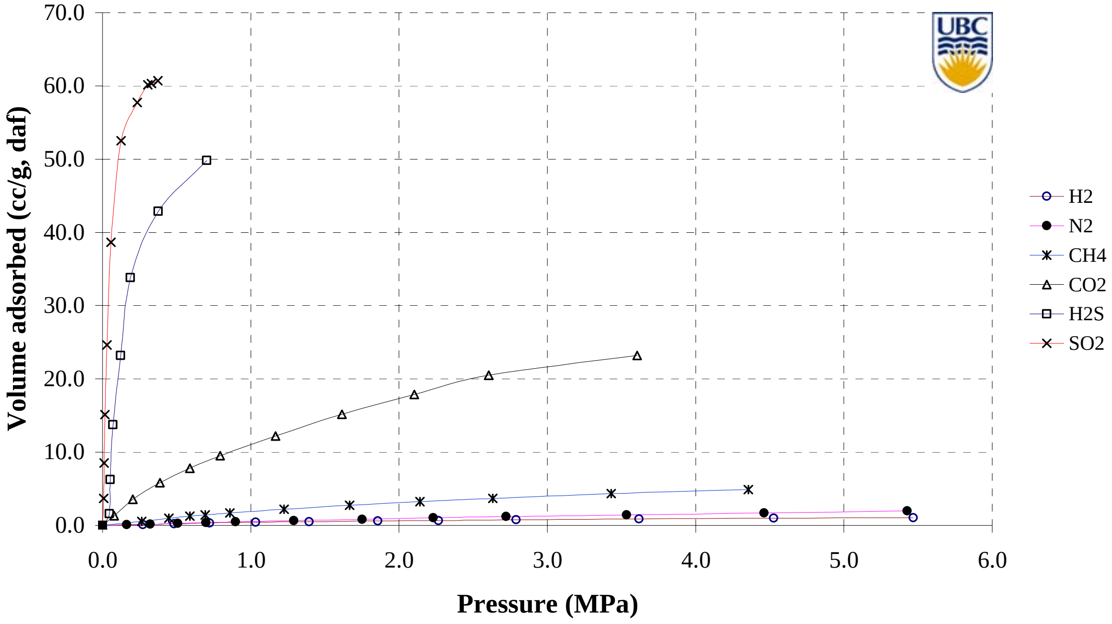

ii. To determine the selectivity of coal to hydrogen sulphide, sulphur dioxide, carbon dioxide, methane, nitrogen

A series of experiments on selected coals utilising mixtures of carbon dioxide and hydrogen sulphide to characterize the separation factors during adsorption and desorption. The figure below shows the change in gas composition during 60 minute desorption test of a coal that was exposed to 50:50 mix of carbon dioxide and hydrogen sulphide. This result and our similar experiments clearly show the selectivity of coal for hydrogen sulphide followed by carbon dioxides and methane, which is critical to quantifying sequestration of acid gas with co-production of methane.

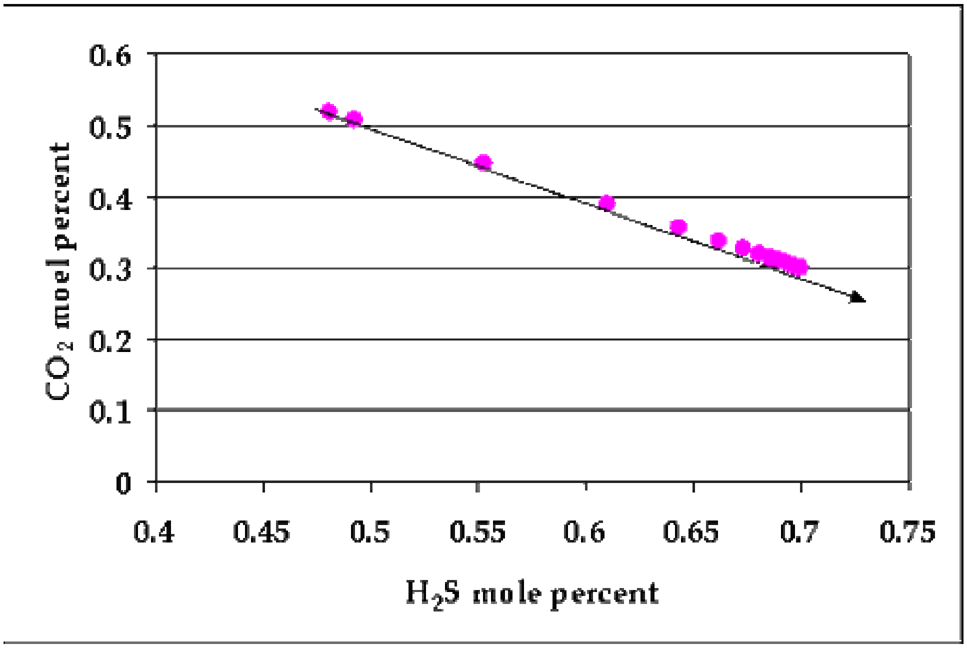

iii. To determine the effects of pressure, temperature and moisture content on quantity of sorbable gas

Experiments to determine quantitatively the effects of temperature, pressure and moisture content on sorption capacity were undertaken. The experimental data is utilized in quantitative assessment of the storage capacity of coals under various conditions. The graph below typifies some of data and shows the results of measuring sorption capacity at various reservoir temperatures. The data confirms previous studies that argue that temperature plays a major role is sorption capacity but also provides a quantitative assessment of temperature effects that is integrated into our numerical simulator.

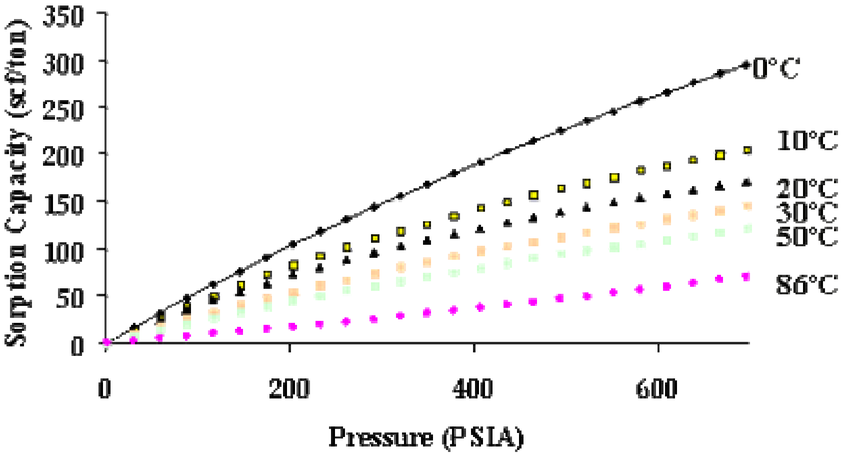

iv. **To document variation in permeability associated matrix volume changes associated with acid sorption and methane desorption**

Strain experiments using CO_2, CH_4, N_2, He and H_2S were determined for four selected coal samples. The results of the strain experiments show that the volumetric swelling is directly proportional to the quantities of gas adsorbed and increases with coal rank. Comparison of strain with different gases show that the volumetric swelling with H_2S is about 5-20 times higher than CH_4 and 40-130 times higher than N_2. Desorption strain data could not be collected for H_2S as after 1 MPa pressure step gas started reacting with the strain gages. The desorption runs for CH_4 and N_2 show that CH_4 creates a volumetric shrinkage of 0.3% to 1.8% and H_2S adsorption results in marked swelling of about 2% to 10% which varies with coal rank and likely composition. These results are very critical for evaluating the optimum coals for sequestration of acid gases with co-production of methane. The typical strain plot for Quinsam (Nanaimo coal) is shown below.

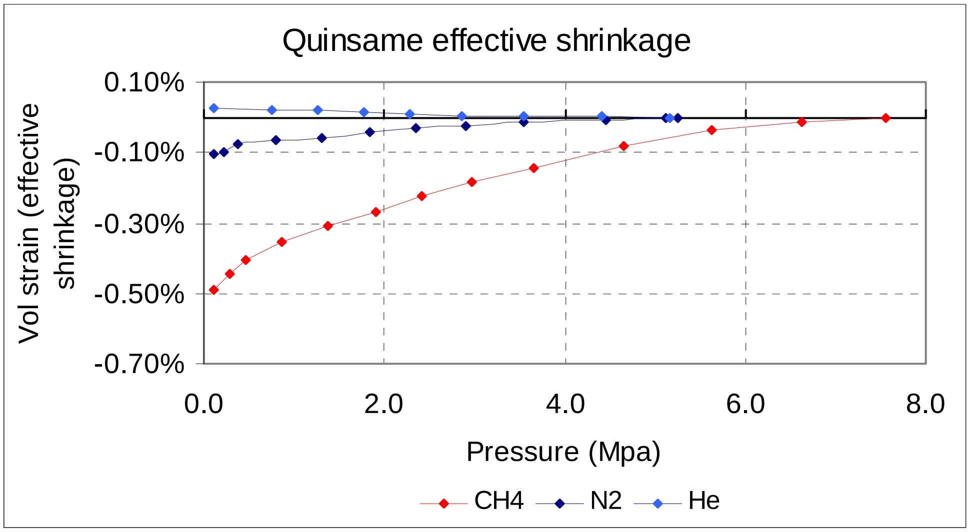

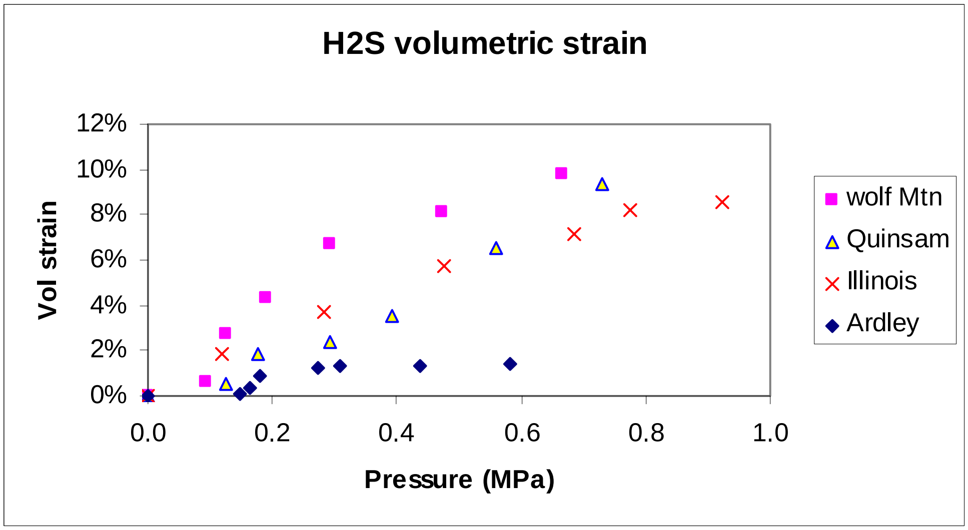

v. Numerical modeling to simulate acid gas injection to determine possible rates of injection and volume of acid gas that can be sequestered.

Practical sequestration of CO_2 and H_2S requires the maintenance of a minimum permeability for injection efficiency. However, our experimental data show that the adsorption of CO_2 and H_2S into coals causes strong swelling of coals and thus likely reduces coal permeability significantly by closing or narrowing the cleat apertures. To quantify the impacts of the coal swelling on coal permeability and thus acid gas injection efficiency, we have derived a stress-dependent permeability model and incorporated it into a two-dimensional finite difference model that is capable of simulatating acid gas injection and CH_4 recovery process. With constraints from experimental gas adsorption and coal swelling data for three Canadian coals, the permeability change during injection of CO_2 and H_2S into those coals were evaluated. Because of the much larger adsorption capacity and stronger adsorption affinity of H_2S and CO_2 than CH_4, injection of pure CO_2 or H_2S is significantly inhibited with more than several order of magnitude of permeability reduction. Owing to low adsorption capacity and affinity of N_2 in coals, injection of gas mixture of N_2 and CO_2 can markedly improve the efficiency of CO_2 sequestration and CH_4 recovery. However, injection of H_2S and N_2 mixture does not enhance markedly the H_2S sequestration efficiency because of the extreme swelling associated H_2S sorption. Coal fabric (e.g., cleat spacing) plays an important role in the dynamic change in cleat permeability and the breakthrough of injected CO_2 and H_2S. For a given cleat permeability, larger (as compared to smaller) cleat spacing retards diffusion and adsorption of injected gas into coal particles, resulting in an early breakthrough of injected gas, which can also be promoted by the cleat permeability enhancement due to the cleat pressure elevation by initial gas injection. Furthermore, coal seams with large cleat spacing likely have lower initial cleat porosity and thus the larger cleat permeability reduction may occur during sequestration of H_2S and CO_2. Therefore, an optimal coal seam for CO_2 and H_2S sequestration would be high-rank coals that commonly have denser cleat networks and less differential adsorption capacities between acid gases and CH_4.

Partnership and Collaboration

Contact and association has been made with industrial supporters of the project. Shell, BP Amoco and the Alberta Research Council extended the use of facilities for the toxic gas experiments. A choice was made to utilize the Alberta Research Council facility at Devon because of its proximity to Edmonton (and the airport) and because the facility offered was specifically designed for the type of hazardous experiments that we are running. Robert Lee, formally of Air Liquide and Bill Gunter of ARC have been a very vocal supporters and key advisor on the design of sorption experiments. The Alberta Research Council support in man power and supplies and expenses. Other support and collaboration includes discussion and logistic support from Encana, Husky, Suncor, Martlet, and the federal and provincial geological surveys. The support was mainly re-discussion with engineering and/or geological staff and access to data. Data on problems associated with deep injection of acid gas into depleted reservoirs had been made available by some industry collaborators and this data will be a valuable asset as the study moves forward into the last phase.

Training of Research Personnel

The research personal described below are funded in part by funding from OGC and partly my NSERC and support from the Alberta Research Council.

Four post-doctoral fellows have been directly involved as outlined below. Additionally two of my MSc students (Ramos, Mackin) have been associated with some aspects of the study although their research thesis topics are not directly part of the project.

One UBC colleague, Dr. G. Dipple is assisting in integrating the experimental data into a numerical models and provided guidance to X. Cui in formulating the models. His interests are mainly in the areas of carbon dioxide sequestration by carbonation reactions but there are many commonalities with my study.

The following post-doctoral fellows have been the contributors and benefactors of the project to date.

R. Wust (post-doctoral fellow: Sept. 01-June 02)

Raphael was responsible for carrying out deformation experiments to access the effects of strain on pore size distribution in coals and hence sorption capacity. Raphael has left to take up a faculty position at James Cook University, Australia.

Maristela Bagatin Silva (post-doctoral fellow Jan. 01- Dec. 01)

Maris was responsible for petrographically and chemically characterizing coal samples prior to and following sorption experiments. Maris has now taken up a faculty position in Brazil.

Laxmi Chikatamarla (post-doctoral fellow Jan. 01- present)

Laxmi has the main responsibility for building the equipment for running the sorption and strain experiments, analyzing and interpreting the sorption and strain data.

X. Cui (Albert) (post-doctoral fellow July 02-present)

Albert is responsible for the numerical modeling of the results. Albert developed programs to take integrate the diffusion data, matrix swelling characteristics and gas separations factors to attempt to predict the results of acid gas injection into coal.

Accessibility of Results to Supporting Organizations

Discussions and informal presentations of the study have taken place with most industrial supporters. The results of the study were presented at the Canadian CO2 Sequestration Consortium Forum in Calgary, in April, 2001, and on April 29th and 22nd October, 2002 and papers were presented (and published) as part of the 2003 and 2004 International Coalbed methane symposium, The University of Alabama. Representatives from most of the industrial supporters of the research program attended these meetings and had the opportunity to comment and provide direction. Several additional manuscripts are in various states of preparation. During the next year the results of the research program will be presented at several international conferences.

1. Bustin, R.M. and Xiaojun CUI, 2004, Coal Swelling with Acid Gas injection: Coal-SEQ III, Baltimore (Sponsored by Dept. of Energy, US)

2 Laxminarayana, C., Xiaojun CUI and R. Marc Bustin (2004). Implications of Volumetric Swelling/ Shrinkage of Coal in Sequestration of Acid Gases, Paper #0435, The 2004 International Coalbed Methane Symposium held on 3-7th May 2004 at Tuscaloosa, Alabama, USA.

3. Laxminarayana, C. and R. Marc Bustin (2003) (Abstract). Volumetric Swelling/Shrinkage Characteristics of Western Canadian Coals: Implications for Sequestration of Acid Gases. Geological Society of America, November 2003, Seattle, USA.

4. Laxminarayana, C. and R. Marc Bustin (2003). Acid gas sorption by BC coal: Implications for permanent disposal of acid gas in deep coal seams with possible co-production of methane. The First Annual Science and Community Environmental Knowledge Forum and Workshop. Organized by Oil and Gas Commission, May 29-30, 2003 Fort St John, BC, Canada.

5. Laxminarayana, C. and R. Marc Bustin (2003). Sequestration potential Acid gases in Western Canadian coal, Paper # 0360, The 2003 International Coalbed Methane Symposium held on 5-8th May 2003 at Tuscaloosa, Alabama, USA.

6. Laxminarayana, C. and R. Marc Bustin (2002). H2S, SO2 and CO2 sorption on coals: Implications for sequestration of acid gas in coal beds with possible co-production of methane. Coalbed Methane: A Fossil Fuel Resource with The Potential of Zero Greenhouse Gas Emissions, Phase IV Technical meeting held in Calgary on 22nd October 2002.

7. R. Marc Bustin and Laxminarayana, C., (2002). Adsorption of H2S and SO2 on Coal and their implication for sequestration. Coalbed Methane: A Fossil Fuel Resource with The Potential Of Zero Greenhouse Gas Emissions, Phase III-A Technical meeting held in Calgary on 29th April 2002.

8. Bustin, R.M., and Laxmi Chikatamarla 2002, Acid Gas sequestration potential of British Columbian Coals, 3rd Technical meeting of Canadian CO2 Sequestration Consortium Forum in Calgary, April 29.

9. Bustin R.M., 2002, Research activities on carbon dioxide, hydrogen sulphide and sulphur dioxide sequestration, First International Forum on Geological Sequestration of Carbon Dioxide in Deep, Unmineable Coal seams (Coal-Seq I), Houston, March 14-15, 2002

Benefits and Legacy of the Research

The results of the research provide the first attempt to quantify the sorption capacity of coals of various ranks to acid and other gases and to evaluate the potential impact on permeability of injections of these gases. The results of this study will be critical to evaluate coals that may suitable for a field pilot project which is the next step evaluating the feasibility of the disposal in coal seams of acid and flue gases and potentially co-production of methane.

As part of the research program four post-doctoral fellow and two graduate students received invaluable training and experience in research and in the field of unconventional gas exploration and development.

A important legacy of the research is the development of protocols for analyses and the development of numerical models that will be useful in forth coming research programs. The fuding by the OGC has facilitated UBC becoming the world leader is the study of the sequestration potential for acid gas in geological formations.

TECHNICAL REPORT

Part 1.

ACID GAS SORPTION BY BC COALS: IMPLICATIONS FOR PERMANENT DISPOSAL OF ACID GAS IN DEEP COAL SEAMS AND POSSIBLE CO-PRODUCTION OF METHANE

Dr R. M. Bustin
Department of Earth and Ocean Sciences
The University of British Columbia
Vancouver, B.C.
V6T 1Z4
ph 604 822 6179 fax 604 822 6088
bustin@interchange.ubc.ca

1. Introduction

The contract to investigate the acid gas sorption by BC coals was undertaken with the objective of providing essential information to assist in the design and implementation of a pilot injection project for sequestering greenhouse and acid gases into deep coal seams with a possible co-production of methane. Measurements were carried out to quantify the volumetric swelling of two BC coal samples with N_2, CH_4, CO_2, H_2S and also the volumetric shrinkage with CH_4 desorption. In this part we provide the results of the study.

2. Experimental design

An experiment was set-up to measure the volumetric strain within the coal matrix under changing gas pressure. The design and experimental procedure is similar to the work done by Harpalani and Schraufnagel (1990) and George and Barakat (2001) but differs in equilibrium timings and gas dosage methods. The equipment we designed is fully automated for gas dosage (valve opening and closing) and equilibrium timings with a proprietary software interface to minimize the human error in deciding the equilibrium conditions, which is critical for the experiments.

A new volumetric adsorption apparatus (Fig.1) was constructed to do adsorption isotherm as well as strain measurements simultaneously. The equipment is designed using high precision pressure transducers (0-15 MPa) and data was collected by utilizing a computer interface. The equilibrium stage at each isothermal point is decided by the proprietary software where the conditions are pre-specified before the experiment. Experiments are performed according to the pre-determined pressure steps. Once all the steps are finished the experiment stops automatically. The data is filtered using a macro where the equilibrium data points for isotherm and strain are collected. A volume adsorbed at each pressure step is calculated using gas compressibility determined with the Peng-Robinson Equation of State and the liquid density of gas at its boiling point. The temperature of the bath is maintained at target temperature (in this case it is 25°C) ± <0.1°C using temperature controller.

The strain experiments on an average took between 6 – 10 days to reach equilibrium each pressure step. Thus for a 12 step adsorption-strain experiment the time required would be between 72 – 120 days depending upon the coal-gas adsorption system. It might even take longer time if temperature of the bath is not maintained constant.

2.1. Specimen preparation for strain experiments

Coal samples in big lumps were cored in the laboratory to 37 mm in diameter and about 100 mm in length and the specimen ends were ground parallel. The specimens were then sealed in polyethylene bags and kept in the freezer to prevent the oxidation and loss of moisture. Three sets of core samples were prepared, one set is used for non toxic gases i.e. N2, CH_4, CO_2 and second set for H_2S and SO_2 strain experiments. The third set was kept as back up. However, SO_2 strain experiments were not carried out hence not discussed in this report. The samples were analyzed for its moisture and ash content (Annexure I; Table 1).

Four strain gages were used per specimen; they were adhered 180° apart, two axial and two radial for each sample. The length of strain gages were such that it covers nearly 90% of sample length so that the representative strain is measured. The strain gage wires from the sample were soldered to another set of wires passing through a hermitically sealed gland assembly and to the computer via an interface to collect the strain data along with isotherm data (Fig. 2).

2.2. Sample preparation for adsorption isotherm experiments

Selected BC coal samples (Annexure I; Table 2) were first crushed to <1 mm and a representative split were taken for petrography. The remaining sample was further crushed to <60 mesh sieve (<0.250 mm) for isotherm analysis. The samples were then split into 6 sub-samples, for running adsorption isotherms with H_2, N_2, CH_4, CO_2, H_2S and SO_2 gases, sealed in polyethylene bags and preserved in cold storage to prevent oxidation. The samples were then brought to equilibrium moisture state using standard techniques (Australian Standard, 1989).

The samples were characterised by proximate analysis (moisture and ash content), maceral content, vitrinite reflectance (Annexure I; Table 2) [4, 5], Micro- FTIR and adsorption characteristics of H_2, N_2, CH_4, CO_2, H_2S and SO_2 were determined.

2.3. Strain experimental procedure

Prior to start of the experiments strain gages were calibrated for temperature variation coefficients and the same were incorporated into the proprietary strain measuring software for calculating the volumetric changes during adsorption and desorption process. Coal sample volume was determined with helium expansion runs up to5 MPa in increasing steps and also to measure the dead volume inside the vessel which are used for adsorption isotherm calculations. After the void volume runs, the samples were evacuated for one-half hour and system was allowed for equilibrium. The strains were then set to zero. Since our objective was to quantify the volumetric shrinkage of coal during methane production/ desorption and also volumetric swelling during sequestration of acid gases, the adsorption strain cycle for CH_4 was carried out in two steps up to 8 MPa to save time. Whereas for N_2, CO_2, and H_2S the adsorption isotherm and strain data was collected for gradual increasing pressure steps. The strains were continuously recorded using computer interface. After the adsorption isotherms for CH_4 finished, desorption run was started with gradual decreasing pressure steps (Annexure III; Tables 13 & 14) for methane.

Once the CH_4 isotherm-strain data collected, the samples were evacuated thoroughly and the similar procedure was adopted for N_2, CO_2 and H_2S adsorption isotherm-strain runs. However, for N_2, CO_2 and H_2S adsorption cycles pressures steps varied (Annexure-III; Tables 13a, 13b, 14a & 14b). In the case of N_2 and CO_2 the adsorption steps were carried out up to 5 MPa with gradual increasing pressure steps. In the case of H_2S 11 steps up to 1.5 MPa (max pressure available at 25°C) were programmed but at about 0.6 MPa the strain gauges started reacting with gas so the experiment was stopped.

3.0 Data Analysis

The Langmuir model [6] was used for adsorption data analysis as is conventionally used in the field. The equation is generally expressed as:

$$V = \frac{V_L P}{P_L + P}$$

Eq.

1 Where V = volume of gas adsorbed

P = pressure

V_L= Langmuir Volume

P_L= Langmuir pressure

Since the pressure *vs.* strain data follows the trend of isotherm shape i.e. pressure *vs.* volume of gas adsorbed, an equation having the same mathematical form as the Langmuir equation was used to model the strain data and gives fairly good fit to the strain experimental data.

$$\varepsilon_v = \frac{\varepsilon_L p}{p + p_e}$$

Eq.

2

Where, ε_v is the volumetric strain at a given pressure 'p' and ε_L and p_ε are the model constants which are derived by best fitting a linearised form of Eq. 2 where $\frac{p}{\varepsilon}$ versus p is plotted and have the similar meaning as of Langmuir model constants V_L and P_L derived for isotherm i.e. ε_L represents maximum theoretical strain at infinite pressure and p_ε is the pressure at which 50% of its maximum strain can be attained.

Volumetric strain calculation

The volumetric strain was calculated by taking the average of vertical and horizontal strains and then temperature corrections were applied. The following volumetric strain (ε) equation for the cylindrical samples was derived assuming isotropic swelling/shrinkage in the sample during adsorption/desorption process.

$$\varepsilon = \frac{\Delta V}{V} = \varepsilon_r^2 + 2\varepsilon_r + \varepsilon_a + \varepsilon_r^2 \varepsilon_a + 2\varepsilon_a \varepsilon_r \qquad \text{Eq. 3}$$

where V= original volume

ΔV = change in volume

ε_a = axial strain

ε_r = radial strain

4. Results and Discussions

4.1 Potential volume of acid gas that maybe sequestered in BC coals

A sub-bituminous sample suite of BC coals of rank varying from sub-bituminous 'A' (R_r 0.62%) to medium volatile (R_r 1.31%) from the sedimentary Basins of BC (Annexure I; Table 2) was analyzed for its sorption capacity to H_2, N_2, CH_4, CO_2, H_2S and SO_2 at various pressures at 25°C. The non-toxic gas analyses were done at UBC. For the H_2S and SO_2 experiments a safe module at the Devon research facility of the Alberta Research Council was utilized. The data of BC coals isotherm analysis is provided at Annexure II; Tables 5a to 12b.

The composite isotherm plots of all gases quantifying the sequestration potential of the BC coal samples are shown in Figs. 3 to 10 and the individual gas isotherm plots along with Langmuir fits are shown in Figs. 3a to 10f. The Langmuir constants are provided at Tables 3 & 3a of Annexure I. The data clearly indicate the tremendous sorption capacity of coal to hydrogen sulphide and sulphur dioxide and the real potential for utilizing BC coals as sink for these gases. The order of adsorption invariably was SO_2 > H_2S> CO_2> CH_4> N_2> H_2.

The adsorption ratios of CO_2, H_2S & SO_2 to CH_4 at 0.6 MPa suggests that CO_2 has 2.5 to 13 times higher storage potential than CH_4, 6-40 times higher for H_2S and 4-50 times higher storage potential for SO_2 relative to CH_4 for the sample suites investigated (Annexure I; Table 4). Interestingly, these ratios broadly show decreasing trend with increasing coal rank and average variation was observed from about 8:1 to 4:1 for CO_2; 25:1 to 15:1 for H_2S and 16:1 to 8:1 for SO_2 (Fig. 10g).

The BC coals were chemically and physically characterized in detail prior to and following sorption by acid gas. Micro-FTIR analyses prior to and following sorption of acid gases indicate that no measurable change in functionality of the organics during the adsorption-desorption experiment. Hence we conclude that acid gas does not chemically alter the structure or surface chemistry of the coal.

4.2. Volumetric changes in BC coals due to adsorption/desorption of CH_4, N_2, CO_2 and H_2S

Volumetric strain experiments adsorbing N_2, CH_4, CO_2 and H_2S were determined for Wolf Mtn and Quinsam coal samples (Figs. 11 to 22). With increasing adsorption pressure of N_2, CH_4, CO_2 and H_2S resulted in marked swelling of coal matrix. It is interesting to note that the volumetric strain and pressure follows the trend of isotherm i.e. similar to pressure vs. gas concentration and can be modeled fairly well using Langmuir type equation (Eq.2) for strain modeling. The modeled data fits fairly well to the experimental strain data for all the gases (Figs. 16 & 22). For comparison of strains at a common base, all the strains were calculated at 0.6 MPa using Eq. 2, since the H_2S experiment was done at low pressures up to 0.6 MPa as stated previously. The order of volumetric swelling observed at 0.6 MPa in descending order is H_2S (8.4% to 9.3%)> CO_2 (0.46%-0.66%)> CH_4 (0.12%- 0.29%)> N_2 (0.012% - 0.026%) (Figs.16 &

22; Table 4a). The volumetric strain (swelling) with H_2S is markedly very high about 12-20 times higher than CO_2 and about 30-70 times higher than CH_4 shrinkage. Similarly swelling caused by CO_2 is 2-5 times higher than the CH_4 Shrinkage and CH_4 shrinkage is 10 times higher than the swelling caused by the N_2 adsorption for the sample suite investigated (Table 4b; Figs. 16 & 22). The volumetric strains are strongly and positively correlated with adsorbed gas quantities and are linearly proportional to the amount of gas adsorbed (Figs. 11a to 15a; 17a to 21a).

It may be noted that the moisture content of Wolf Mtn and Quinsam for strain experiment samples is 2.26% and 4.14% which is different from the equilibrium moisture content for isotherm samples at 4.56% and 6.69% respectively. This is because the solid core samples looses some moisture during the strain adhering processes, which is a time consuming and has to be done in dry environment for curing the strain gauges.

From the adsorption isotherms and volumetric strain data suggests that N_2 injection will enhance the CH_4 production from coalbeds due to increase in N_2 partial pressure coupled with increased permeability of coal beds because of shrinkage by CH_4. Pure injection of H_2S or CO_2 may completely or significantly reduce the permeability of coal seams as injection of H_2S and CO_2 causes up to 4.5 times higher swelling than the shrinkage created by the CH_4 desorption on unit concentration basis. The results suggest that the injection of a mixture of N_2 and CO_2 or N_2 and H_2S may inhibit the swelling of coals and may facilitate sequestration of acid gas.

5. Conclusions

Adsorption isotherm and volumetric strain experiments on BC coals with various gases provide critical information on the coal reservoir behavior when acid gas is injected for pure sequestration or for ECBM purposes. The volumetric swelling/shrinkage is strongly and positively correlated with gas concentration in all the cases. The volumetric strain related to pressure behaves like an isotherm and can be reasonably modeled using Langmuir model type equation similar to isotherm modeling. The parameters derived from modeling the strain can be used for interpreting the strain caused due to pressure change in the reservoir and also the change in gas concentration using the relationship between volumetric strain vs. gas concentration.

Sorption capacity increases in the order H_2> N_2> CH_4> CO_2> H_2S > SO_2 in the BC coals. Overall the sorption capacity and volumetric strain increases with increasing pressure steps until they reach their saturation pressures. Comparison of strain at about 0.6 MPa pressure step with the above gases show that the volumetric strain (swelling) with H_2S is very high and about 20 times higher than CO_2 and about 70 times higher than CH_4. The order of volumetric swelling at 0.6 MPa in decreasing order is H_2S (up to 10.0%)> CO_2 (up to 0.66%)> CH_4 (up to 0.29%)> N_2 (up to 0.026%).

Attempts to sequester H_2S and CO_2 in BC coals will result in significant swelling of the coal to a markedly greater extent than the initial shrinkage caused due to methane production. Hence, may result in substantial loss of permeability of the coal reservoir. Depending on initial coal permeability and composition, the potential for sequestration of CO_2, H_2S or SO_2 may be limited by the swelling of coal and resulting decline in permeability during injection.

References

1. Harpalani, S. and Schraufnagel, R. 1990: Shrinkage of coal matrix with release of gas and its impact on permeability of coal. Fuel, v 69, pp 551-556.

2. George, J. D. St. and Barakat, M. A. 2001: The change in effective stress associated with shrinkage from gas desorption in coal. International Journal of Coal Geology, v. 45, pp. 5-113.

3. Australian Standard AS 1038.17-1989, 1989: “Methods for the analysis and testing of coal and coke. Part 17: Determining the moisture-holding capacity (equilibrium moisture) of higher rank coal”; Standards Association of Australia, North Sydney. 8 p.

4. Australian Standard AS 2486-1989, 1989: “Methods for microscopic determination of the reflectance of coal macerals”; Standards Association of Australia, North Sydney. 15 p.

5. Australian Standard AS 2856-1986, 1986: “Coal-Maceral Analysis”; Standards Association of Australia, North Sydney. 22 p.

6. Langmuir, I. 1918: The adsorption of gases on plane surfaces of glass, mica and platinum. The Journal of American Chemical Society, v 40, pp. 1361-1403.

FIGURES

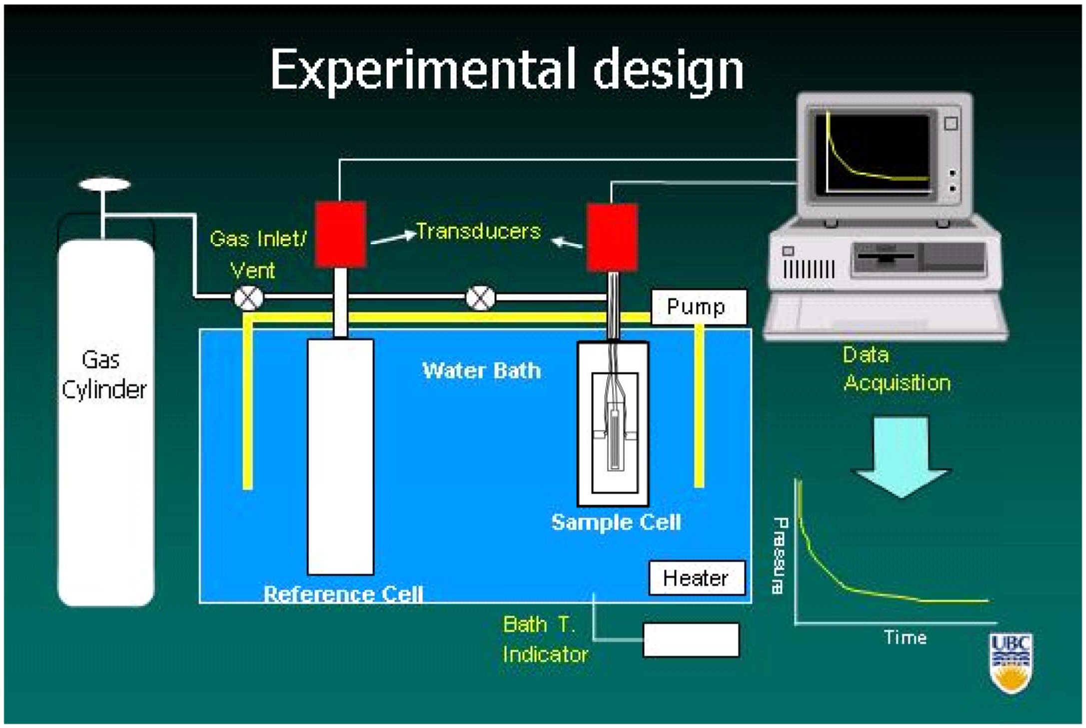

Figure 1: Experimental set up for adsorption isotherms

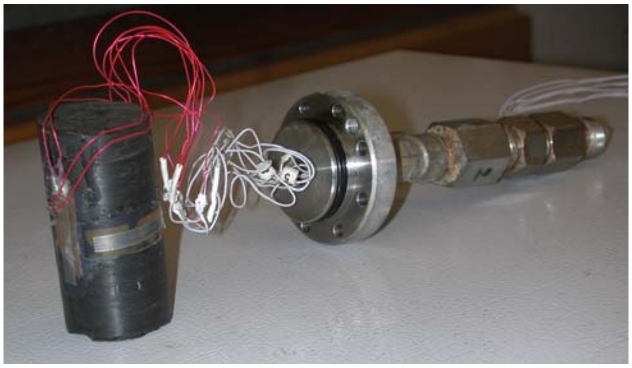

Figure 2: Strain gauge set up to core sample

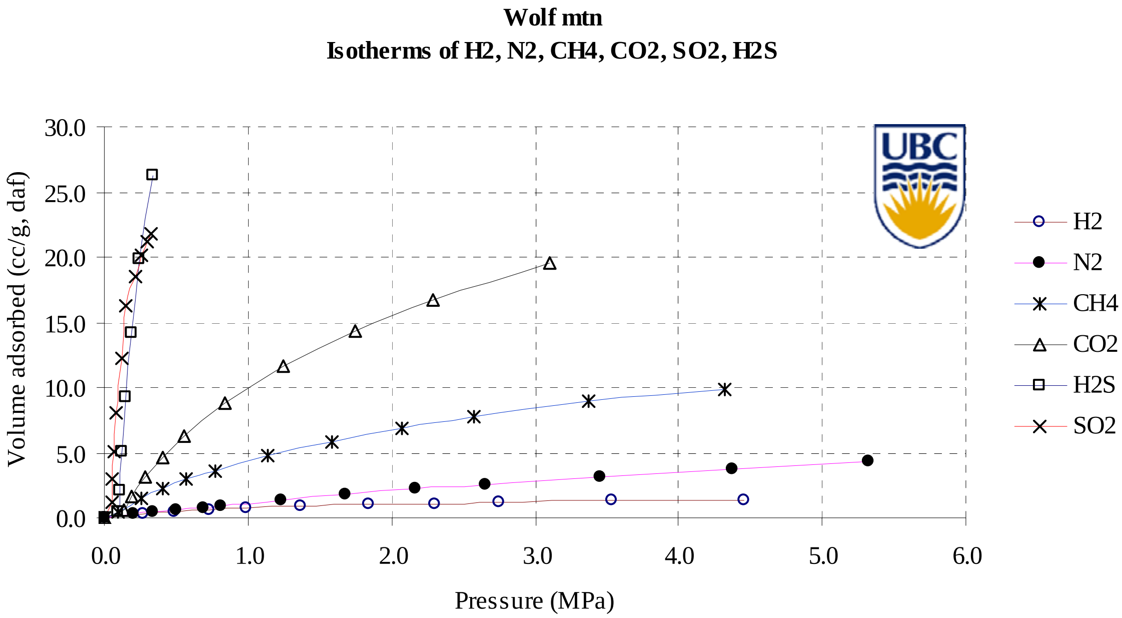

Figure 3: Wolf Mtn adsorption isotherms for H_2, N_2, CH_4, CO_2, H_2S and SO_2

Wolf Mtn: Isotherm plots for individual gases

(Figures 3a to 3f)

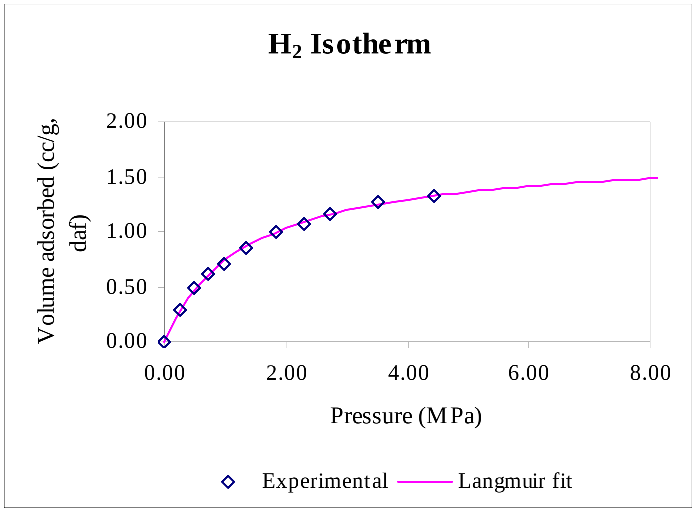

Figure 3a: Isotherm plot with Langmuir fit for H_2

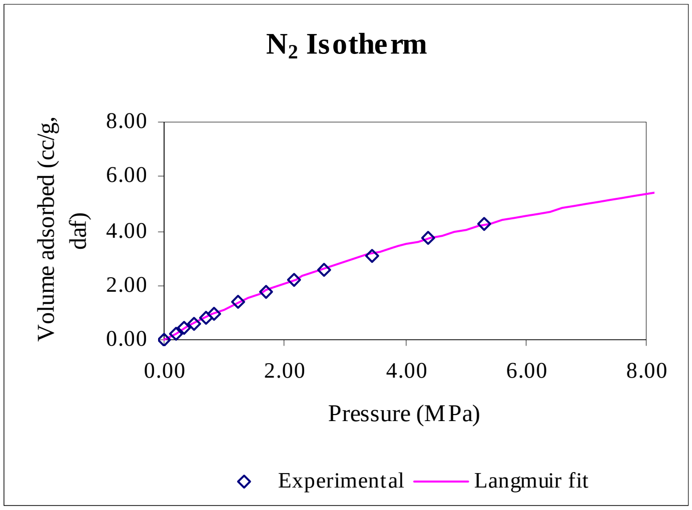

Figure 3b: Isotherm plot with Langmuir fit for N2

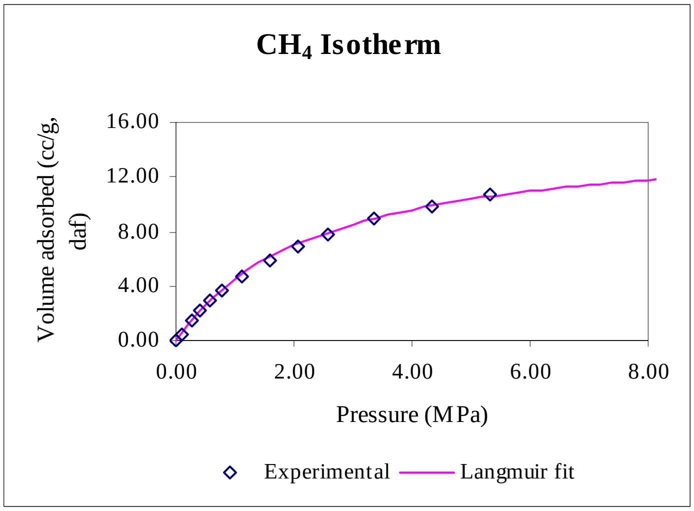

Figure 3c: Isotherm plot with Langmuir fit for CH_4

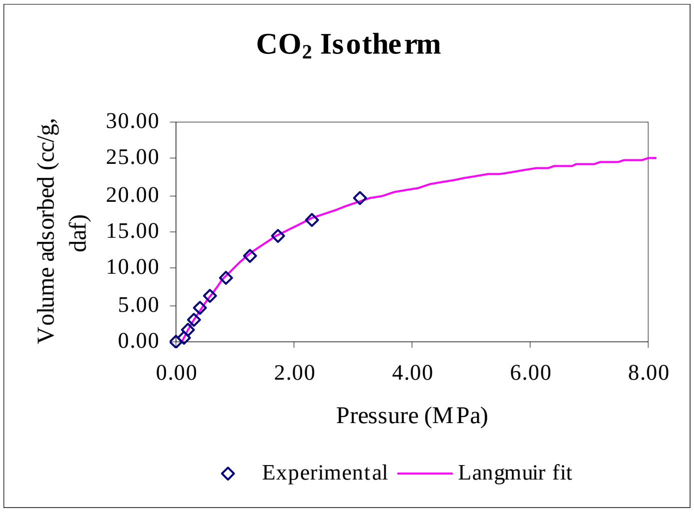

Figure 3d: Isotherm plot with Langmuir fit for CO_2

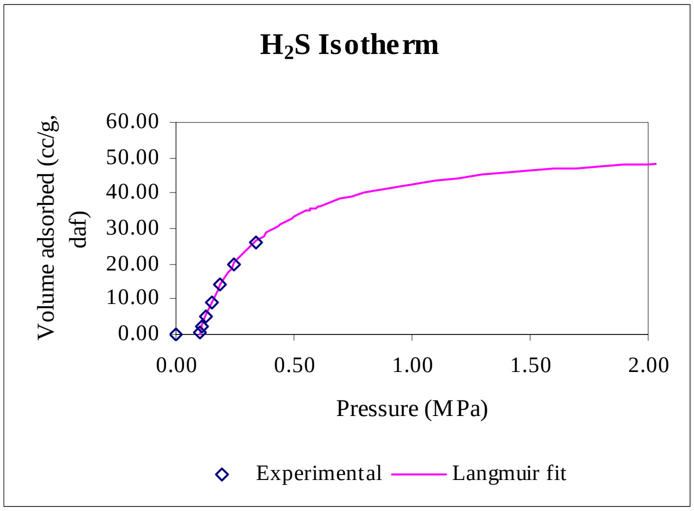

Figure 3e: Isotherm plot with Langmuir fit for H_2S

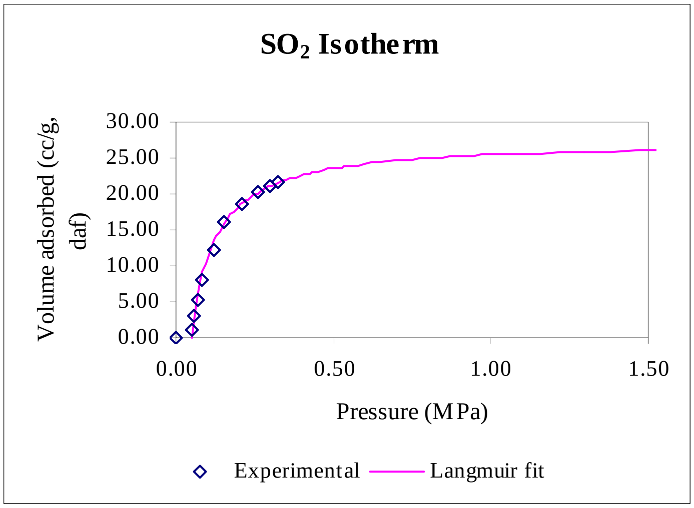

Figure 3f: Isotherm plot with Langmuir fit for SO_2

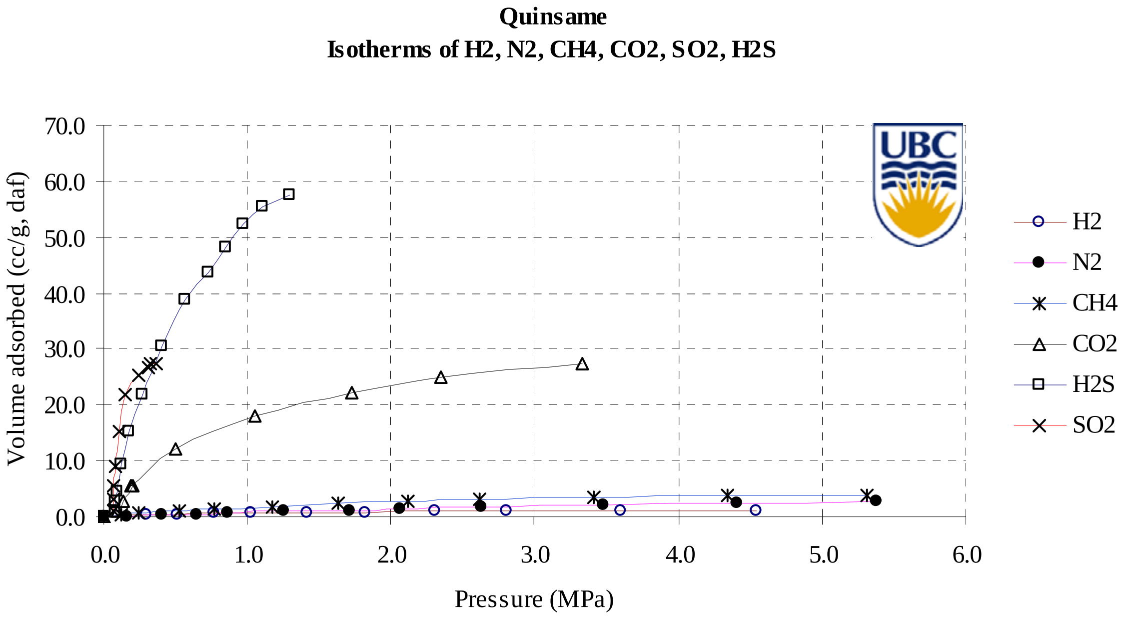

Figure 4: Quinsam adsorption isotherms for H_2, N_2, CH_4, CO_2, H_2S and SO_2

Quinsam: Isotherm plots for individual gases

(Figures 4a to 4f)

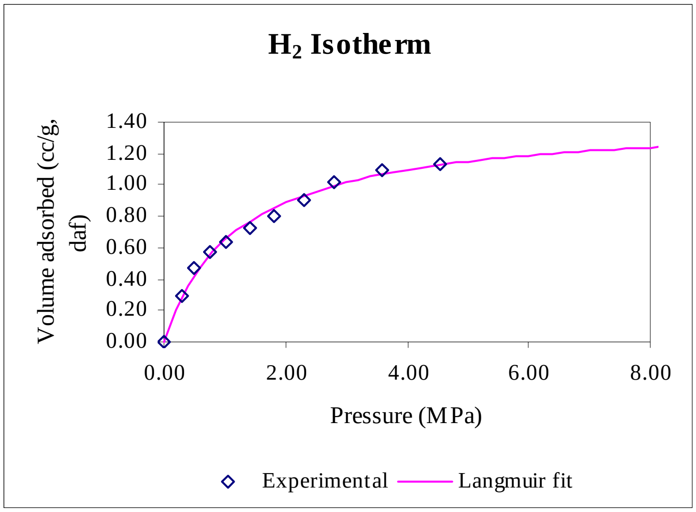

Figure 4a: Isotherm plot with Langmuir fit for H_2

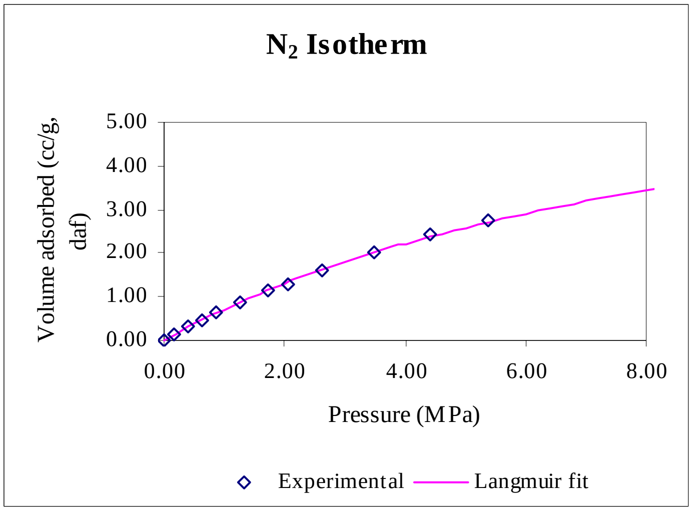

Figure 4b: Isotherm plot with Langmuir fit for N_2

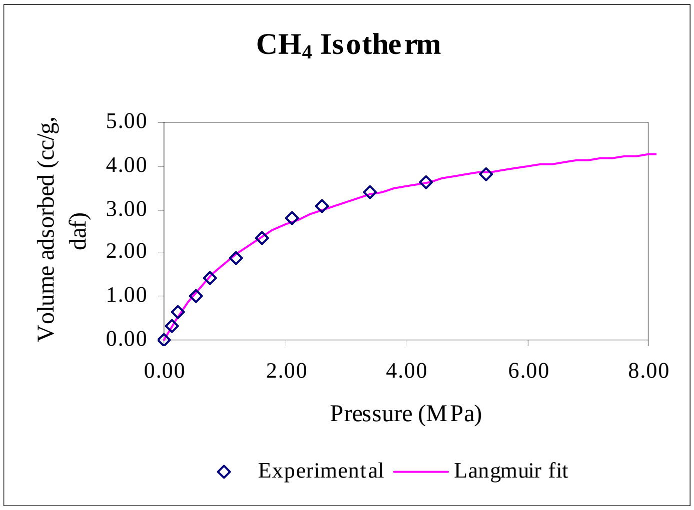

Figure 4c: Isotherm plot with Langmuir fit for CH_4

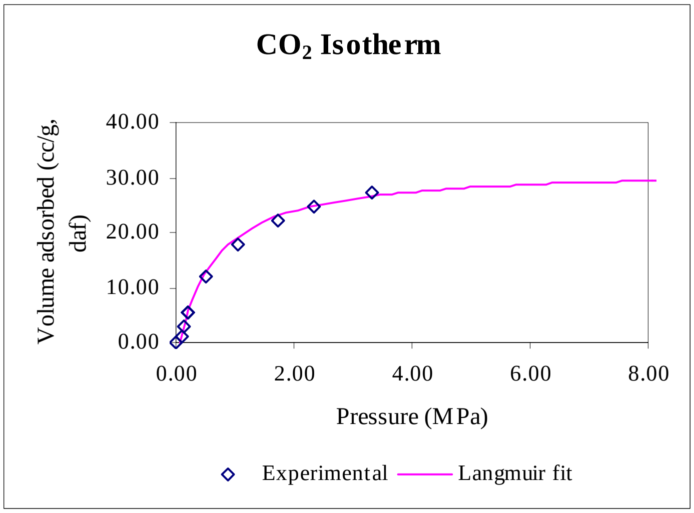

Figure 4d: Isotherm plot with Langmuir fit for CO_2

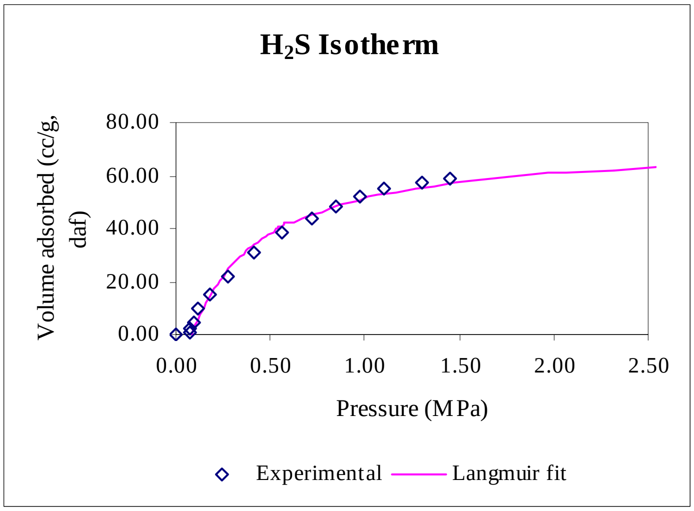

Figure 4e: Isotherm plot with Langmuir fit for H_2S

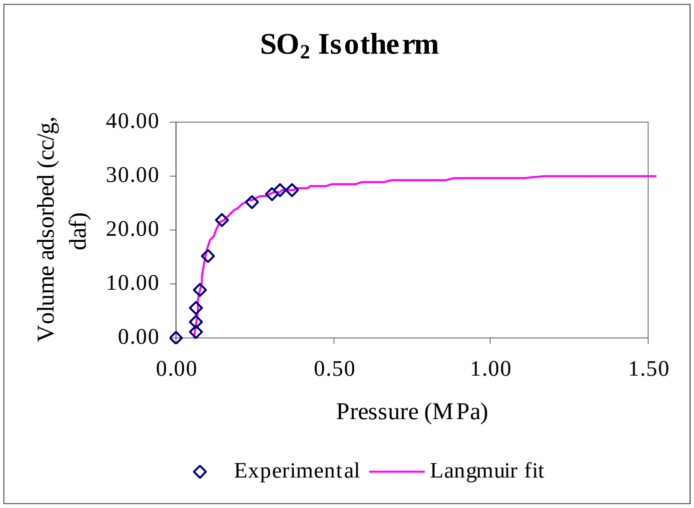

Figure 4f: Isotherm plot with Langmuir fit for SO_2

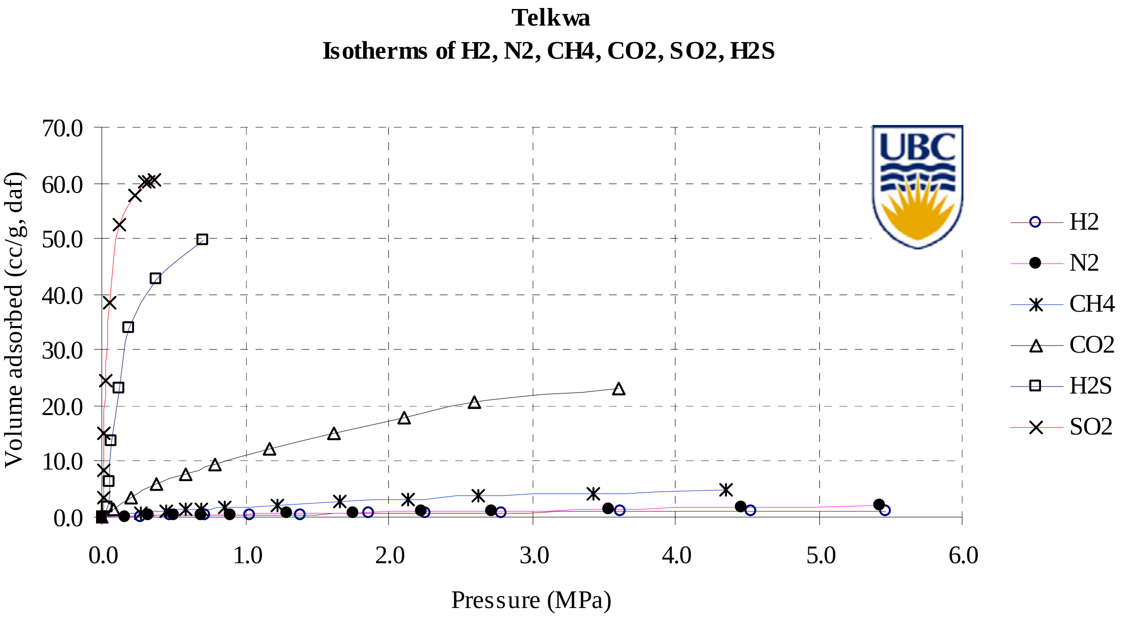

Figure 5: Telkwa adsorption isotherms for H_2, N_2, CH_4, CO_2, H_2S and SO_2

Telkwa: Isotherm plots for individual gases

(Figures 5a to 5f)

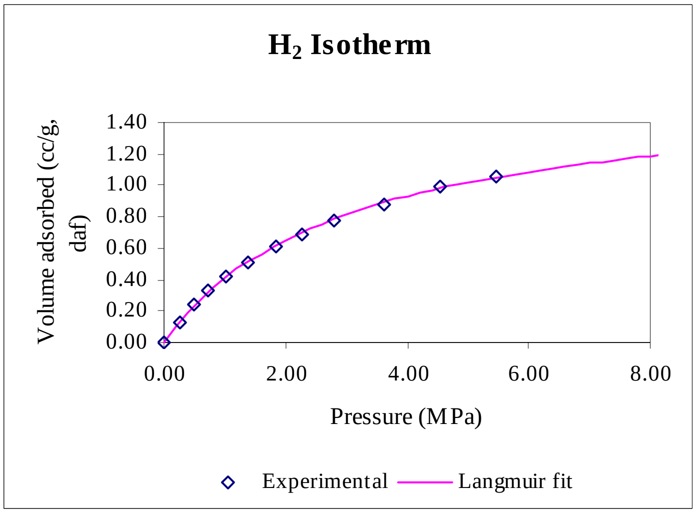

Figure 5a: Isotherm plot with Langmuir fit for H_2

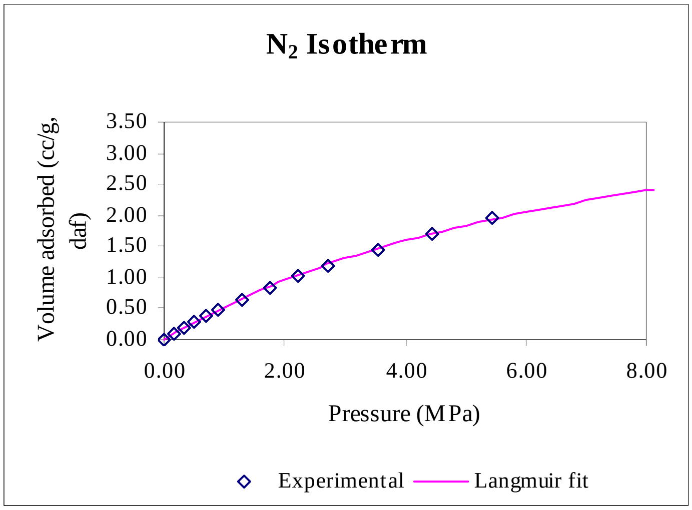

Figure 5b: Isotherm plot with Langmuir fit for N_2

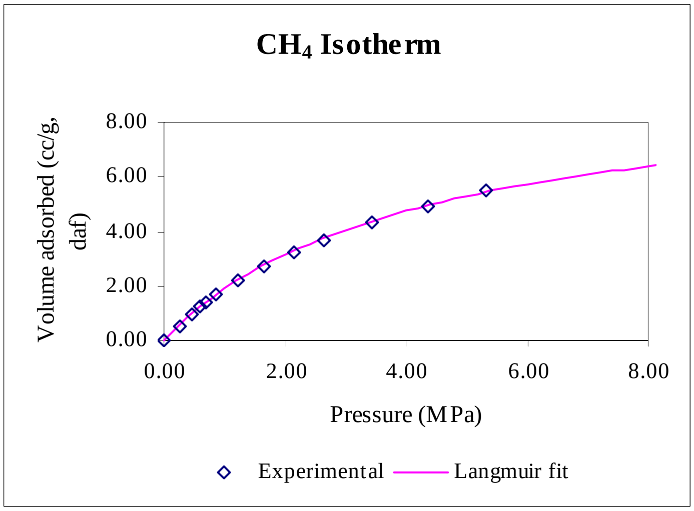

Figure 5c: Isotherm plot with Langmuir fit for CH_4

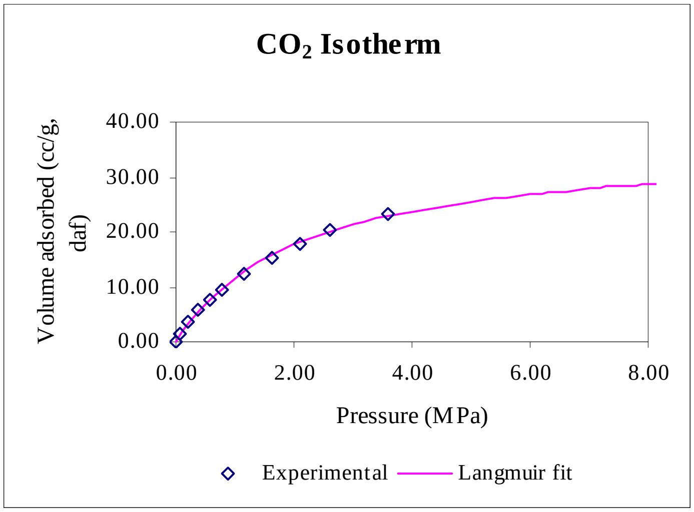

Figure5d: Isotherm plot with Langmuir fit for CO_2

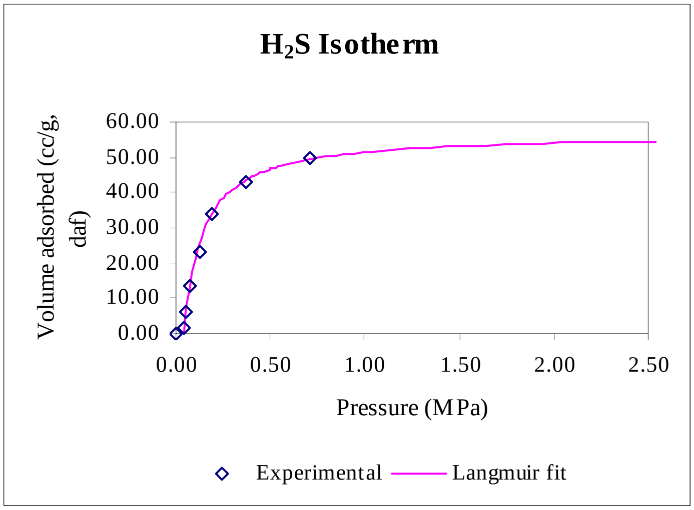

Figure 5e: Isotherm plot with Langmuir fit for H_2S

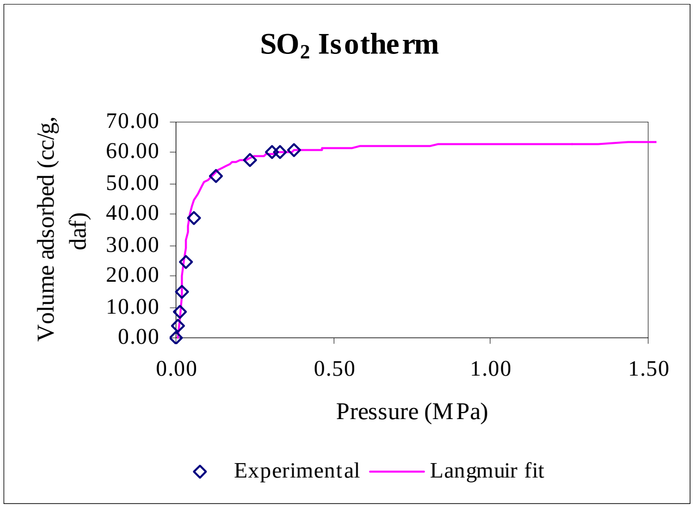

Figure 5f: Isotherm plot with Langmuir fit for SO_2

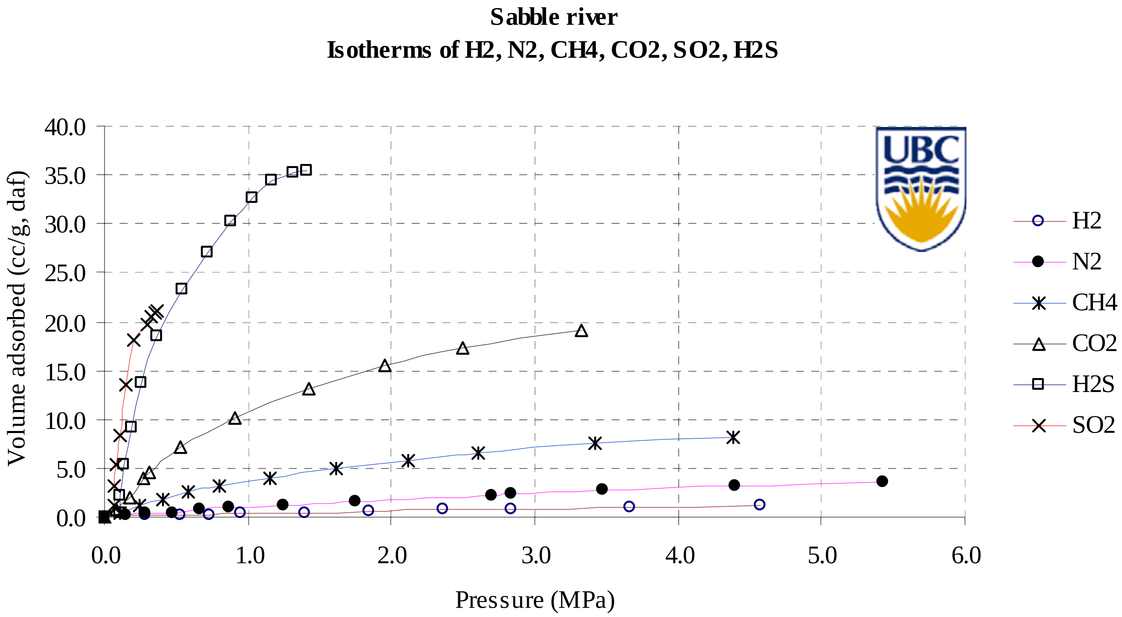

Figure 6: Sable River adsorption isotherms for H_2, N_2, CH_4, CO_2, H_2S and SO_2

Sable River: Isotherm plots for individual gases

(Figures 6a to 6f)

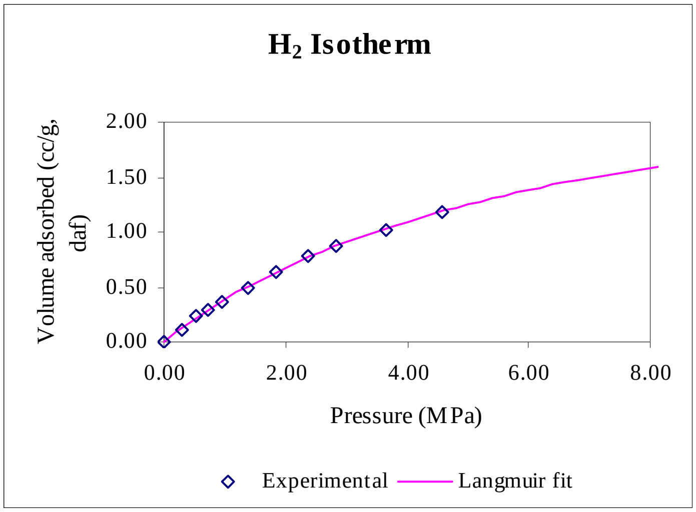

Figure 6a: Isotherm plot with Langmuir fit for H_2

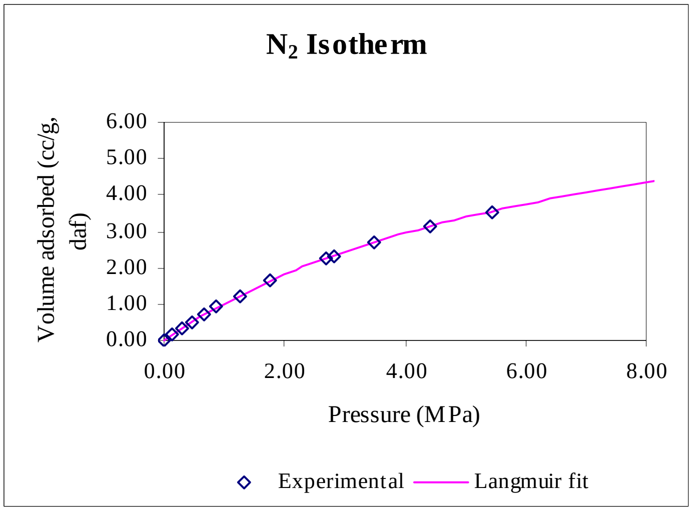

Figure 6b: Isotherm plot with Langmuir fit for N_2

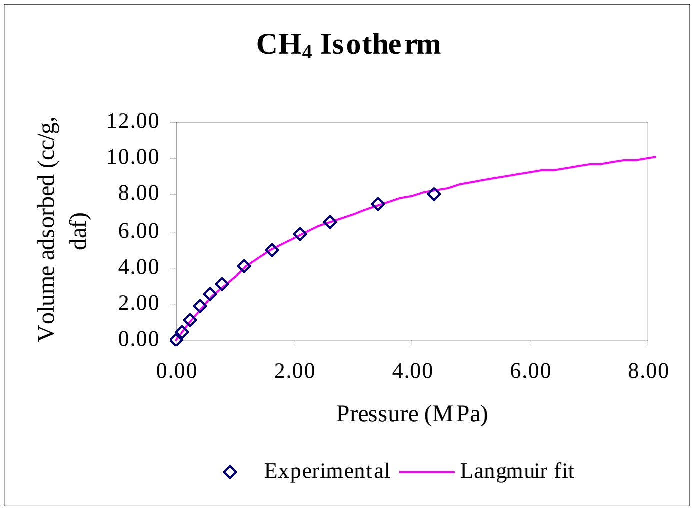

Figure 6c: Isotherm plot with Langmuir fit for CH_4

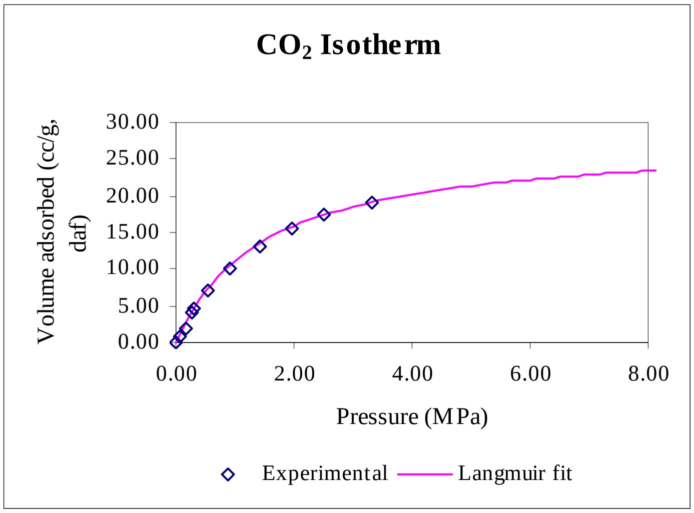

Figure 6d: Isotherm plot with Langmuir fit for CO_2

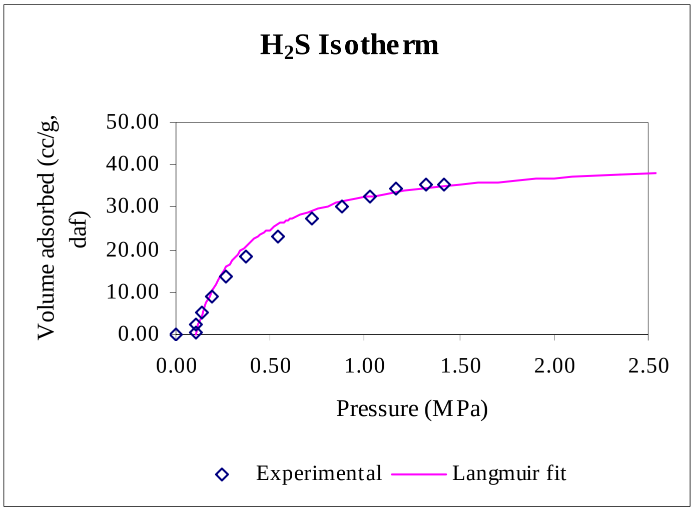

Figure 6e: Isotherm plot with Langmuir fit for H_2S

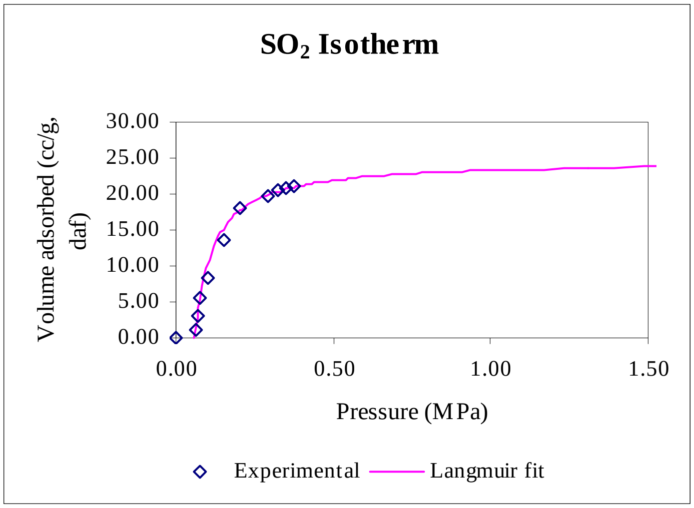

Figure 6f: Isotherm plot with Langmuir fit for SO_2

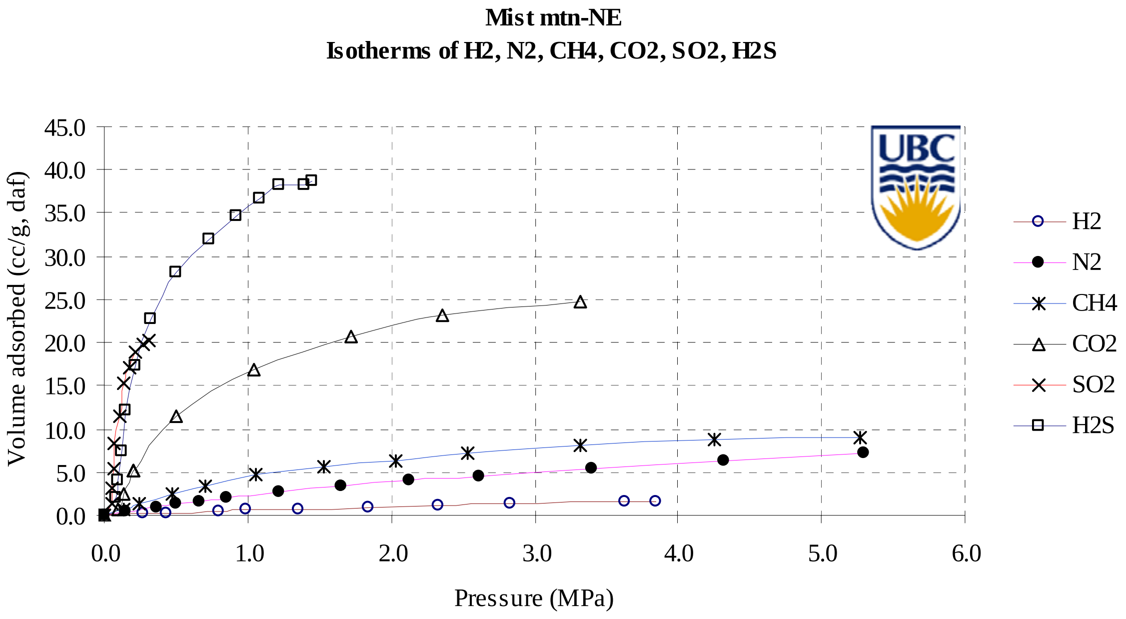

Figure 7: Mist Mtn-NE adsorption isotherms for H_2, N_2, CH_4, CO_2, H_2S and SO_2

Mist Mtn-NE: Isotherm plots for individual gases

(Figures 7a to 7f)

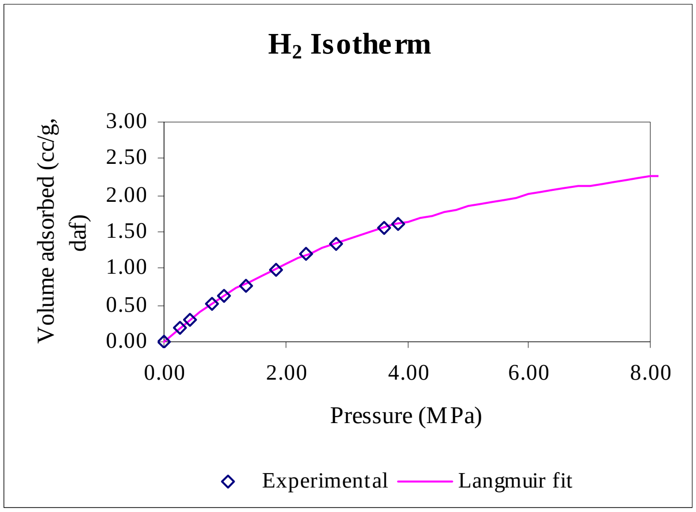

Figure 7a: Isotherm plot with Langmuir fit for H_2

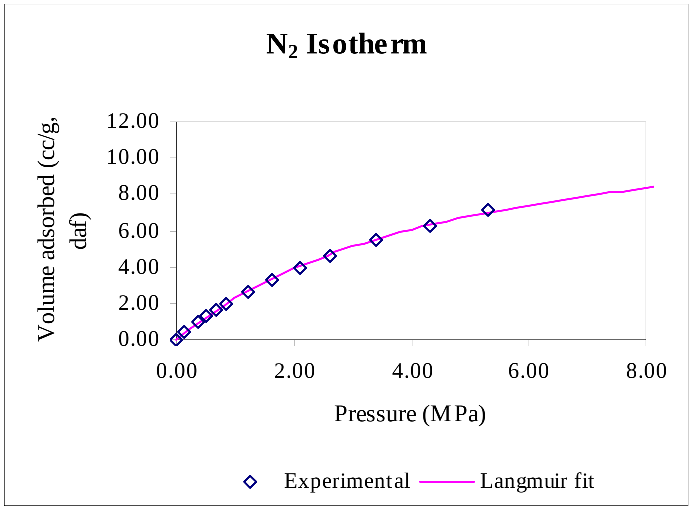

Figure 7b: Isotherm plot with Langmuir fit for N_2

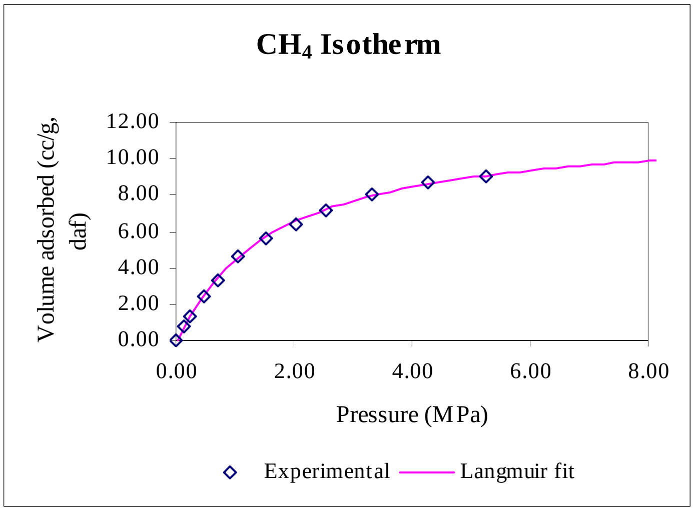

Figure 7c: Isotherm plot with Langmuir fit for CH_4

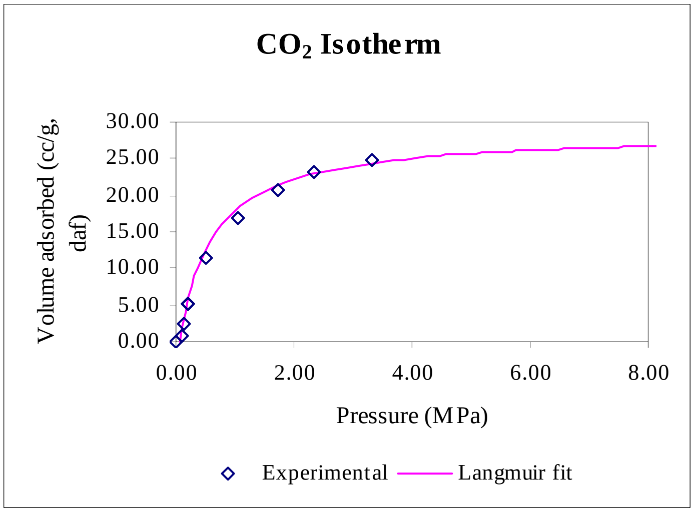

Figure 7d: Isotherm plot with Langmuir fit for CO_2

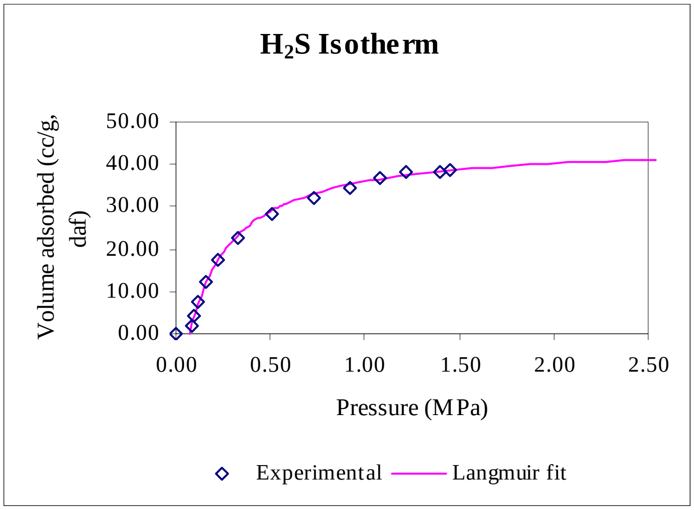

Figure 7e: Isotherm plot with Langmuir fit for H_2S

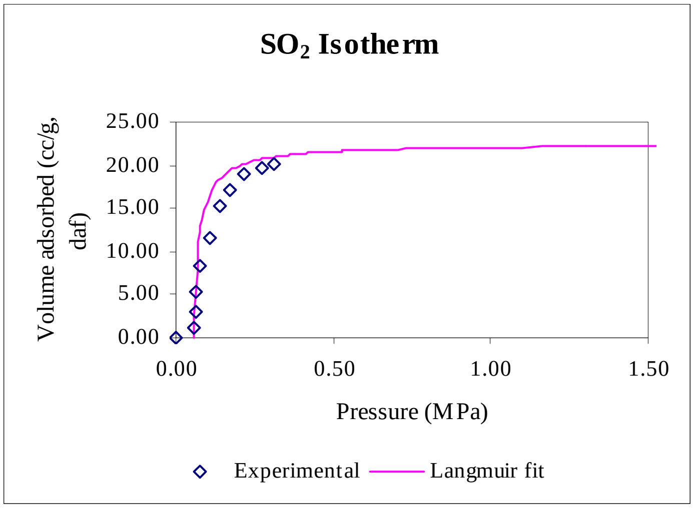

Figure 7f: Isotherm plot with Langmuir fit for SO_2

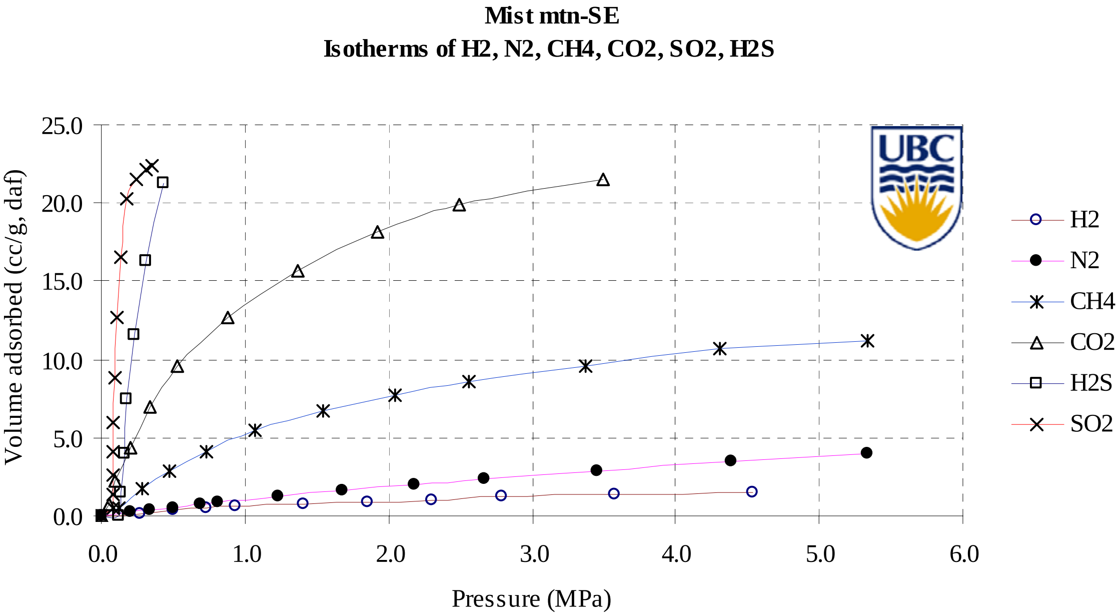

Figure 8: Mist Mtn-SE adsorption isotherms for H_2, N_2, CH_4, CO_2, H_2S and SO_2

Mist Mtn-SE: Isotherm plots for individual gases

(Figures 8a to 8f)

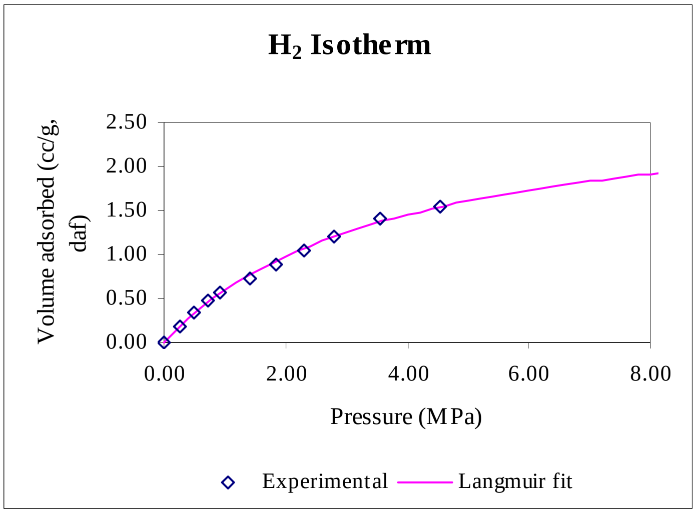

Figure 8a: Isotherm plot with Langmuir fit for H_2

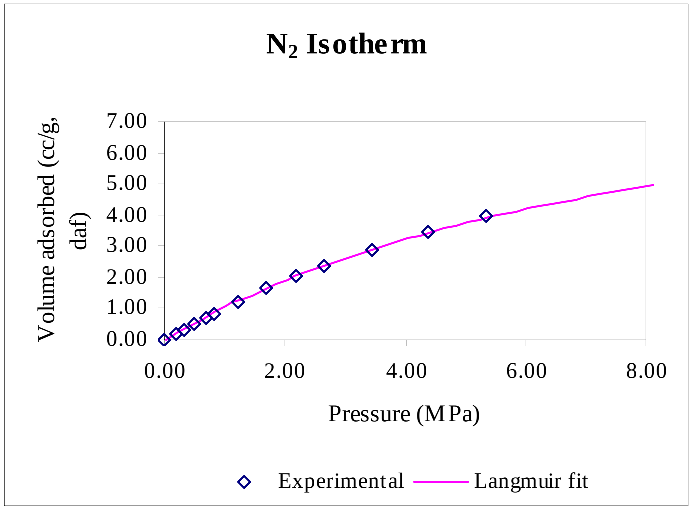

Figure 8b: Isotherm plot with Langmuir fit for N_2

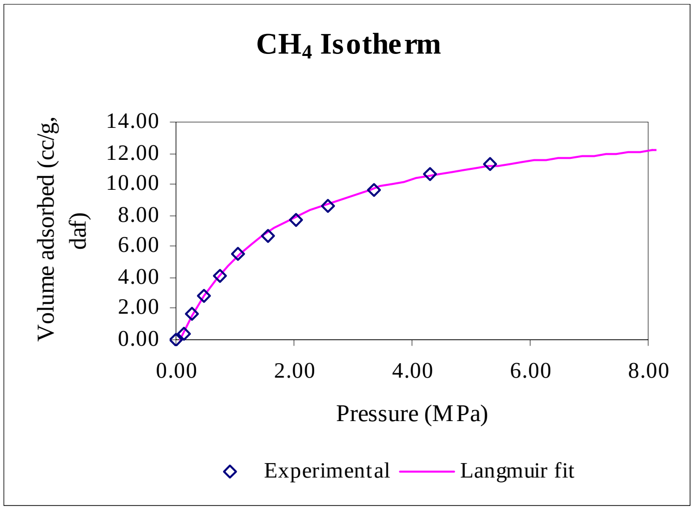

Figure 8c: Isotherm plot with Langmuir fit for CH_4

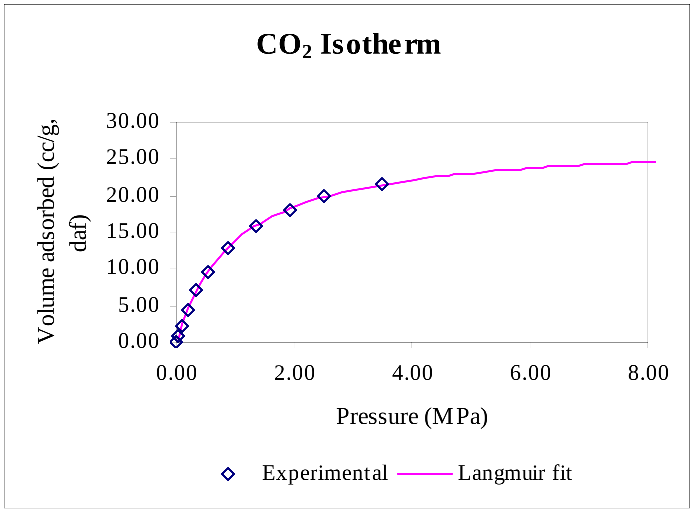

Figure 8d: Isotherm plot with Langmuir fit for CO_2

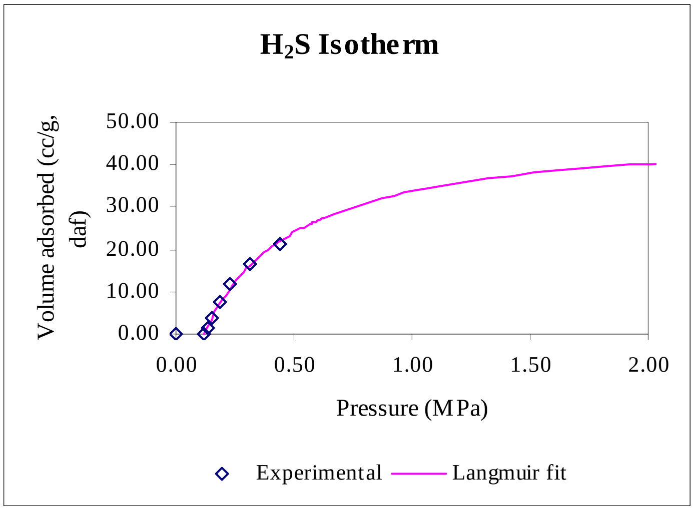

Figure 8e: Isotherm plot with Langmuir fit for H_2S

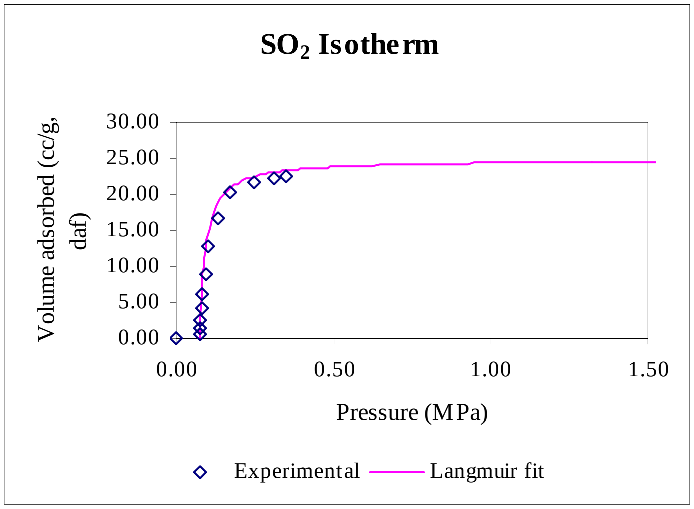

Figure 8f: Isotherm plot with Langmuir fit for SO_2

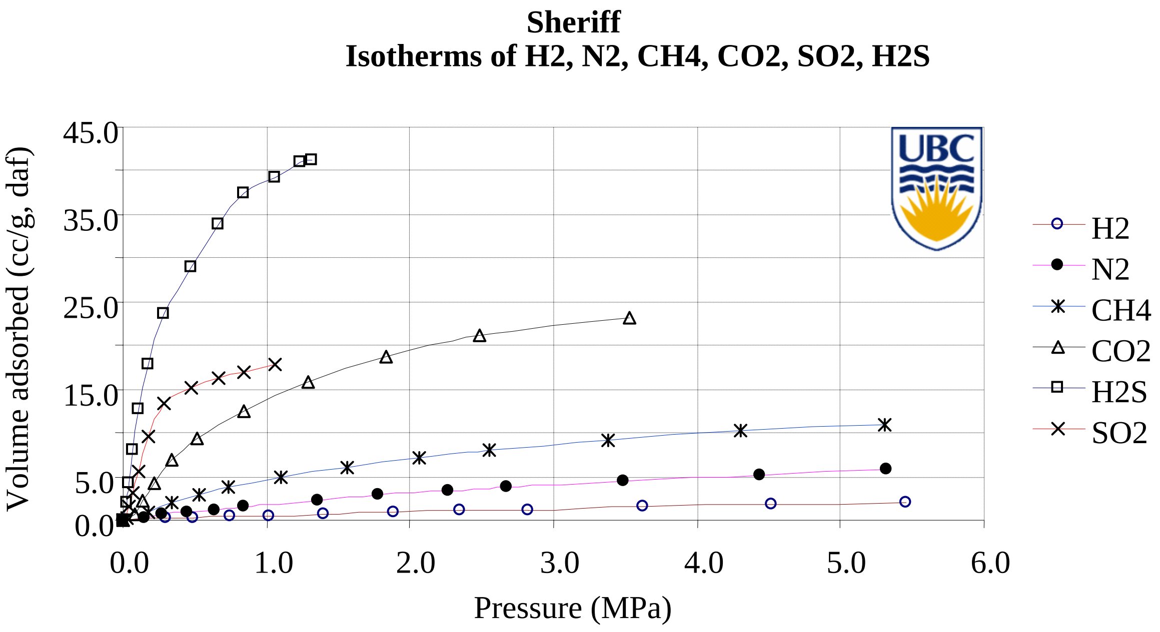

Figure 9: Sheriff adsorption isotherms for H_2, N_2, CH_4, CO_2, H_2S and SO_2

Sheriff: Isotherm plots for individual gases

(Figures 9a to 9f)

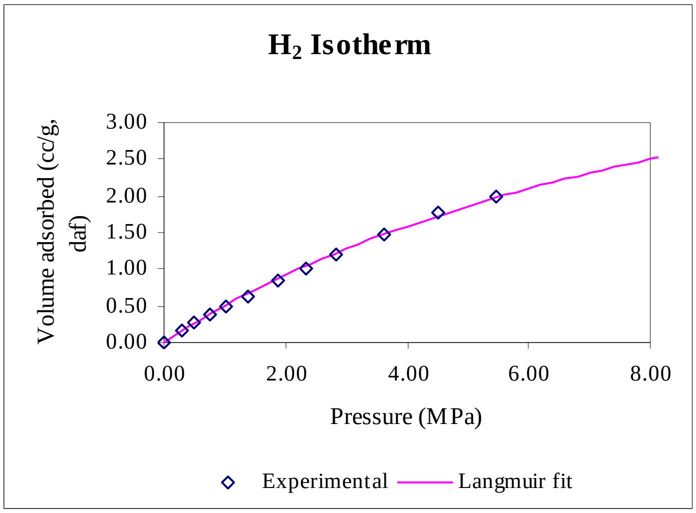

Figure 9a: Isotherm plot with Langmuir fit for H_2

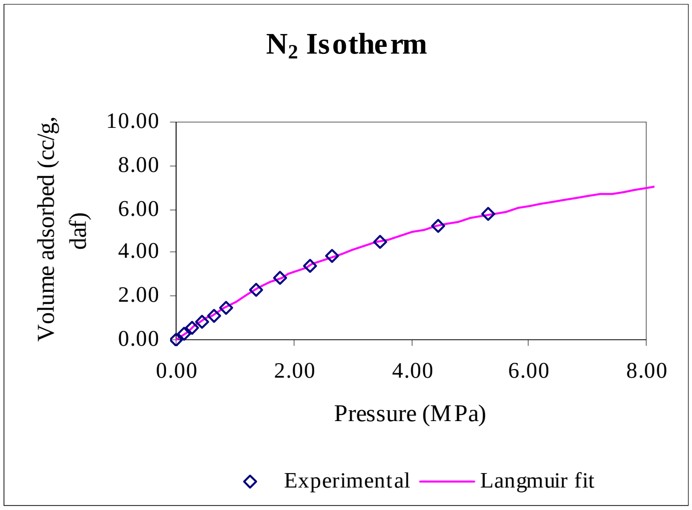

Figure 9b: Isotherm plot with Langmuir fit for N_2

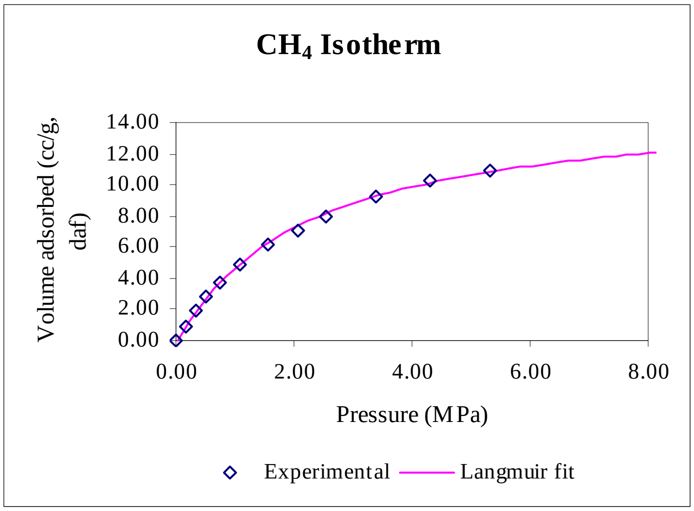

Figure 9c: Isotherm plot with Langmuir fit for CH_4

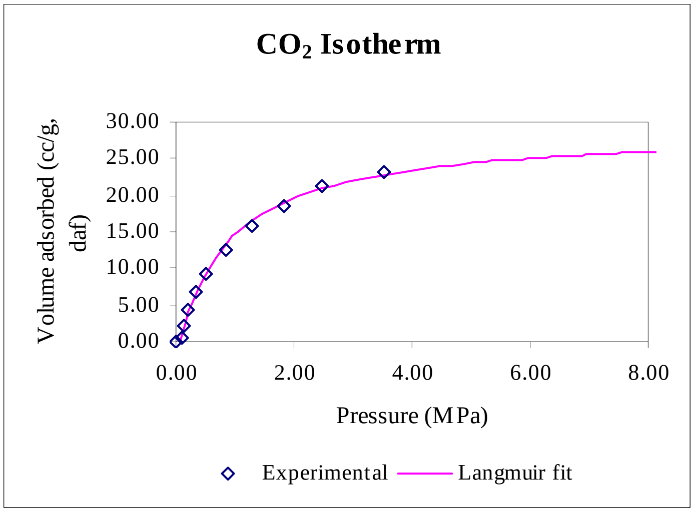

Figure 9d: Isotherm plot with Langmuir fit for CO_2

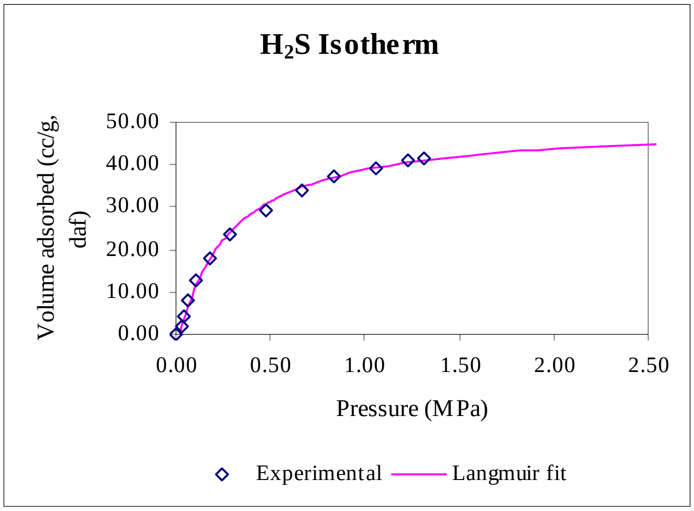

Figure 9e: Isotherm plot with Langmuir fit for H_2S

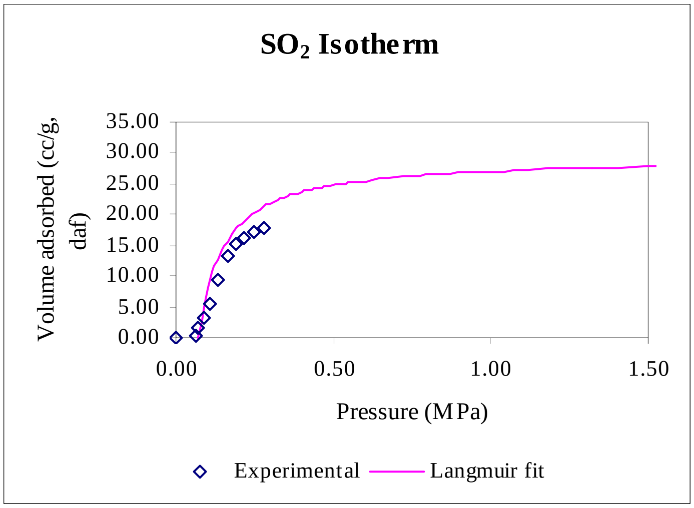

Figure 9f: Isotherm plot with Langmuir fit for SO_2

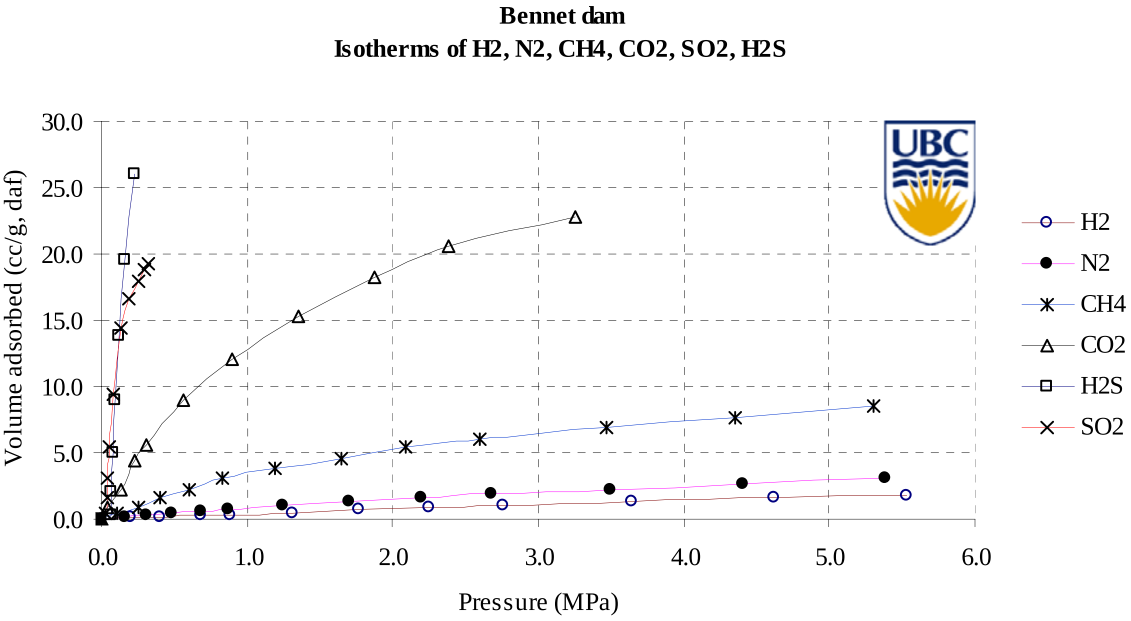

Figure 10: Bennet Dam adsorption isotherms for H_2, N_2, CH_4, CO_2, H_2S and SO_2

Bennet Dam: Isotherm plots for individual gases

(Figures10a to 10f)

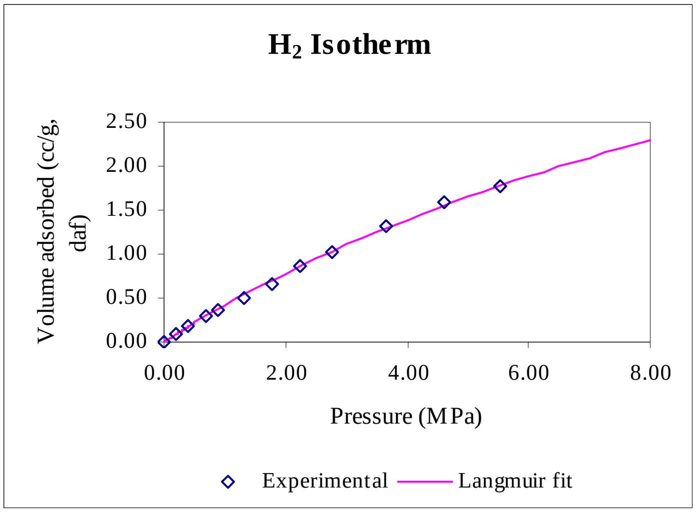

Figure 10a: Isotherm plot with Langmuir fit for H_2

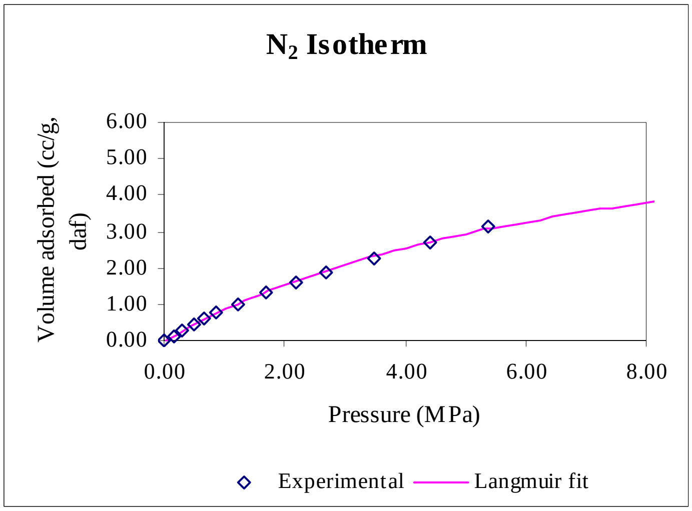

Figure 10b: Isotherm plot with Langmuir fit for N_2

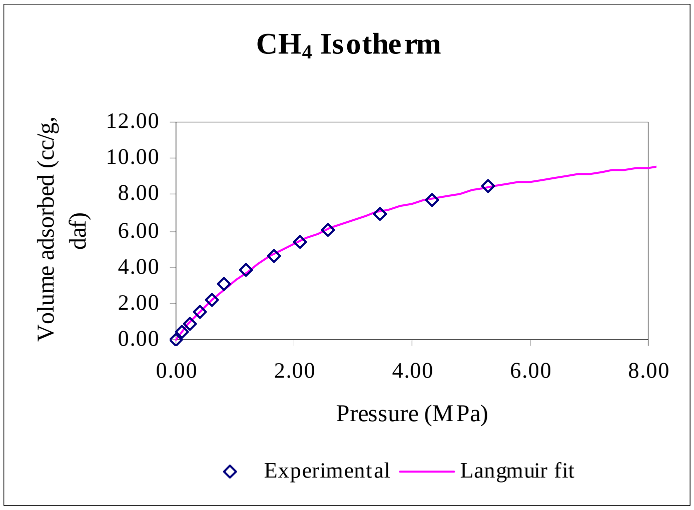

Figure 10c: Isotherm plot with Langmuir fit for CH_4

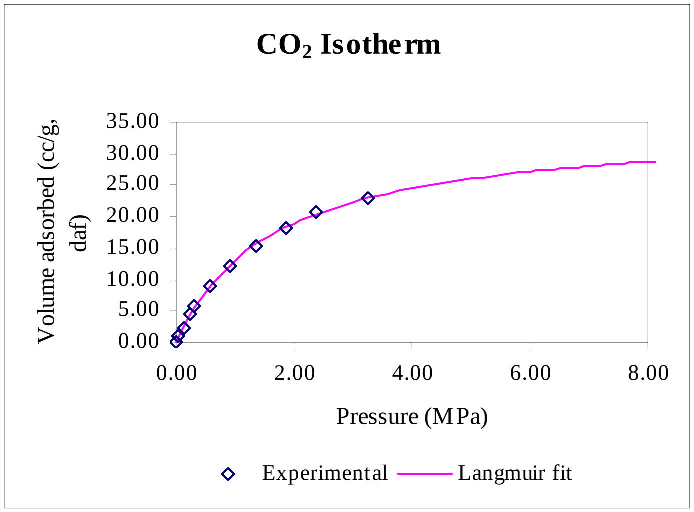

Figure 10d: Isotherm plot with Langmuir fit for CO_2

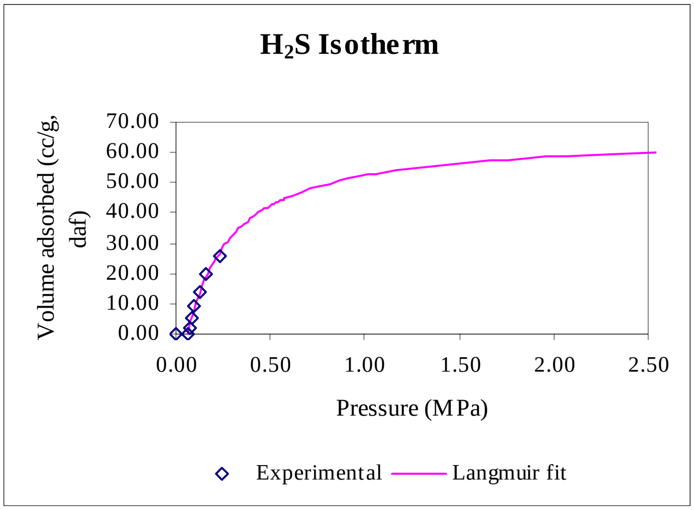

Figure 10e: Isotherm plot with Langmuir fit for H_2S

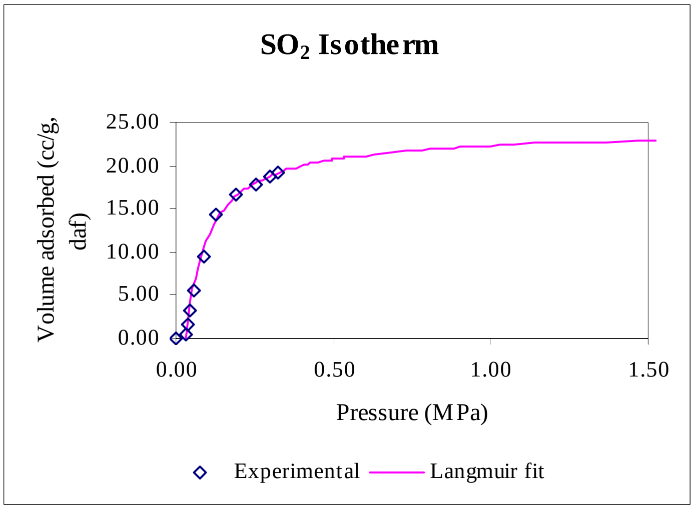

Figure 10f: Isotherm plot with Langmuir fit for SO_2

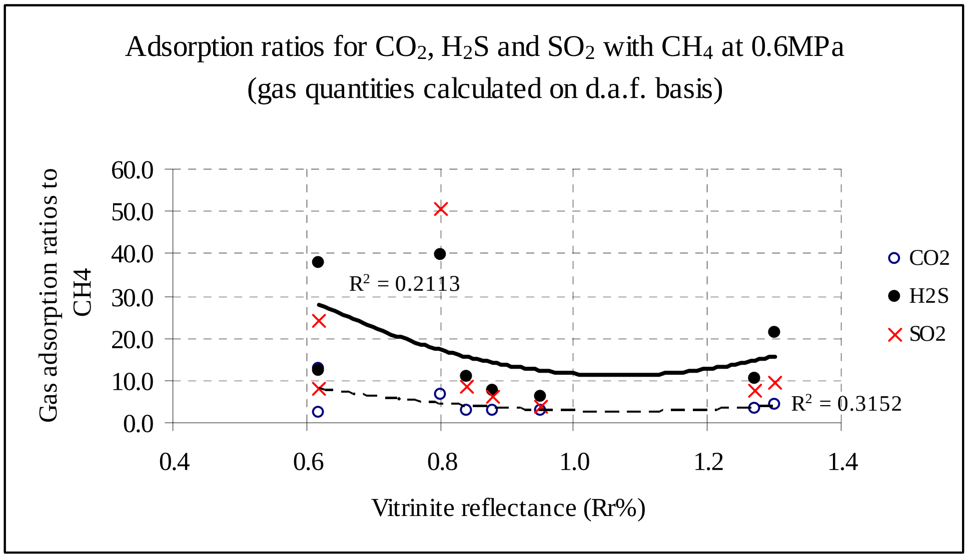

Figure 10g: Adsorption ratios with rank for CO_2, H_2S and SO2 with CH_4. R^2 values shown are for H_2S and CO_2 indicate a broad trend.

Strain plots: Wolf Mtn

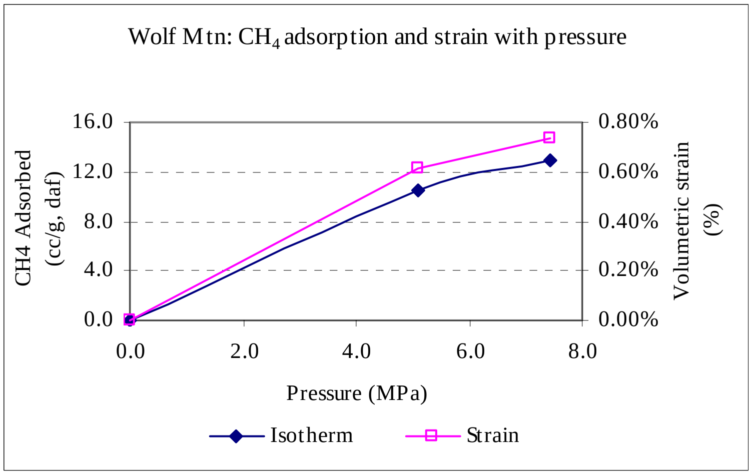

Figure 11: Pressure, gas concentration and volumetric strain plot for CH_4 adsorption run

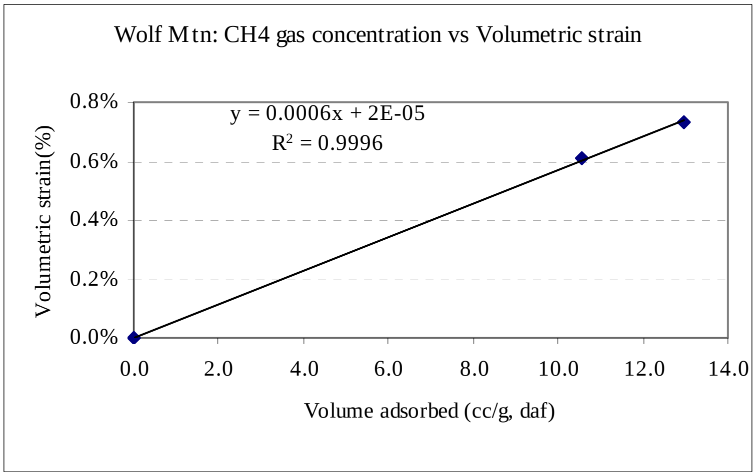

Figure 11a: Gas concentration and volumetric strain relationship for CH_4 adsorption run

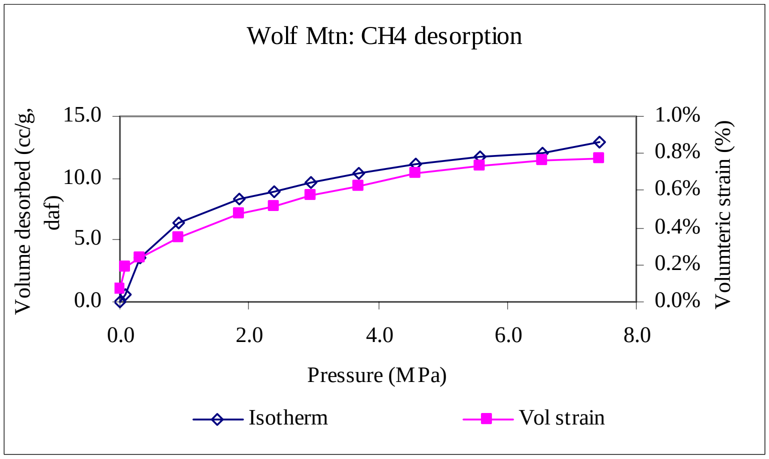

Figure 12: Pressure, gas concentration and volumetric strain plot for CH_4 desorption run

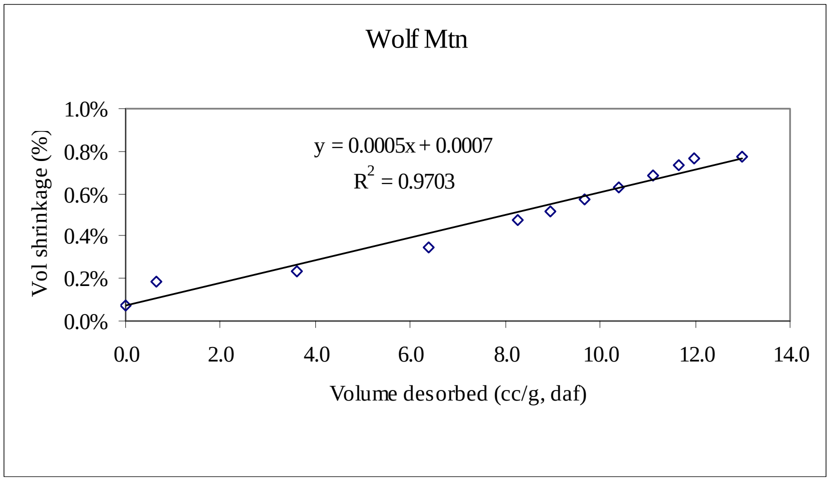

Figure 12a: Gas concentration and volumetric strain relationship for CH_4 desorption run

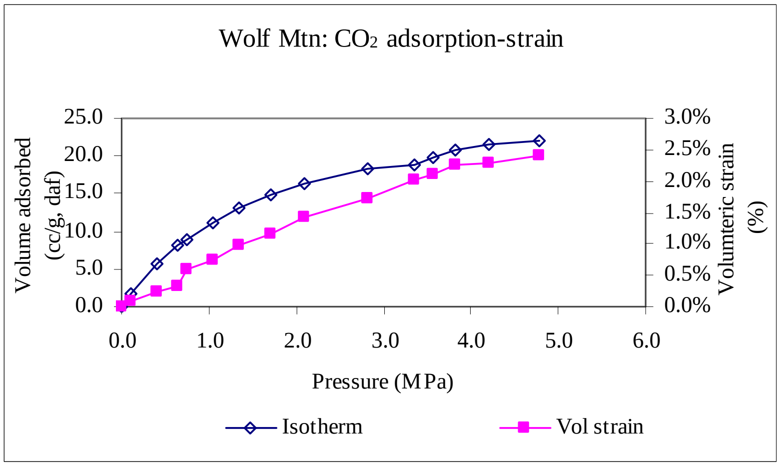

Figure 13: Pressure, gas concentration and volumetric strain plot for CO_2 adsorption run

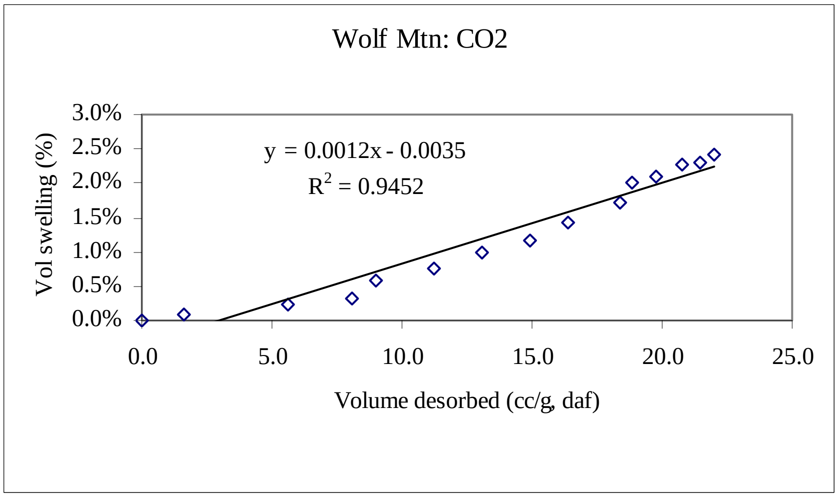

Figure 13a: Gas concentration and volumetric strain relationship for CO_2 adsorption run

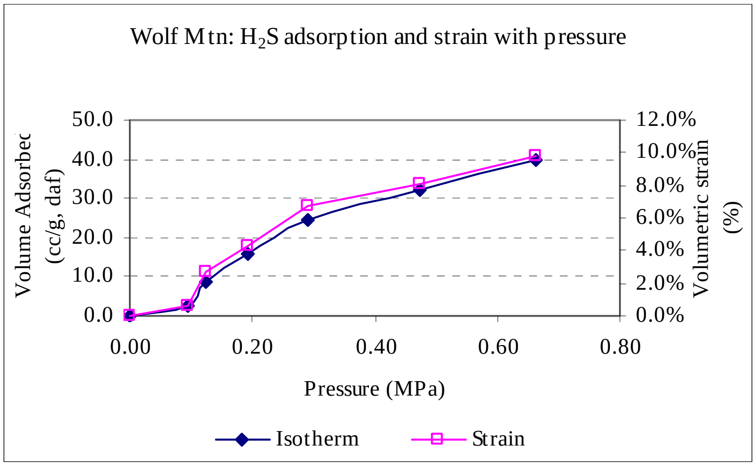

Figure 14: Pressure, gas concentration and volumetric strain plot for H_2S adsorption run

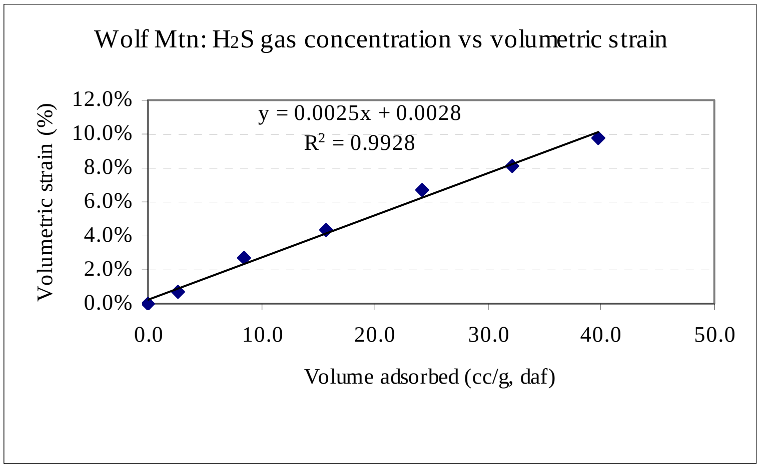

Figure 14a: Gas concentration and volumetric strain relationship for H_2S adsorption run

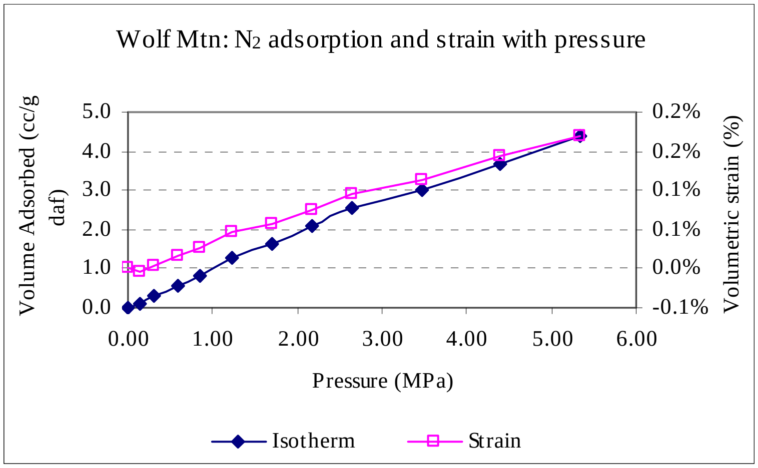

Figure 15: Pressure, gas concentration and volumetric strain plot for N_2 adsorption run

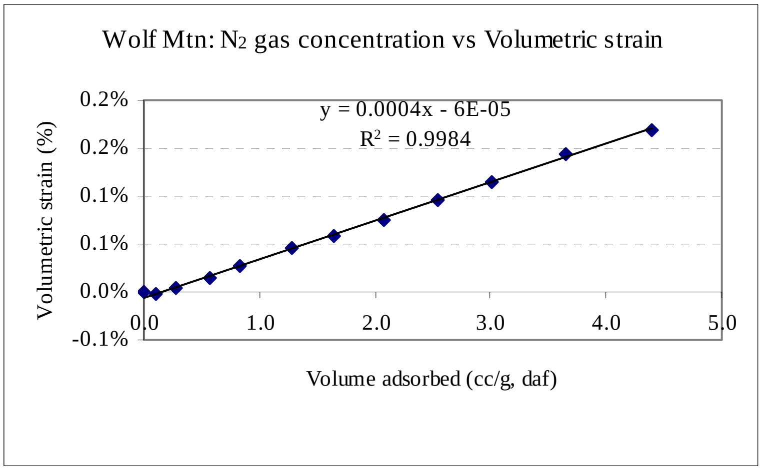

Figure 15a: Gas concentration and volumetric strain relationship for N_2 adsorption run

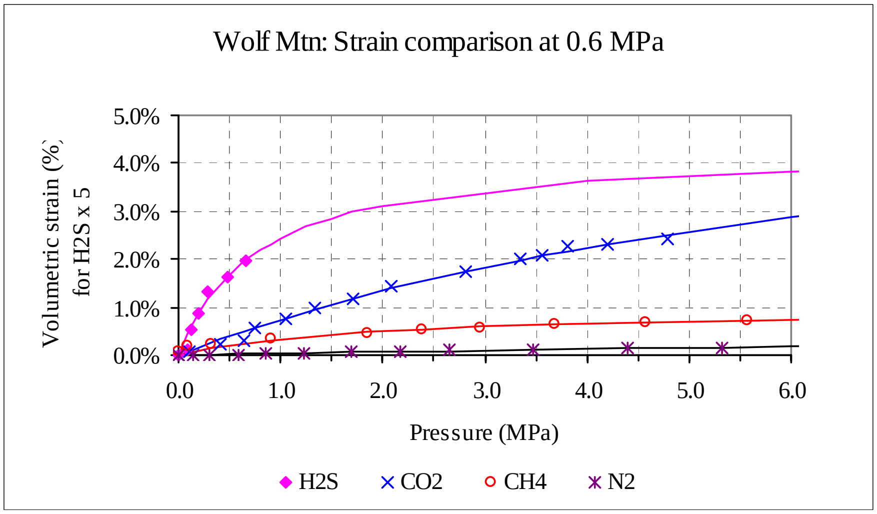

Figure 16: Wolf Mtn adsorption volumetric strain (swelling) for N_2, CH_4, CO_2 and H_2S. The points show experimental data and line shows model fit

Strain plots: Quinsam

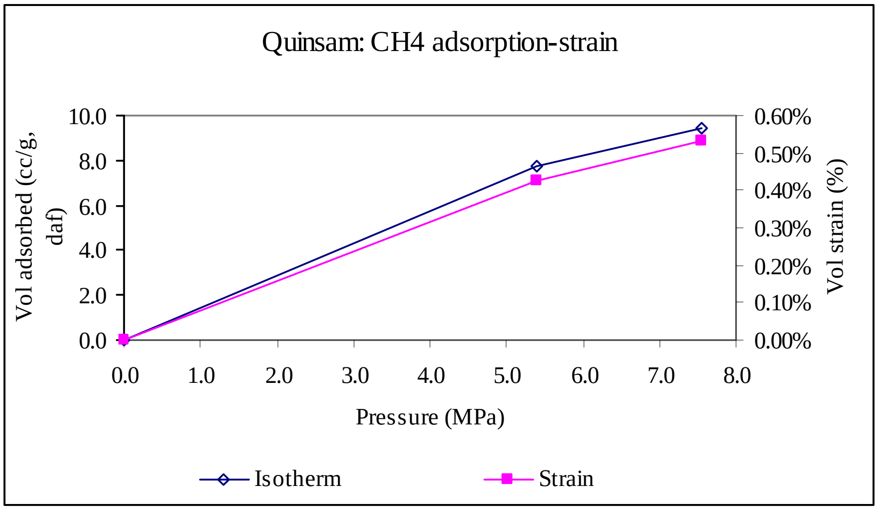

Figure 17: Pressure, gas concentration and volumetric strain plot for CH_4 adsorption run

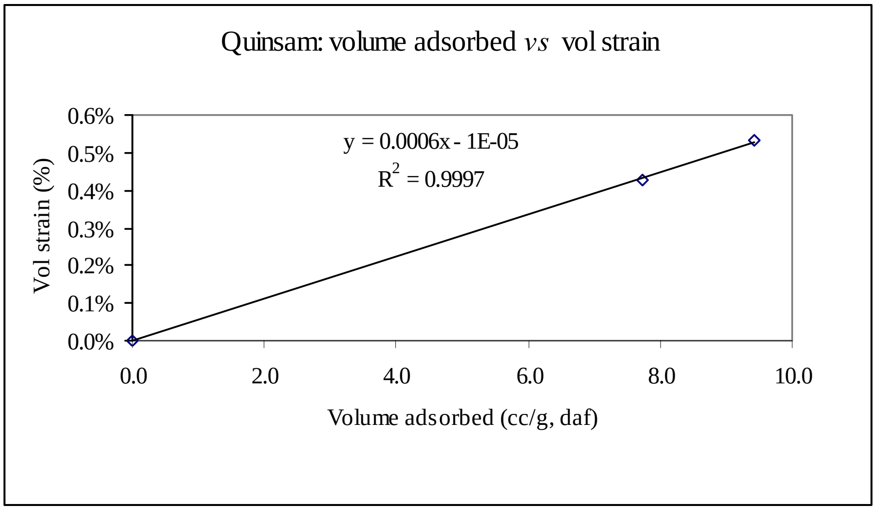

Figure 17a: Gas concentration and volumetric strain relationship for CH_4 adsorption run

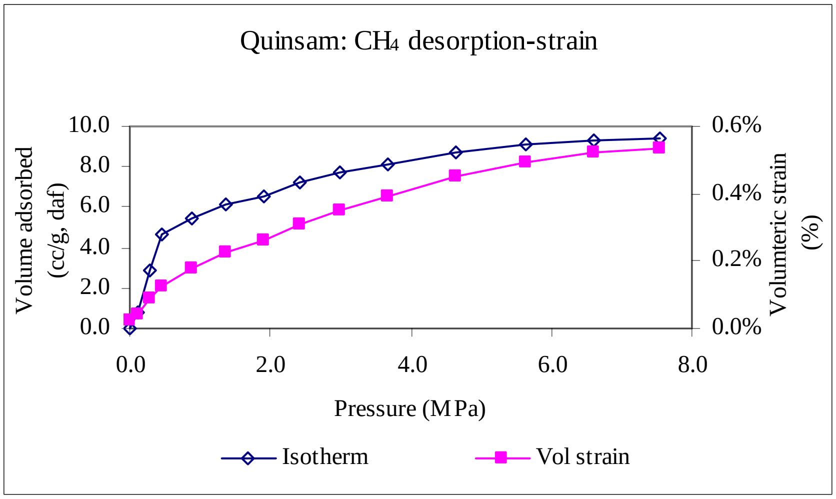

Figure 18: Pressure, gas concentration and volumetric strain plot for CH_4 desorption run

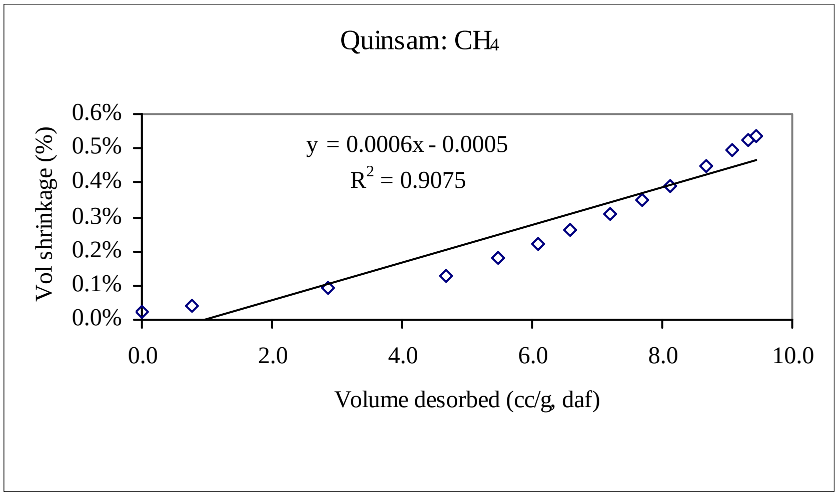

Figure 18a: Gas concentration and volumetric strain relationship for CH_4 desorption run

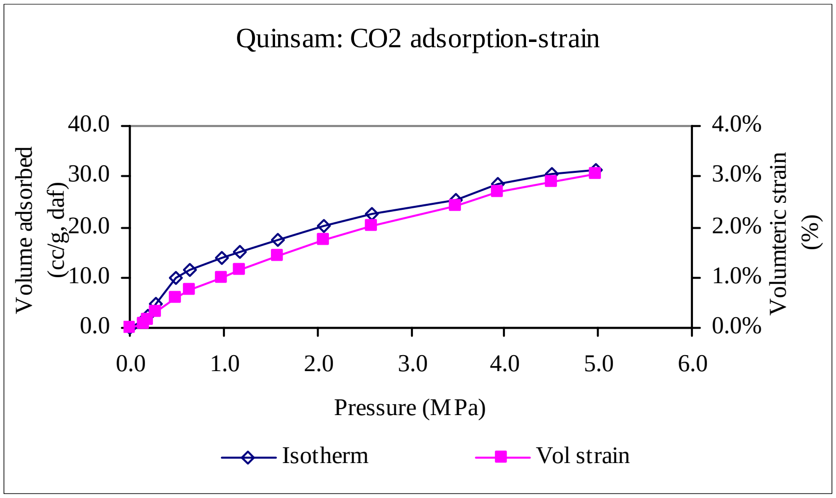

Figure 19: Pressure, gas concentration and volumetric strain plot for CO_2 adsorption run

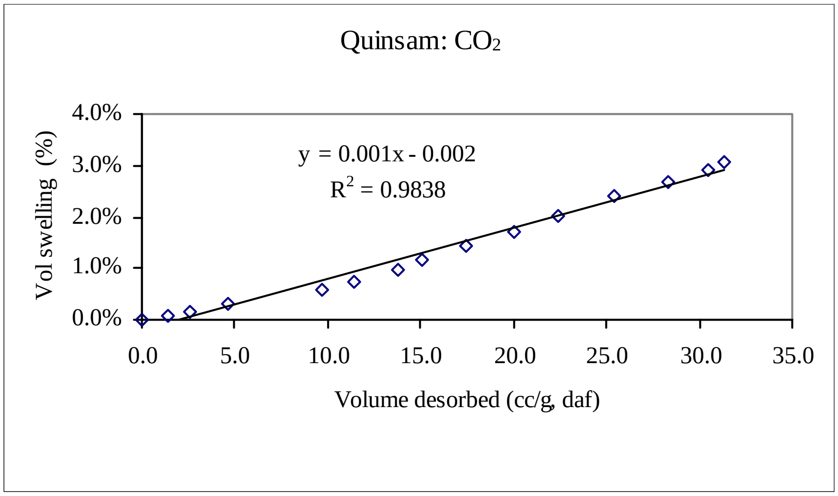

Figure 19a: Gas concentration and volumetric strain relationship for CO_2 adsorption run

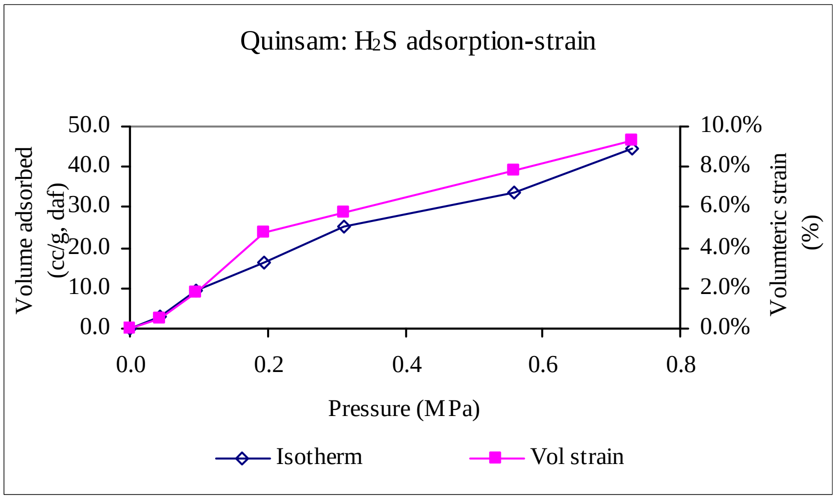

Figure 20: Gas concentration and volumetric strain relationship for H_2S adsorption run

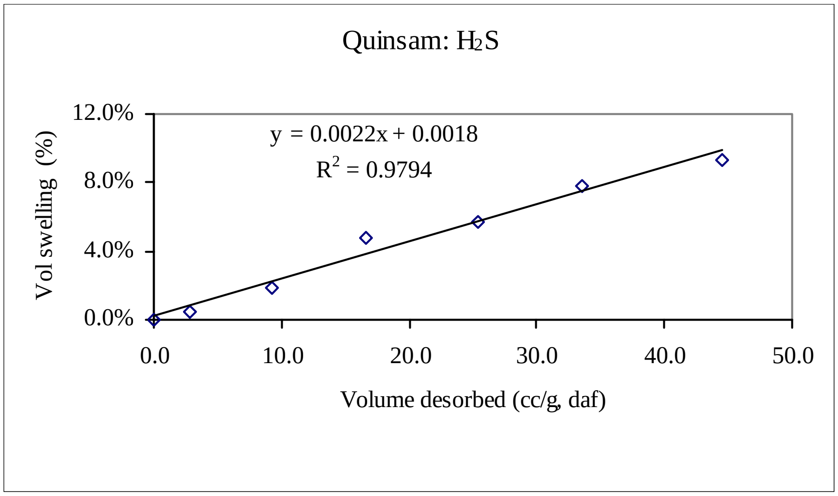

Figure 20a: Gas concentration and volumetric strain relationship for H_2S adsorption run

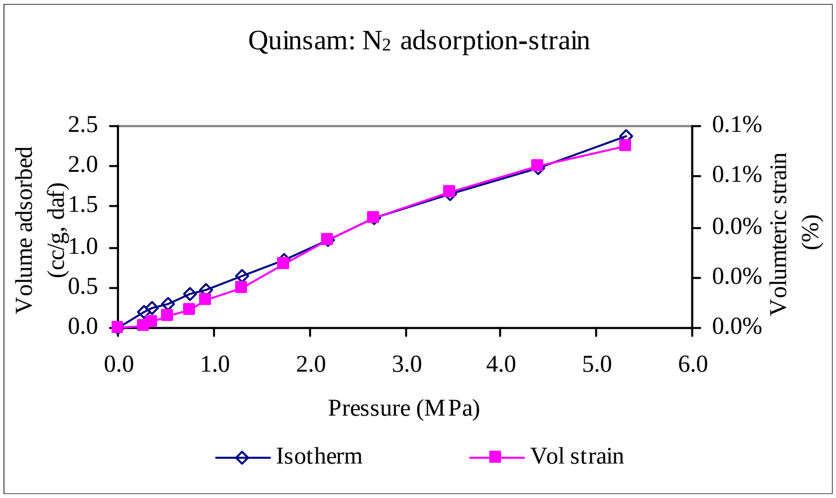

Figure 21: Gas concentration and volumetric strain relationship for N_2 adsorption run

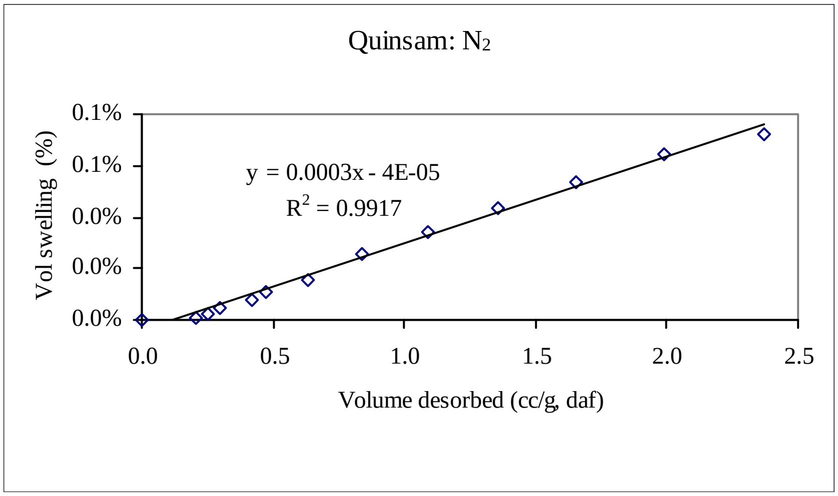

Figure 21a: Gas concentration and volumetric strain relationship for N_2 adsorption run

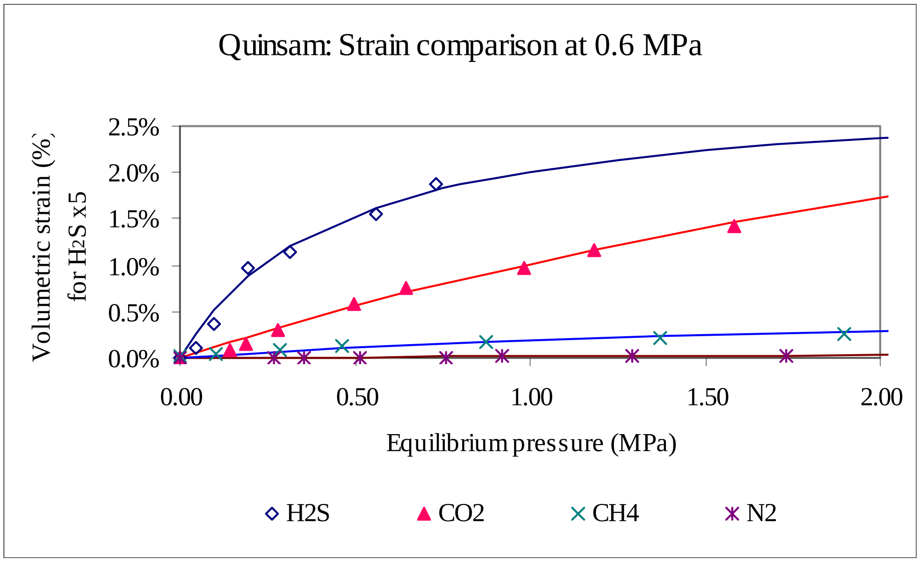

Figure 22: Quinsam adsorption volumetric strain (swelling) for N_2, CO_2, CH_4 and H_2S. The points represent the experimental data and line represent the model fit

ANNEXURES

ANNEXURE I

Table 1: Composition of BC coals for strain experiments

Samples	Petrography analysis				Vitrinite reflectance (Rr %)	Proximate analysis	
	Vitrinite (%)	Liptinite (%)	Inertinite (%)	Mineral matter (%)		Moisture (%)	Ash (%)
Wolf Mtn	81.4	4.0	13.4	1.2	0.62	2.26	5.05
Quinsam	82.8	4.2	11.6	1.4	0.62	4.14	9.30

Table 2: Composition of BC coals for isotherm experiments

Samples	Petrography analysis				Vitrinite reflectance (Rr %)	Proximate analysis	
	Vitrinite (%)	Liptinite (%)	Inertinite (%)	Mineral matter (%)		Moisture (%)	Ash (%)
Wolf Mtn	81.4	4.0	13.4	1.2	0.62	4.56	5.05
Quinsam	82.8	4.2	11.6	1.4	0.62	6.69	9.30
Telkwa	39.8	4.0	52.8	3.4	0.80	8.88	10.12
Sable River	72.8	4.2	12.4	10.6	0.84	2.12	14.28
Mist Mtn-NE	51.9	4.6	37.9	5.6	0.95	2.27	8.47
Mist Mtn-SE	68.2	8.2	17.4	6.2	0.88	2.16	8.49
Sheriff	67.4	0.0	30.6	2.0	1.27	2.23	8.17
Bennet Dam	46.4	1.4	51.6	0.6	1.31	4.84	2.01

Table 3: Langmuir constants for H_2, N_2 and CH_4

Sample ID	V_L as recd	V_L with moist and ash free	V_L dry with ash	V_L daf	P_L	Regression coefficient (R^2)	Type of Gas
Wolf Mtn.	1.57	1.65	1.64	1.73	1.35	0.9985	H2
Quinsam	1.20	1.32	1.29	1.43	1.22	0.9917	H2
Telkwa	1.32	1.47	1.45	1.63	3.02	0.9931	H2
Sable River	2.42	2.82	2.47	2.90	6.58	0.9732	H2
Mist Mtn-NE	3.20	3.44	3.22	3.60	4.77	0.9950	H2
Mist Mtn-SE	2.50	2.74	2.56	2.80	3.71	0.9863	H2
Sheriff	5.04	5.49	5.16	5.85	10.71	0.9298	H2
Bennet Dam	4.27	4.36	4.49	4.58	13.04	0.9914	H2
Wolf Mtn.	10.34	10.88	10.83	11.43	9.06	0.9956	N2
Quinsam	6.42	7.08	6.89	7.65	9.76	0.9876	N2
Telkwa	3.90	4.34	4.28	4.82	8.09	0.9900	N2
Sable River	6.90	8.05	7.05	8.25	7.18	0.9926	N2
Mist Mtn-NE	11.58	12.65	11.85	13.44	4.87	0.9961	N2
Mist Mtn-SE	9.05	9.90	9.25	10.13	8.44	0.9958	N2
Sheriff	10.65	11.59	10.89	11.88	5.66	0.9819	N2
Bennet dam	6.61	6.74	6.94	7.44	7.66	0.9925	N2
Wolf Mtn.	13.42	14.14	14.06	15.30	2.38	0.9956	CH4
Quinsam	4.56	5.03	4.89	5.34	2.04	0.9926	CH4
Telkwa	7.57	8.42	8.30	9.68	4.14	0.9930	CH4
Sable River	11.31	13.19	11.56	13.54	2.81	0.9736	CH4
Mist Mtn-NE	10.04	10.97	10.27	11.88	1.62	0.9975	CH4
Mist Mtn-SE	13.18	14.40	13.47	14.75	1.70	0.9982	CH4
Sheriff	13.73	14.96	14.05	15.33	2.19	0.9961	CH4
Bennet dam	11.82	12.06	12.42	12.97	2.90	0.9929	CH4

Table 3a: Langmuir constants for CO_2, H_2S and SO_2

Sample ID	V_L as recd	V_L with moist and ash free	V_L dry with ash	V_L daf	P_L	Regression coefficient (R^2)	Type of Gas
Wolf Mtn.	27.78	29.26	29.11	30.73	1.82	0.9955	CO2
Quinsam	26.69	29.43	28.61	31.78	0.63	0.9961	CO2
Telkwa	29.32	32.62	32.18	36.20	2.10	0.9871	CO2
Sable River	23.14	26.99	23.64	27.68	1.48	0.9937	CO2
Mist Mtn-NE	25.48	27.84	26.07	28.55	0.55	0.9971	CO2
Mist Mtn-SE	24.62	26.90	25.16	27.55	0.98	0.9989	CO2
Sheriff	25.85	28.15	26.44	28.86	0.91	0.9956	CO2
Bennet dam	32.28	32.94	33.92	34.65	1.67	0.9944	CO2
Wolf Mtn.	49.55	52.19	51.92	54.82	0.26	0.9920	H2S
Quinsam	62.17	68.54	66.62	74.00	0.39	0.9773	H2S
Telkwa	45.99	51.17	50.47	56.78	0.10	0.9976	H2S
Sable River	35.37	41.27	36.14	42.31	0.28	0.9842	H2S
Mist Mtn-NE	40.32	44.05	41.25	45.17	0.24	0.9990	H2S
Mist Mtn-SE	43.36	47.39	44.32	48.53	0.39	0.9370	H2S
Sheriff	44.98	48.98	46.01	50.20	0.29	0.9980	H2S
Bennet Dam	61.39	62.66	64.52	65.91	0.24	0.7271	H2S
Wolf Mtn.	24.87	26.19	26.06	27.51	0.08	0.9718	SO2
Quinsam	25.85	28.50	27.71	30.77	0.04	0.9991	SO2
Telkwa	52.12	57.99	57.20	64.35	0.02	0.9973	SO2
Sable River	20.64	24.08	21.09	24.69	0.06	0.9866	SO2
Mist Mtn-NE	20.09	21.95	20.55	22.50	0.03	0.9935	SO2
Mist Mtn-SE	22.17	24.23	22.66	24.81	0.03	0.9989	SO2
Sheriff	26.20	28.53	26.80	29.24	0.12	0.9509	SO2
Bennet Dam	22.36	22.82	23.50	24.01	0.07	0.9895	SO2

Table 4: Adsorption ratios for BC coals with different gases

	Adsorption at 0.6 MPa (daf basis)	Adsorption ratios of gas/methane at 0.6 MPa (daf basis)

Sample ID	CH_4	N_2	CO_2	H_2	H_2S	SO_2	N_2	CO_2	H_2	H_2S	SO_2
Wolf Mtn	3.10	0.71	7.63	0.53	38.32	24.38	0.23	2.47	0.17	12.38	7.88
Quinsam	1.19	0.44	15.45	0.47	45.01	28.98	0.37	12.95	0.40	37.73	24.30
Telkwa	1.23	0.33	8.04	0.27	48.74	61.97	0.27	6.53	0.22	39.61	50.36
Sable River	2.67	0.64	7.98	0.24	28.96	22.55	0.24	2.99	0.09	10.86	8.45
Mist Mtn-NE	5.40	1.47	14.90	0.40	32.31	21.35	0.27	2.76	0.07	5.98	3.95
Mist Mtn-SE	3.85	0.67	10.46	0.39	29.45	23.72	0.17	2.72	0.10	7.65	6.16
Sheriff	3.30	1.14	11.47	0.31	33.91	24.23	0.34	3.48	0.09	10.27	7.34
Bennet Dam	2.23	0.54	9.15	0.20	46.98	21.38	0.24	4.10	0.09	21.07	9.59

Table 4a: Strain model parameters and strains at 0.6 MPa for BC coals with different gases

Sample Id	Gas type	ε_L	p_ε	Vol strain at 0.6 MPa
Wolf Mtn	H2S	18.05%	0.56	9.327%
Quinsam	H2S	14.42%	0.43	8.378%
Wolf Mtn	CO2	6.74%	8.04	0.468%
Quinsam	CO2	5.90%	4.80	0.656%
Wolf Mtn	CH4	0.87%	1.16	0.297%
Quinsam	CH4	0.74%	3.01	0.123%
Wolf Mtn	N2	0.42%	9.02	0.026%
Quinsam	N2	0.21%	10.28	0.012%

Table 4b: Strain ratios at 0.6 MPa for BC coals

Samples	Ratios of volumetric strains at 0.6 MPa
H2S/CH4	
Wolf Mtn	31.41
Quinsam	68.00
	CO2/CH4
Wolf Mtn	1.58
Quinsam	5.33
	N2/CH4
Wolf Mtn	0.09
Quinsam	0.10
	H2S/CO2
Wolf Mtn	19.9
Quinsam	12.8

ANNEXURE – II

BC coals adsorption isotherm data for individual gases on daf basis

(Ash and Moisture as given in Table2)

Sample: Wolf Mtn

Table 5a: Experimental adsorption isotherm values for H_2, N_2 and CH_4

H_2		N_2		CH_4	
Pressure (MPa)	Volume adsorbed cc/g, daf	Pressure (MPa)	Volume adsorbed cc/g, daf	Pressure (MPa)	Volume adsorbed cc/g, daf
0.00	0.00	0.00	0.00	0.00	0.00
0.26	0.28	0.20	0.25	0.09	0.39
0.49	0.48	0.33	0.41	0.26	1.45
0.74	0.63	0.51	0.61	0.40	2.18
0.99	0.70	0.69	0.81	0.57	2.96
1.36	0.86	0.81	0.95	0.77	3.65
1.84	1.00	1.23	1.37	1.13	4.72
2.30	1.08	1.68	1.79	1.58	5.82
2.74	1.16	2.17	2.20	2.07	6.84
3.54	1.27	2.66	2.56	2.57	7.72
4.46	1.33	3.45	3.11	3.37	8.93
		4.37	3.71	4.33	9.81
		5.32	4.28	5.31	10.77

Table 5b: Experimental adsorption isotherm values for CO_2, H_2S and SO_2

CO_2		H_2S		SO_2	
Pressure (MPa)	Volume adsorbed cc/g, daf	Pressure (MPa)	Volume adsorbed cc/g, daf	Pressure (MPa)	Volume adsorbed cc/g, daf
0.00	0.00	0.00	0.00	0.00	0.00
0.14	0.67	0.10	0.38	0.05	1.23
0.19	1.64	0.11	2.16	0.06	3.03
0.29	3.09	0.13	5.13	0.07	5.14
0.41	4.56	0.15	9.19	0.08	7.99
0.56	6.26	0.19	14.18	0.12	12.23
0.84	8.76	0.25	19.90	0.15	16.22
1.24	11.59	0.34	26.24	0.21	18.52
1.74	14.33			0.26	20.18
2.29	16.65			0.30	21.13
3.11	19.60			0.32	21.77

Sample: Quinsam

Table 6a: Experimental adsorption isotherm values for H_2, N_2 and CH_4

H_2	N_2	CH_4

Pressure (MPa)	Volume adsorbed cc/g, daf	Pressure (MPa)	Volume adsorbed cc/g, daf	Pressure (MPa)	Volume adsorbed cc/g, daf
0.00	0.00	0.00	0.00	0.00	0.00
0.30	0.29	0.17	0.13	0.12	0.31
0.51	0.47	0.40	0.31	0.25	0.63
0.76	0.58	0.64	0.48	0.53	1.00
1.03	0.64	0.86	0.63	0.77	1.40
1.42	0.72	1.26	0.88	1.18	1.86
1.82	0.81	1.71	1.14	1.63	2.32
2.31	0.91	2.06	1.29	2.12	2.79
2.81	1.02	2.64	1.59	2.62	3.08
3.60	1.09	3.48	2.00	3.42	3.40
4.55	1.13	4.40	2.41	4.34	3.64
		5.38	2.74	5.32	3.81

Table 6b: Experimental adsorption isotherm values for CO_2, H_2S and SO_2

CO_2		H_2S		SO_2	
Pressure (MPa)	Volume adsorbed cc/g, daf	Pressure (MPa)	Volume adsorbed cc/g, daf	Pressure (MPa)	Volume adsorbed cc/g, daf
0.00	0.00	0.00	0.00	0.00	0.00
0.09	0.97	0.08	0.81	0.06	1.18
0.13	2.82	0.08	2.60	0.06	3.01
0.20	5.53	0.09	4.48	0.07	5.48
0.19	5.56	0.12	9.50	0.08	8.95
0.20	5.60	0.18	15.40	0.10	15.17
0.50	12.09	0.27	21.81	0.14	21.68
1.05	17.86	0.41	30.63	0.24	25.25
1.72	22.08	0.56	38.70	0.31	26.71
2.35	24.80	0.72	43.74	0.33	27.31
3.32	27.21	0.85	48.18	0.37	27.49
		0.97	52.22		
		1.11	55.44		
		1.30	57.40		
		1.45	59.17		

Sample: Telkwa

Table 7a: Experimental adsorption isotherm values for H_2, N_2 and CH_4

H_2		N_2		CH_4	

Pressure (MPa)	Volume adsorbed cc/g, daf	Pressure (MPa)	Volume adsorbed cc/g, daf	Pressure (MPa)	Volume adsorbed cc/g, daf
0.00	0.00	0.00	0.00	0.00	0.00
0.27	0.13	0.16	0.09	0.27	0.55
0.48	0.24	0.32	0.19	0.45	0.97
0.72	0.33	0.51	0.29	0.59	1.24
1.03	0.42	0.70	0.39	0.69	1.43
1.39	0.50	0.90	0.48	0.86	1.70
1.86	0.62	1.29	0.65	1.22	2.22
2.27	0.69	1.75	0.84	1.67	2.74
2.79	0.78	2.23	1.02	2.14	3.25
3.62	0.88	2.72	1.19	2.63	3.70
4.53	0.99	3.54	1.45	3.43	4.34
5.468	1.057	4.46	1.72	4.35	4.91
		5.43	1.97	5.31	5.54

Table 7b: Experimental adsorption isotherm values for CO_2, H_2S and SO_2

CO_2		H_2S		SO_2	
Pressure (MPa)	Volume adsorbed cc/g, daf	Pressure (MPa)	Volume adsorbed cc/g, daf	Pressure (MPa)	Volume adsorbed cc/g, daf
0.00	0.00	0.00	0.00	0.00	0.00
0.08	1.31	0.05	1.61	0.01	3.66
0.21	3.58	0.05	6.25	0.01	8.53
0.39	5.84	0.07	13.75	0.02	15.14
0.59	7.80	0.12	23.19	0.03	24.63
0.79	9.52	0.19	33.82	0.06	38.66
1.17	12.18	0.38	42.87	0.12	52.52
1.61	15.19	0.70	49.81	0.23	57.73
2.10	17.90			0.31	60.18
2.60	20.51			0.33	60.30
3.61	23.20			0.37	60.70

Sample: Sable River

Table 8a: Experimental adsorption isotherm values for H_2, N_2 and CH_4

H_2		N_2		CH_4	
Pressure (MPa)	Volume adsorbed cc/g, daf	Pressure (MPa)	Volume adsorbed cc/g, daf	Pressure (MPa)	Volume adsorbed cc/g, daf

0.00	0.00	0.00	0.00	0.00	0.00
0.29	0.12	0.14	0.17	0.11	0.41
0.52	0.23	0.28	0.30	0.25	1.14
0.74	0.30	0.48	0.50	0.40	1.85
0.95	0.36	0.67	0.72	0.59	2.52
1.40	0.50	0.87	0.91	0.79	3.14
1.85	0.64	1.25	1.24	1.16	4.06
2.36	0.79	1.75	1.63	1.61	4.97
2.83	0.87	2.70	2.25	2.11	5.82
3.66	1.02	2.83	2.34	2.61	6.52
4.57	1.19	3.48	2.69	3.42	7.47
		4.40	3.15	4.39	8.08
		5.43	3.52		

Table 8b: Experimental adsorption isotherm values for CO_2, H_2S and SO_2

CO_2		H_2S		SO_2	
Pressure (MPa)	Volume adsorbed cc/g, daf	Pressure (MPa)	Volume adsorbed cc/g, daf	Pressure (MPa)	Volume adsorbed cc/g, daf
0.00	0.00	0.00	0.00	0.00	0.00
0.08	0.80	0.11	0.43	0.06	1.21
0.17	2.00	0.11	2.28	0.07	3.11
0.28	3.96	0.14	5.29	0.08	5.44
0.31	4.54	0.19	9.13	0.10	8.42
0.53	7.13	0.26	13.66	0.15	13.48
0.91	10.22	0.37	18.50	0.21	18.03
1.42	13.16	0.54	23.24	0.29	19.71
1.96	15.44	0.72	27.14	0.33	20.48
2.50	17.34	0.88	30.18	0.35	20.88
3.33	19.15	1.03	32.59	0.37	21.05
		1.17	34.44		
		1.32	35.28		
		1.42	35.43		

Sample: Mist Mtn-NE

Table 9a: Experimental adsorption isotherm values for H_2, N_2 and CH_4

H_2		N_2		CH_4	
Pressure (MPa)	Volume adsorbed cc/g, daf	Pressure (MPa)	Volume adsorbed cc/g, daf	Pressure (MPa)	Volume adsorbed cc/g, daf
0.00	0.00	0.00	0.00	0.00	0.00
0.26	0.19	0.15	0.40	0.13	0.72

0.44	0.30	0.37	0.97	0.25	1.36
0.79	0.53	0.50	1.27	0.47	2.44
0.99	0.62	0.67	1.64	0.70	3.34
1.35	0.78	0.85	2.02	1.06	4.62
1.84	0.99	1.21	2.67	1.53	5.59
2.34	1.19	1.65	3.36	2.04	6.38
2.83	1.34	2.13	4.01	2.54	7.14
3.63	1.56	2.61	4.60	3.32	8.08
3.85	1.60	3.41	5.48	4.26	8.73
		4.33	6.32	5.27	9.03
		5.30	7.13		

Table 9b: Experimental adsorption isotherm values for CO_2, H_2S and SO_2

CO_2		H_2S		SO_2	
Pressure (MPa)	Volume adsorbed cc/g, daf	Pressure (MPa)	Volume adsorbed cc/g, daf	Pressure (MPa)	Volume adsorbed cc/g, daf
0.00	0.00	0.00	0.00	0.00	0.00
0.09	0.78	0.08	2.00	0.06	1.25
0.13	2.57	0.10	4.09	0.06	3.11
0.20	5.19	0.12	7.50	0.06	5.40
0.20	5.22	0.15	12.16	0.07	8.42
0.20	5.26	0.22	17.33	0.11	11.58
0.50	11.48	0.33	22.82	0.14	15.38
1.05	16.92	0.51	28.13	0.17	17.20
1.72	20.75	0.73	31.92	0.22	18.89
2.35	23.09	0.92	34.60	0.28	19.74
3.32	24.83	1.09	36.64	0.31	20.21
		1.22	38.18		
		1.39	38.30		
		1.45	38.60		

Sample: Mist Mtn-SE

Table 10a: Experimental adsorption isotherm values for H_2, N_2 and CH_4

H_2		N_2		CH_4	
Pressure (MPa)	Volume adsorbed cc/g, daf	Pressure (MPa)	Volume adsorbed cc/g, daf	Pressure (MPa)	Volume adsorbed cc/g, daf
0.00	0.00	0.00	0.00	0.00	0.00
0.27	0.19	0.20	0.19	0.12	0.44
0.49	0.35	0.33	0.34	0.28	1.72

0.74	0.48	0.51	0.53	0.48	2.85
0.94	0.58	0.69	0.72	0.73	4.10
1.40	0.74	0.82	0.85	1.06	5.53
1.86	0.89	1.23	1.25	1.55	6.67
2.30	1.04	1.69	1.64	2.04	7.73
2.80	1.21	2.17	2.03	2.56	8.55
3.57	1.41	2.66	2.36	3.37	9.63
4.54	1.55	3.46	2.88	4.30	10.66
		4.38	3.44	5.33	11.25
		5.34	3.97		

Table 10b: Experimental adsorption isotherm values for CO_2, H_2S and SO_2

CO_2		H_2S		SO_2	
Pressure (MPa)	Volume adsorbed cc/g, daf	Pressure (MPa)	Volume adsorbed cc/g, daf	Pressure (MPa)	Volume adsorbed cc/g, daf
0.00	0.00	0.00	0.00	0.00	0.00
0.05	0.73	0.12	0.05	0.08	0.54
0.10	2.26	0.13	1.47	0.08	1.40
0.21	4.36	0.16	3.95	0.08	2.58
0.34	7.00	0.18	7.41	0.08	4.10
0.53	9.56	0.23	11.60	0.09	6.00
0.88	12.74	0.31	16.29	0.09	8.80
1.37	15.68	0.44	21.24	0.10	12.68
1.92	18.10			0.13	16.57
2.49	19.92			0.17	20.23
3.50	21.48			0.24	21.55
				0.311	22.145
				0.352	22.415

Sample: Sheriff

Table 11a: Experimental adsorption isotherm values for H_2, N_2 and CH_4

H_2		N_2		CH_4	
Pressure (MPa)	Volume adsorbed cc/g, daf	Pressure (MPa)	Volume adsorbed cc/g, daf	Pressure (MPa)	Volume adsorbed cc/g, daf
0.00	0.00	0.00	0.00	0.00	0.00
0.29	0.16	0.15	0.28	0.18	0.87
0.48	0.27	0.26	0.57	0.34	1.98
0.75	0.39	0.44	0.85	0.52	2.88
1.01	0.49	0.64	1.13	0.73	3.75

1.40	0.64	0.84	1.50	1.10	4.94
1.88	0.84	1.36	2.28	1.56	6.12
2.34	1.02	1.78	2.84	2.06	7.10
2.83	1.21	2.27	3.37	2.56	8.01
3.62	1.48	2.67	3.81	3.38	9.19
4.52	1.78	3.49	4.48	4.30	10.26
5.456	2.000	4.44	5.22	5.31	10.95
		5.32	5.80		

Table 11b: Experimental adsorption isotherm values for CO_2, H_2S and SO_2

CO_2		H_2S		SO_2	
Pressure (MPa)	Volume adsorbed cc/g, daf	Pressure (MPa)	Volume adsorbed cc/g, daf	Pressure (MPa)	Volume adsorbed cc/g, daf
0.00	0.00	0.00	0.00	0.00	0.00
0.09	0.59	0.03	1.94	0.06	0.25
0.13	2.15	0.05	4.30	0.07	1.55
0.21	4.33	0.07	7.95	0.09	3.17
0.34	6.81	0.11	12.59	0.11	5.61
0.52	9.27	0.18	17.89	0.13	9.55
0.84	12.50	0.29	23.62	0.16	13.31
1.30	15.79	0.47	29.03	0.19	15.10
1.83	18.68	0.67	33.87	0.22	16.20
2.49	21.15	0.84	37.35	0.25	17.03
3.53	23.21	1.06	39.20	0.28	17.76
		1.23	41.00		
		1.32	41.29		

Sample: Bennet Dam

Table 12a: Experimental adsorption isotherm values for H_2, N_2 and CH_4

H_2		N_2		CH_4	
Pressure (MPa)	Volume adsorbed cc/g, daf	Pressure (MPa)	Volume adsorbed cc/g, daf	Pressure (MPa)	Volume adsorbed cc/g, daf
0.00	0.00	0.00	0.00	0.00	0.00
0.21	0.10	0.16	0.13	0.10	0.45
0.41	0.18	0.31	0.26	0.25	0.92
0.69	0.30	0.49	0.42	0.40	1.55
0.89	0.37	0.68	0.59	0.60	2.23
1.31	0.51	0.87	0.74	0.83	3.06
1.77	0.67	1.24	1.02	1.20	3.84

2.25	0.85	1.70	1.30	1.64	4.59
2.76	1.03	2.19	1.61	2.09	5.43
3.64	1.33	2.68	1.88	2.59	6.04
4.62	1.58	3.49	2.28	3.47	6.98
5.536	1.779	4.40	2.72	4.35	7.71
		5.38	3.12	5.30	8.50

Table 12b: Experimental adsorption isotherm values for CO_2, H_2S and SO_2

CO_2		H_2S		SO_2	
Pressure (MPa)	Volume adsorbed cc/g, daf	Pressure (MPa)	Volume adsorbed cc/g, daf	Pressure (MPa)	Volume adsorbed cc/g, daf
0.00	0.00	0.00	0.00	0.00	0.00
0.04	0.86	0.06	0.32	0.03	0.40
0.13	2.26	0.07	2.05	0.04	1.55
0.23	4.41	0.08	4.98	0.04	3.15
0.30	5.65	0.10	8.94	0.06	5.47
0.56	8.92	0.12	13.85	0.09	9.43
0.90	12.07	0.16	19.57	0.13	14.42
1.35	15.27	0.23	26.02	0.19	16.55
1.88	18.27			0.25	17.91
2.38	20.58			0.30	18.85
3.25	22.82			0.32	19.24

ANNEXURE – III

Wolf Mtn strain data for N2, CH4, CO2 and H2S gases

(Ash 5.05%; Moisture 2.26%)

Table 13: Wolf Mtn coal Strain data for CH_4 adsorption and desorption run

Wolf Mtn: CH4-Adsorption			Wolf Mtn: CH4-Desorption		
Pressure (MPa)	Volume adsorbed, cc/g, daf)	Volumetric strain (%)	Pressure (MPa)	Volume desorbed (cc/g, daf)	Volumetric shrinkage Strain (%)
0.00	0.00	0.000%	7.42	12.98	0.772%
5.08	10.56	0.611%	6.54	12.00	0.764%
7.42	12.98	0.772%	5.57	11.67	0.736%
			4.58	11.12	0.689%
			3.69	10.39	0.626%
			2.95	9.66	0.574%

2.39	8.94	0.518%
1.86	8.28	0.473%
0.91	6.39	0.350%
0.32	3.60	0.237%
0.10	0.65	0.186%
0.00	0.00	0.070%

Table 13a: Wolf Mtn Strain data for CO_2 and H_2S adsorption run

Wolf Mtn: CO_2-Adsorption			Wolf Mtn: H_2S-Adsorption		
Pressure (MPa)	Volume adsorbed, cc/g, daf)	Volumetric strain (%)	Pressure (MPa)	Volume adsorbed, cc/g, daf)	Volumetric strain (%)
0.00	0.00	0.000%	0.00	0.00	0.000%
0.10	1.63	0.089%	0.09	2.64	0.658%
0.41	5.61	0.240%	0.12	8.42	2.713%
0.65	8.08	0.313%	0.19	15.73	4.323%
0.75	8.98	0.580%	0.29	24.27	6.698%
1.05	11.22	0.745%	0.47	32.14	8.116%
1.34	13.05	0.979%	0.66	39.76	9.759%
1.71	14.90	1.158%			
2.09	16.41	1.430%			
2.82	18.40	1.727%			
3.35	18.86	2.017%			
3.56	19.76	2.100%			
3.81	20.80	2.260%			
4.20	21.43	2.300%			
4.78	22.00	2.420%			

Table 13b: Wolf Mtn Strain data for N_2 adsorption run

Wolf Mtn: CH4-Adsorption		
Pressure (MPa)	Volume adsorbed, cc/g, daf)	Volumetric strain (%)
0.00	0.00	0.000%
0.15	0.11	-0.003%
0.30	0.28	0.005%
0.59	0.57	0.015%
0.85	0.82	0.027%
1.22	1.28	0.046%
1.70	1.65	0.058%
2.17	2.08	0.076%
2.65	2.54	0.096%
3.48	3.02	0.114%

4.39	3.65	0.144%
5.33	4.39	0.154%

Quinsam strain data for CH4, N2 and H2S gases

(Ash 9.30%; Moisture 4.14%)

Table 14: Quinsam coal Strain data for CH_4 adsorption and desorption run

Quinsam: CH4-Adsorption		
Pressure (MPa)	Volume adsorbed, cc/g, daf)	Volumetric strain (%)
0.00	0.00	0.000%
5.40	7.73	0.428%
7.55	9.43	0.534%

Quinsam: CH4-Desorption		
Pressure (MPa)	Volume desorbed (cc/g, daf)	Volumetric shrinkage Strain (%)
7.55	9.43	0.534%
6.62	9.31	0.522%
5.64	9.07	0.495%
4.65	8.69	0.450%
3.66	8.13	0.392%
2.98	7.69	0.349%
2.41	7.19	0.308%
1.89	6.57	0.262%
1.37	6.10	0.224%
0.87	5.49	0.179%
0.46	4.67	0.127%
0.28	2.87	0.091%
0.10	0.78	0.043%
0.00	0.00	0.021%

Table 14a: Quinsam Strain data for CO_2 and H_2S adsorption run

Quinsam: CO_2-Adsorption		
Pressure (MPa)	Volume adsorbed, cc/g, daf)	Volumetric strain (%)
0.00	0.00	0.000%
0.14	1.40	0.078%
0.19	2.54	0.154%
0.28	4.59	0.307%
0.50	9.74	0.580%
0.65	11.46	0.745%
0.98	13.81	0.979%
1.18	15.08	1.158%
1.58	17.48	1.430%

Quinsam: H_2S-Adsorption		
Pressure (MPa)	Volume adsorbed, cc/g, daf)	Volumetric strain (%)
0.00	0.00	0.000%
0.04	2.78	0.512%
0.10	9.19	1.816%
0.19	16.55	4.800%
0.31	25.39	5.730%
0.56	33.59	7.800%
0.73	44.46	9.352%

2.06	20.03	1.727%
2.58	22.44	2.017%
3.48	25.39	2.411%
3.92	28.34	2.681%
4.51	30.47	2.905%
4.98	31.31	3.061%

Table 14b: Quinsam: N_2-Adsorption strain data

Pressure (MPa)	Volume adsorbed, cc/g, daf)	Volumetric strain (%)
0.00	0.00	0.000%
0.27	0.21	0.001%
0.35	0.25	0.003%
0.51	0.30	0.005%
0.76	0.42	0.007%
0.92	0.47	0.011%
1.29	0.63	0.016%
1.73	0.84	0.025%
2.19	1.09	0.034%
2.67	1.35	0.044%
3.47	1.66	0.054%
4.40	1.99	0.064%
5.32	2.37	0.072%

TECHNICAL REPORT

Part 1I

IMPACTS OF ADSORPTION-INDUCED COAL SWELLING ON PERMEABILITY AND ACID GAS SEQUESTRATION INTO COAL SEAMS: INSIGHTS FROM EXPERIMENTAL AND NUMERICAL STUDIES

Dr R. M. Bustin
Department of Earth and Ocean Sciences
The University of British Columbia
Vancouver, B.C.
V6T 1Z4
ph 604 822 6179 fax 604 822 6088
bustin@interchange.ubc.ca

1. Introduction

Because of the large adsorption capacity and adsorption strength of coals, a large amount of CO_2 and H_2S can be adsorbed into coals in a near liquid (adsorbate) state. The adsorption of CO_2 and H_2S may further displace CH_4 out of coals as a clean resource. Therefore, sequestration of CO_2 and H_2S into deep, unminable coal seams becomes an attractive option. Injection of CO_2 into geological formations is already being practiced by the petroleum industry for enhanced oil recovery.

The practical sequestration of CO_2 and H_2S into unminable coal seams requires that the coal seams have well interconnected pathways for the injected gases to permeate into coal seams efficiently. Besides the primary, mainly-micro pores, coal seams commonly have secondary fractures/cleats formed during coalification or in response to afterward tectonic events. The cleat networks are the major conduits for gas and water flow in coal seams, whereas gas is adsorbed into microporous coal particles by diffusion. The cleat permeability contributed by the cleat network may vary strongly due to the hydro-mechanic responses of coal seams during gas injection. For example, injection of gas into coal seams likely elevates the cleat pressure significantly, widens the cleat apertures, and enhances the permeability. In contrast, the adsorption of acid gas likely causes strong swelling of coals, consequently narrowing the cleat aperture and reducing the permeability. Models have been formulated to account for the dynamic permeability changes during primary coalbed methane recovery or enhanced recovery by CO_2 injection (e.g., Sawyer et al., 1990; Palmer and Masoori, 1998; Pekot and Reeves, 2003; Shi and Durucan, 2003). However, how the permeability varies and the consequent impacts on CO_2 and H_2S sequestration into coal seams remain poorly understood because of lack of experimental data. Moreover, previous studies were limited mainly to CH_4 recovery. The possible permeability variation induced by CO_2 or H_2S or flue gas (e.g., CO_2+N_2 or H_2S+N_2) injection has not been studied.

In this part we use our experimental data of gas adsorption (CH_4, CO_2, H_2S, and N_2) and the associated volumetric strains measured for three western Canadian coals (namely Ardley, Wolf Mountain, and Quinsam coals), we attempt to investigate the possible permeability changes induced by acid gas sorption and their impacts on the efficiency of sequestration of CO_2 and H_2S, or their N_2-mixtures (flue gas) into those coals. We develop an effective-stress-dependent cleat permeability model by an analogy to a thermo-elastic porous medium. With the constraints of our experimental data, the possible cleat permeability change and its impact on acid gas sequestration are investigated analytically and numerically, which provides insights into the permeability variation during acid gas injection and their impact on acid gas sequestration into coals.

2. Experimental Gas Adsorption and Coal Swelling

The volumetric strain induced by adsorption CH_4, CO_2, H_2S, and N_2 were measured at 25 °C and on received basis for coal cores of three Canadian coals (the Ardley, Wolf Mountain, and Quinsam coals). The detailed experimental procedure is described elsewhere (Chikatamarla et al., 2004). Generally, the volumetric strains induced by gas adsorption are linearly proportional to the volume of adsorbed gas (Fig. 1). Therefore, the total volumetric strain ε_V caused by adsorption of a pure gas or gas mixtures can be described as

$$\varepsilon_V = \sum_{i=1}^{i=n} \varepsilon_{gi} V_{gi} \, , \qquad (1)$$

where subscript i represents a pure gas i or component i in a gas mixture, ε_{gi} is the volumetric strain coefficient of gas i, given by the slope of solid lines that fit the experimental data in Fig. 1. Thus, the coefficient ε_g measures the swelling effect of different gases with respect to a unit volume of adsorbed gas. V_{gi} is the volume of adsorbed gas i, and n is the total number of gas components, which ranges from 1 (pure gas) to 3 (multiple components) in this study. Here it was assumed that, for a gas mixture, the total volumetric strain caused by gas adsorption is simply a linear combination of the volumetric strain induced by each component as we only consider linear-elastic deformation of coal seams and the sorption-induced volumetric strain is linearly dependent on the volume of individual adsorbate.

For an individual gas, the swelling or volumetric strains induced by its sorption into the three coals are quite similar except for the adsorption of H_2S into the Ardley coal. This is likely because that H_2S reacted with the moisture inside the coal matrix forming sulphuric acid which in-turn reacted with strain gauges. The higher moisture content of Ardley sample (8.04%) relative to Wolf Mountain (2.26%) and Quinsam (4.14%) (Table 2) might have caused the early reaction with strain gauges compared to the other two samples, consequently giving the low strain values for the Ardley coal. Among all gases H_2S induces the largest volumetric strain per unit volume of adsorbed gas as indicated by an average ε_{gH_2S} of 2.1×10^{-3} g/cc (Fig. 1c), which is about three times that of CH_4 ($\varepsilon_{gCH_4} \sim 6.9 \times 10^{-4}$ g/cc; Fig. 1a); followed by is CO_2, which has an average ε_{gCO_2} of about 9.9×10^{-4} g/cc (Fig. 1b) or 1.5 times that of CH_4; and N_2 induces the smallest volumetric strain with an average volumetric strain coefficient of 3.1×10^{-4} g/cc (Fig. 1d) or half that of CH_4.

Gas is mostly adsorbed onto the internal surface of microporous coal particles. The adsorbed gas volume (V_{gi}) can be described by the Langmuir isotherm for pure gas *i* or extended Langmuir isotherm for gas component *i* of a gas mixture, taking the form:

$$V_{gi} = \frac{V_{Li}\, y_{mi}\, p_m / p_{Li}}{1 + p_m \sum_{i=1}^{n} y_{mi} / p_{Li}}, \tag{2}$$

where p_{Li} and V_{Li} are the Langmuir pressure and volume for gas *i*, which are the experimental values of pure gases; y_i is mole fraction of gas *i* in the gas mixture; p_m is the total gas pressure in microporous coal particles. The Langmuir constants for CH_4, CO_2, H_2S, and N_2 of the three Canadian coals were measured on coal cores and crushed coals at equilibrium moisture conditions and at 25 °C. Although the Langmuir constants determined with coal cores or crushed coals are similar, only those data that could reproduce well the experimental volumetric strain data at different pressures using eqs. 1 and 2 (Fig. 2) were adopted here (Table 1). As commonly observed, the general gas adsorption capacity (V_L) in increasing order is $N_2 < CH_4 < CO_2 < H_2S$, and so does approximately the adsorption affinity or adsorption strength (approximated to be $1/P_L$) for the three coals. However, the adsorption properties for a specific gas are quite different among the coals.

Because of their large adsorption capacity and high adsorption strength, under similar pressures, H_2S and CO_2 cause much larger volumetric strain than CH_4 (Fig. 2).

The volumetric strain ratios of different gases relative to CH_4 are high at low pressures (i.e. below 2 MPa) and at high pressures these ratios narrow down (Fig. 2). At the intermediate to high pressures the volumetric strain ratios ($\varepsilon_{H2S}/\varepsilon_{CH4}$) are about 8, 20 and 30 for the Ardley, Wolf Mountain and Quinsam coals, respectively; similarly, the ratios of $\varepsilon_{CO2}/\varepsilon_{CH4}$ are about 7, 3, and 5; but the ratios of $\varepsilon_{N2}/\varepsilon_{CH4}$ are 0.2, 0.3, and 0.3 for Ardley, Wolf Mountain and Quinsam coals. Therefore, the displacement of CH_4 from these coal seams by H_2S or CO_2 injection without significant pressure change will cause net coal expansion. However, injecting N_2 to displace CH_4 from these coals likely causes net coal shrinkage. How the coal permeability changes with the volumetric strain induced by gas adsorption or desorption is investigated quantitatively in following sections.

3. Permeability Model of Coal Seams

Volumetric strain induced by gas sorption is linear proportional to the volume of gas adsorbate. Thus, the effects of gas sorption on the deformation of isothermal coal seams can be treated analogously as the effects of temperature for non-isothermal elastic porous medium (e.g., Palmer and Mansoori, 1998). Therefore, similar to the constitutive relation of non-isothermal poro-elastic medium (e.g., Palciauskas and Domenico, 1982; Neuzil, 2003), the stress (σ_{ij}) and strain (ε_{ij}) relation for deforming coal seams can be described as:

$$\sigma_{ij} = \frac{E}{1+v}(\varepsilon_{ij} + \frac{v}{1-2v}\varepsilon_b\delta_{ij}) + \zeta p\delta_{ij} + K\varepsilon_V\delta_{ij}\,, \tag{3}$$

where E is Young's module of the porous medium, v is the Poisson's ratio, ε_b is the bulk volumetric strain, p is pore fluid pressure, ε_V is the sorption-induced volumetric strain given by eq. 1, $K = E/3(1-2v)$ is the bulk module of the porous medium, δ_{ij} is Kronecker's delta, and i or j is the directional index (x, y, and z). The Boit constant ζ is defined as (e.g., Palciauskas and Domenico, 1982):

$$\zeta = 1 - \frac{K}{K_s}\,, \tag{4}$$

where K_s is the modulus of the solid matrix.

The bulk volumetric strain increment $d\varepsilon_b = d\varepsilon_{xx} + d\varepsilon_{yy} + d\varepsilon_{zz}$ can be derived from eq. 3 as

$$d\varepsilon_b = -\frac{dV_b}{V_b} = \frac{1}{K}(d\sigma - \zeta dp) - d\varepsilon_V \,, \tag{5}$$

where V_b is the bulk volume, and σ is the confining pressure or the mean normal stress, $(\sigma_{xx} + \sigma_{yy} + \sigma_{zz})/3$. The pore volume strain increment $d\varepsilon_p$ can be expressed as (e.g., Zimmerman et al, 1986; Zimmerman, 2000):

$$d\varepsilon_p = -\frac{dV_p}{V_p} = \frac{1}{K_p}d\sigma - (\frac{1}{K_p} - \frac{1}{K_s})dp \,, \tag{6}$$

where V_p is the pore volume, K_p is the modulus of the pores. No terms that consider the effects of gas sorption enter into eq. 6 because gas is mostly adsorbed into microporous coal particles instead of the macroscopic pores that we considered here.

The macroscopic porosity (ϕ) of a coal seam is defined as

$$\phi = \frac{V_p}{V_b} \,. \tag{7}$$

Thus, the porosity change of a deforming coal seam can be described as

$$d\phi = d\left(\frac{V_p}{V_b}\right) = \frac{V_p}{V_b}\left(\frac{dV_p}{V_p} - \frac{dV_b}{V_b}\right). \tag{8}$$

Substituting eqs. 5 - 7 into eq. 8 and making some reorganizations yield

$$\frac{d\phi}{\phi} = \left(\frac{1}{K} - \frac{1}{K_p}\right)(d\sigma - dp) - d\varepsilon_V \,. \tag{9}$$

Assuming constant K and K_p, integrating eq. 9 with time yields

$$\frac{\phi}{\phi_0} = \exp\left\{\left(\frac{1}{K} - \frac{1}{K_p}\right)[(\sigma - \sigma_0) - (p - p_0)] - (\varepsilon_V - \varepsilon_{V0})\right\}, \tag{10}$$

where subscript $_0$ represents the initial values.

For most coal seams, the permeability for gas and water flow is mainly contributed by the macroscopic cleat/fracture porosity. The micro pores in coal matrix contribute negligible permeability to water and gas flow. Therefore, the cleat permeability (κ) can be described in terms of cleat porosity (ϕ) as

$$\frac{\kappa}{\kappa_0} = \left(\frac{\phi}{\phi_0}\right)^3 , \qquad (11)$$

where κ_0 is the initial cleat permeability. The initial permeability and porosity of a coal seam can be determined from the coal fabric, such as the cleat spacing (a) and aperture width (b), by using the match-stick model (Sawyer et al., 1990; Harpalani and Chen, 1997):

$$\phi_0 = \frac{2b}{a} \text{ and } k_0 = \frac{b^3}{12a} . \qquad (12)$$

In practice, initial permeability (k_0) and cleat spacing (a) can be determined by well testing and examining coal cores. Then the initial porosity (ϕ_0) can be determined with eq. 12. The combination of eqs. 10 and 11 describes the permeability variation induced by stress, pore pressure, and gas sorption or desorption during acid gas injection or methane production.

With assumptions of uniaxial strain (e.g., $\varepsilon_{xx} = \varepsilon_{yy} = 0$), a constant reservoir loading σ_{zz}, and $K_s >> K$ or $\zeta = 1$, which is commonly assumed for sedimentary basin compaction or reservoir modeling as done in this study, then the horizontal stress σ_{xx} or σ_{yy} is given as

$$\sigma_{xx} = \sigma_{yy} = \frac{\nu}{1-\nu}\sigma_{zz} + \frac{1-2\nu}{1-\nu} p + \frac{1-2\nu}{1-\nu} K\varepsilon_V , \qquad (13)$$

and the mean normal stress change (σ-σ_0) becomes

$$\sigma - \sigma_0 = \frac{2(1-2\nu)}{3(1-\nu)} [(p - p_0) + K(\varepsilon_V - \varepsilon_{V0})] . \qquad (14)$$

Furthermore, the pore volume modulus K_p can be approximated as $\phi K/\zeta$ (e.g., Kümpel, 1991) or ϕK for $\zeta = 1$. Thus eq. 10 may be approximated as

$$\frac{\phi}{\phi_0} = \exp\left\{\frac{1-\phi_0}{\phi_0}\left[\frac{(1+\nu)(1-2\nu)}{E(1-\nu)}\left(p - p_0\right) - \frac{2(1-2\nu)}{3(1-\nu)}\left(\varepsilon_V - \varepsilon_{V0}\right)\right] - \left(\varepsilon_V - \varepsilon_{V0}\right)\right\} . \qquad (15)$$

On the other hand, equation 9 can be simplified as

$$d\phi = -\frac{1}{K}\left(1-\phi\right)\left(d\sigma - dp\right) - \phi d\varepsilon_V . \qquad (16)$$

For small porosity as for the macroscopic cleat porosity $\phi << 1\%$, equation 16 can be further simplified as

$$d\phi=-\frac{1}{K}\left(d\sigma-dp\right). \tag{17}$$

Integrating eq. 17 fields

$$\phi-\phi_0=-\frac{1}{K}\left[\left(\sigma-\sigma_0\right)-\left(p-p_0\right)\right]. \tag{18}$$

Substituting eq. 14 into eq. 18, replacing *K* with *E*/*3*(*1-2v*), and making some reorganizations give

$$\phi-\phi_0=\frac{(1-2\nu)(1+\nu)}{E(1-\nu)}(p-p_0)-\frac{2}{3}\left(\frac{1-2\nu}{1-\nu}\right)(\varepsilon_v-\varepsilon_{v0}). \tag{19}$$

Combination of eqs. 11 and 19 gives a stress- and sorption-dependent permeability model that is similar to the porosity model proposed by Palmer and Mansoori (1998). By assuming that the apertures of the vertical cleats or fractures of coal seams are only affected by the horizontal effective stress (e.g., $\sigma_{xx}-p$, or $\sigma_{yy}-p$) on their surfaces, then the stress-dependent porosity may be described as (e.g., Seidle et al., 1992; Shi and Durucan, 2004):

$$\frac{\phi}{\phi_0}=\exp\left\{\frac{1}{K_p}\left[\frac{\nu}{1-\nu}\left(p-p_0\right)-\frac{E}{3(1-\nu)}\left(\varepsilon_V-\varepsilon_{V0}\right)\right]\right\}, \tag{20}$$

which is similar to eq. 15 in that the porosity is an exponential function of the changes in fluid pressure and sorption-induced volumetric strain.

The cleat porosity and permeability change during gas injection or production can be approximated by any of the three eqs. 15, 18, or 20 when combined with eq. 11. However, differences exist among these models. The derivation of eq. 15 is achieved by only assuming constant bulk and pore modulus. More assumptions, such as $\phi << 1\%$ was made to derive eq. 19. Equation 20 may be obtained by replacing the mean normal stress σ with horizontal stress σ_{xx} or σ_{yy} and dropping out the last term ε_V - ε_{V0} in eq. 10. From comparative analyses of these models it is found that for small porosity changes or mild gas-sorption-induced volumetric strain, equations 15 and 19 predict nearly identical permeability variation. But for strong gas-sorption-induced volumetric strain or large porosity change, equation 19 is no longer valid as it may predict negative porosity and permeability. On the other hand, equation 20 generally predicts much stronger reduction or enhancement of porosity and permeability than either eq. 15 or eq.19. Therefore, we adopt eq. 15 in this study although all three models are compared for a specific case.

As indicated by eqs. 15, 19, or 20, an increase in pressure will enhance the cleat porosity and permeability and vice versa. In contrast, an increase in volumetric strain induced by gas sorption will result in a decrease in porosity and permeability. The magnitudes of the influence of pressure and gas sorption on porosity and permeability are closely controlled by the mechanical properties such as bulk and pore modulus or Young's modulus and Poisson's ratio and the initial conditions of the coalbed reservoirs.

4. Gas Sorption-Induced Permeability Change

With our measured coal properties (e.g., gas adsorption and adsorption-induced volumetric strain), here we consider quantitatively the change in coal permeability during CH_4 recovery or CO_2 and H_2S sequestration. It is assumed that the coals are initially saturated with methane and have a hydrostatic fluid pressure estimated from their average depths (Table 2). The likely initial permeability and cleat spacing are given, and thus the initial porosity is calculated with eq. 12. Different porosities are also tested for their effects on the coal permeability variations.

During injection of CO_2 and H_2S into the coal seam, the cleat permeability is likely reduced by the adsorption-induced swelling of coals. On the contrary, the pressure elevation in cleats due to gas injection tends to enhance the permeability. Due to the dual porosity structure of coal seams, adsorption of the injected gas is likely retarded by relatively slow, diffusive transport of injected gas into the microporous coal matrix from the cleats. Therefore, the gas pressure in cleats may be significantly different from that in coal matrix. Thus, there exists a dynamic/kinetic coupling of cleat pressure and sorption in coal matrix on permeability change, which is considered rigorously in next section by numerical modeling. To predict analytically the permeability change induced by gas sorption, we assumed an instantaneous or equilibrium displacement of CH_4 by injected gases without changes in the total reservoir pressure. But the reservoir pressure will be elevated after all CH_4 is depleted or when the partial pressure of injected gas becomes equal to the initial pressure by injecting more gases. Such a presumable scenario is applied to estimate the possible permeability change for injection of CO_2, H_2S, N_2 or their mixtures to displace the preadsorbed CH_4 in this section. For pure CH_4 cases, however, decreasing pressure from the initial coal-seam pressure implies an instantaneous or equilibrium desorption of CH_4 from microporous coal matrix, whereas the increasing pressure from the initial coal-seam pressure implies an instantaneous or equilibrium adsorption of CH_4 into the coals.

4.1. Ardley Coal

Possible permeability change of the Ardley coal during the primary CH_4 recovery and acid gas injections under various conditions is assessed analytically (Fig. 3). As expected from eq. 15, decreasing gas pressure reduces the porosity and hence the permeability. A coal seam with larger Young's modulus E deforms less in response to change in fluid pressure. Thus, the effects of shrinkage of CH_4 desorption on permeability rebounds likely become predominated for the coal seam with a larger E. For example, if the Ardley coal has a large E value, such as 4 GPa, the coal permeability will increase with pressure draw-down from its initial value of 2 MPa, whereas with a smaller E (e.g., 2 and 3 GPa) the coal permeability decreases with decreasing pressure (Fig. 3a). An increase in Poisson's ratio generally reduces the magnitude of permeability change when the gas pressure is elevated or lowered. But, similar permeability variations for primary CH_4 recovery are predicted for this coal with different Poisson's ratios. Additionally, the lower the initial cleat porosity ϕ_0 of the coal seam, the more significant variation of the coal permeability is predicted. With the relatively small adsorption capacity of CH_4 for the Ardley coal, the volumetric strain caused by CH_4 adsorption or desorption does not play a major role in the variation of permeability, and thus no permeability rebound is predicted or the rebound is limited when methane is desorbed from the coal (Fig. 3a).

Figure 3b shows the possible reduction of cleat permeability caused by the injection of CO_2 into the Ardley coal under various conditions. The adsorption of CO_2 into coals with CH_4 displacement causes the progressive reduction of coal permeability as the partial pressure of CO_2 increases. After the pressure of CO_2 reaches the initial coal-bed pressure (2 MPa), the permeability continues to decrease with pressure without permeability rebound. This trend is predicted for different Poisson's ratios and initial porosities (Fig. 3b). It is interesting to note that the injection of CO_2 could cause about 90% permeability reduction if the coal seam has an initial porosity of 0.58% and almost complete permeability loss occurs if the coal seam has an initial porosity of 0.12% (Fig. 3b). Similarly, injection of H_2S into the Ardley coal results in >95% loss of permeability even if the coal has a large initial cleat porosity of 0.58% (see the reference curve) and a reduction of the permeability by seven order of magnitude if it has a small initial cleat porosity of 0.12% (Fig. 3c). Due to the strong swelling effects of CO_2 or H_2S, different Young's modulus (2, 3, or 4 GPa) predict very similar permeability change and thus only the permeability evolutions predicted with E = 3 GPa are shown here. However, a larger Poisson ratio (i.e., $\nu = 0.4$) predicts much smaller changes in permeability (Fig. 3b-c).

Because of the smaller swelling effects and adsorption capacity and sorption strength of N_2 than CH_4, injection of N_2 to displace CH_4 from the coal seam results in not only in a net decrease of gas mass in the coals but also a significant shrinkage of the coals. Thus, permeability enhancement is predicted for N_2 injection, especially for coal seams with a smaller initial porosity (Fig. 3d). Therefore, it is logic to believe that injection of mixture of CO_2 and N_2 or H_2S and N_2 instead of the pure acid gas will induce less permeability reduction owing to less sorption of acid gas. Indeed, injection of a mixture of $80\%N_2+20\%CO_2$ causes only about 20% permeability reduction instead of a 90% loss for pure CO_2 injection into a coal seam with $\phi_0 = 0.58\%$, and about 60% permeability reduction instead of nearly complete permeability loss for pure CO_2 injection into a coal seam with $\phi_0 = 0.12\%$ (Fig. 3b). Mixing N_2 with H_2S also causes less permeability reduction than pure H_2S injection, but the permeability is still significantly reduced (Fig. 3c).

4.2. Wolf Mountain Coal

For the Wolf Mountain coal, because of the large CH_4 adsorption capacity of this coal, desorbing CH_4 from the coal seam with an initial pressure of 3 MPa can cause a strong rebound of permeability at low pressures (Fig. 4a). Injecting CO_2 into this coal likely causes >1000-fold decrease in coal permeability if the coal has an initial porosity of about 0.17%. Even with a large initial porosity of 0.49%, the coal permeability will be reduced by >90%. However, for a similar amount change in partial pressure of CO_2, the permeability reduction at lower pressures is much stronger than at higher pressures (Fig. 4b). Due to the strong swelling induced by H_2S adsorption, injecting H_2S into this coal likely causes > 6-order of magnitude of permeability reduction for an initial porosity of 1% or more than 95% permeability loss for a very large initial porosity of 5% (Fig. 4c).

Injecting N_2 into the Wolf Mountain coal enhances the cleat permeability by >10 times for coal seams with an initial porosity of 0.17% and smaller Poisson's ratio because of the small adsorption capacity and low adsorption affinity of N_2 and the simultaneously displacement of pre-adsorbed CH_4 (Fig. 4d). Therefore, injection of a flue gas of 50% CO_2 + 50% N_2 causes less than 2-order of magnitude of permeability reduction for an initial porosity of 0.17% and 1-order magnitude of permeability reduction for an initial porosity of 0.49%. Such permeability reductions are significantly less than the permeability loss caused by pure CO_2 injection (Fig. 4b). Injection of a flue gas of 50%H_2S and 50%N_2, however, induces limited recovery of permeability loss caused by pure H_2S injection because of the strong swelling induced by H_2S (Fig. 4c).

4.3. Quinsam Coal

For the Quinsam coal, there are also significant permeability rebounds during primary recovery of methane when the pressure drawdown becomes low (Fig. 5a). Significant permeability reduction is also induced by injecting CO_2 and H_2S into the coal (Fig. 5b-c). Again, injection of N_2 enhances the cleat permeability (Fig. 5d). Thus, injecting gas mixture of CO_2+N_2 causes much lower permeability reductions than pure gas injections by >3-orders of magnitude. However, the 80%N_2+20%H_2S injection still causes >5-orders of magnitude permeability loss for small initial porosity of 0.23% (Fig. 5c).

Overall, the above analyses suggest that injection of pure CO_2 or H_2S into the three coals with relatively low initial cleat porosities likely reduces significantly the coal permeability and consequently makes the sequestration of CO_2 and H_2S into those coals to become impractical or very inefficient, especially for H_2S sequestrations. Injection of flue gas may alleviate the permeability loss and thus likely be more efficient than pure acid gas injection.

5. Acid Gas Sequestration Modeling

We have considered analytically the likely reduction of cleat permeability during primary methane recovery or acid gas injection. In this section, the dynamic changes in cleat permeability due to variation of reservoir pressures and adsorbed gas composition are investigated by rigorous numerical simulations.

5.1. Numerical Model

With the assumption of Darcy's type fluid flow in cleat networks of a coal seam, gas and water mass balances in the cleat networks are described as:

$$\frac{\partial}{\partial t}(s_g \phi \rho_g y_i) - \nabla[s_g \rho_g y_i \frac{k_{rg} k}{\mu_g} \nabla p] = (1-\phi) N_i + Q_i \,, \qquad (21)$$

$$\frac{\partial}{\partial t}(s_w \phi \rho_w) - \nabla(s_w \rho_w \frac{k_{rw} k}{\mu_w} \nabla p) = Q_w \,, \qquad (22)$$

where subscript *g* and *w* represent gas and water phases, respectively; *s* is the saturation factor; ρ is density; k_r is the relative permeability; μ is fluid viscosity; Q_i and Q_w are the sources or sinks of gas *i* and water, respectively; *p* is the fluid pressure in the cleats with a zero capillary pressure; and N_i is the volumetric mass flux of gas *i* out of coal matrices into cleat networks, approximated as

$$N_i = \frac{8\pi \phi_m D_{me}}{a^2} (\rho_m y_{mi} - \rho_g y_i) \,, \qquad (23)$$

where subscript *m* represents the averaged properties within coal matrices; ϕ_m is the porosity; ρ_m is the average density of the free gas; y_{mi} is the molar fraction of free gas *i*; D_{me} is the effective gas diffusion coefficient; To derive Eq. 23, a parabolic gas concentration profile is assumed within the coal matrix block (Yang, 1997), and the coal matrix is further approximated by an equivalent cylindrical matrix (e.g., Sawyer et al., 1991).

Assuming the dominance of gas diffusion through pores within coal matrices, the gas mass balance in the coal matrix is approximated as

$$\frac{\partial}{\partial t}(\phi_m y_{mi} \rho_m) + (1-\phi_m)\frac{\partial q_i}{\partial t} = -N_i \,, \qquad (24)$$

where $q_i = V_{gi}\rho_c$ is the averaged adsorbed gas concentration, and ρ_c is the coal density.

Production or injection wells are simulated with the Peaceman model (Peaceman, 1983), which determines the gas rate (Q) in eq. 21 as

$$Q_i = \frac{\theta k k_{rg} y_i \rho_g}{\mu_g (\ln r_0 - \ln r_w)} (p_w - p) , \tag{25}$$

where θ is a connect factor (i.e., $\theta = 2\pi$ if the well is located within a grid block; $\theta = \pi/2$ if the well is located at corner of a grid block as in this study); r_w and p_w are the well bore radius and well pressure, respectively; and $r_0 = 0.14(\Delta x^2 + \Delta y^2)^{1/2}$ is the pressure equivalent radius and Δx and Δy are the sizes of well blocks. A similar equation can be derived to describe water production or injection, and thus it is omitted here.

We adopted a relative permeability relationship published by Gash (1991) (Fig. 6). The density and viscosity of mixed gas are interpolated from a tabular data determined with SUPERTRAPP with the Peng-Robinson state equation, if liquid and gaseous phases of the injected gas and methane in coal pores coexist, the bulk values of their ideal two-phase mixture are applied. Individual pure gas has a quite different diffusivity while being adsorbed into the microporous colas (e.g., Cui et al., 2004). Hence, the diffusion coefficient (D_{mi}) of each gas in microporous coals is determined with our experimental adsorption rate data with a model given by Do (1998). The diffusion coefficients of CO_2, CH_4, H_2S, and N_2 for the Wolf Mountain coal particles are accordingly determined and given in Fig. 7, which is applied in this study. The effective diffusion coefficient of gas mixture within the microporous coal matrix (D_{me}) is then approximated as

$$D_{me} = \sum_{i}^{n} y_{mi} D_{mi} \; . \tag{26}$$

The water density is approximated with the equation given by Ahmed (2000), and its viscosity is calculated with the model proposed by (Brill and Beggs, 1978).

The coupled governing equations (Eqs. 21 – 25) are discretized implicitly in time and with the up-wind finite-difference method in two-dimension space. The obtained nonlinear algebra system is then solved using the Newton-Raphson method (e.g., Burden and Faires, 1997). A five-spot well pattern is applied (Fig. 8), but the simulated part is only one quarter of the whole domain with a rectangular grid mesh of 20 by 20, which represents a domain of 200 × 200 m with a uniform thickness of 5 m. Therefore, all boundaries of the simulation domain are symmetrical. The properties including fluid pressure, gas concentration and others are assumed to be homogeneous vertically and the coal seam is fully penetrated by the injection or production wells. Gravitational force is also neglected due to relatively small thickness of the coal seam and large horizontal dimensions.

The developed model has been tested against the numerical results of special cases provided by other models (e.g., Law et al., 2003), and our model results are consistent with the results predicted by those different simulators.

5.2. Numerical Results

Using the Wolf Mountain coal as an example, we investigate a couple of representative cases to highlight the permeability variation during acid gas sequestration. The coal seam was assumed to contain initially 100% CH_4 in coal matrices and 65% water in cleats. During all simulations, constant gas injection and production rates are specified. However, the injection-well pressure (p_{wi}) cannot be higher than the specified maximum value (p_{wim}) and the production-well pressure (p_{wp}) of a production well cannot be lower than the specified minimum value (p_{wpm}). Therefore, the injection or production rates are actually adjusted to maintain the well pressure (p_w) within the specified ranges during all simulations (see Table 3 for parameter values).

5.2.1. Modeling of CO_2 sequestration

Modeling results of sequestration of CO_2 into the Wolf Mountain coal with the same properties as the reference values in Fig. 4b are shown in Fig. 9. For pure CO_2 injection, the injection rate is significantly reduced from 10,000 to ~100 m^3 day^{-1} in less than 75 days because of the dramatic reduction of coal permeability caused by CO_2 adsorption (Fig. 9a-b). Even with the strongly reduced CO_2 pumping rate, the CH_4 recovery is still enhanced when compared to the primary CH_4 recovery (Fig. 9a). Furthermore, the primary CH_4 recovery (when taken into consideration the dynamic permeability variation) is much more efficient than that from a coal seam with a constant cleat permeability of 5 md (Fig. 9a). This is because of the enhancement of permeability resulting from desorbing CH_4 from the coals with pressure drawdown as predicted analytically (see Fig. 4a). Because of the significant reduction of CO_2 injection rate, nearly no CO_2 breakthrough occurs and results in the production of pure CH_4 in a period of 10 years.

The coal permeability at different locations evolves dynamically with time (Fig. 9b). The coal permeability close to the injection well (*I*) is enhanced at very beginning due to the elevation of cleat pressure by gas pumping, whereas it is reduced for coals close to the production well (*P*) because of drawdown of cleat pressure by pumping water out of the production well. The injection well block initially undergoes the maximum permeability enhancement and the opposite occurs to the production-well block. However, the enhanced permeability of the injection-well block rapidly and progressively declines with time or adsorption of CO_2 into the coal matrix until the maximum reduction of permeability (>99% permeability loss) is reached in about 30 days (Fig. 9b). The permeability of coals near the production well, however, undergoes enhancement with time because of desorption of CH_4 out of the coal matrices and without significant adsorption of CO_2 (Fig. 9b).

When injecting a gas mixture of 50% CO_2+50% N_2 into the same coal seam, the injection rate is reduced to 500 m^3 day^{-1} over a 200 day period (Fig. 9c). Also the methane recovery is more enhanced with a peak production rate that is about 1.5-times that enhanced by injecting pure CO_2 (Fig. 9a and c). However, the injected N_2 breaks through at about 500 days. The permeability of the injection-well block is doubled at the start of injection and then decreases with adsorption of CO_2 and reaches a minimum value after 200 days rather than the 30 days for pure-CO_2 injection (Fig. 9a and d). As expected, the permeability of the production-well block increases with time because of desorption of CH_4 and essentially no adsorption of CO_2. In this scenario, as more CO_2 is sequestrated into the coal seam and CO_2 migrates further toward the production well, which causes significant permeability reduction of the grid block (5, 5) that is about 50 m away from the injection well at about 2000 days (Fig. 9d).

5.2.2. Modeling of H2S sequestration

As indicated by analytical results (Fig. 4c), H_2S sequestration into the Wolf Mountain coal causes the coal to become nearly impermeable even if the coal has a large initial porosity of 1%. This is further illustrated by numerical modeling here. The effects of injection of 99%H_2S+1%N_2, 50%H_2S+50%N_2, and 20%H_2S+80%N_2 into a coal seam with initial porosity of 1% and a cleat spacing of 1 mm are compared in Fig. 10. Because of the strong coal swelling induced by H_2S sorption, the injection rates for all three cases are dramatically reduced to nearly zero although mixing more N_2 with H_2S gives a higher injection rate (Fig. 10a). Thus very limited amount of H_2S is sequestrated into the coal seam in 10 years and the recoveries of CH_4 for all three cases are almost the same as primary recovery. The occurrences of nearly zero injection rates are owing to the more than 2-orders of magnitude of permeability reduction of the injection-well block in about 100 days (Fig. 10b). However, the permeability of the production-well block is slightly enhanced with time due to desorption of CH_4. Although injection flue gas does promote the injection efficiency and induce less permeability reduction, the overall injection rate is still too low to become practical for H_2S sequestration into the coal seam (Fig. 10).

5.2.3. Influence of coal fabric

As illustrated in last two sections, initial gas injection into coal seams does not immediately cause the sorption-induced coal swelling and the consequent permeability reduction but results in the cleat permeability enhancement as the cleat pressure rises. This is because it takes time for the injected CO_2 to diffuse and be adsorbed into the microporous coal matrices with the relatively slow diffusive gas transfer through microporous coal matrices. Therefore, the coal fabrics (i.e., the cleat spacing) may affect the acid gas sequestration, which is investigated in this section by modeling the CO_2 injection into the Wolf Mountain coal with two different cleat spacing (i.e., 2 mm or 1 cm) but the same initial permeability of 5 md and other properties.

For sequestration of CO_2 into the coal seam (I) with a small cleat spacing of 2 mm, the injection rate of 50%CO_2+50%N_2 is only reduced from 10,000 down to 1700 m^3 day^{-1} in about 50 days (Fig. 11-I-a), in contrast to the counterpart injection-rate reduction from 10,000 down to ~ 100 m^3/day in 700 days for the coal seam (II) with a large cleat spacing of 1 cm (Fig. 11-II-a). This is because, according to eq. 12, coal seam (I) has a larger initial cleat porosity of 0.49% as compared to 0.17% for coal seam (II), which thus causes less permeability reduction for coal seam (I) than for coal seam (II) (Fig. 11-I-b and II-b). Though slightly higher gas production is predicted for coal seam (II), the injected N_2

breaks through the production well with a low concentration of CO_2 at about 50 days (Fig. 11-II-a), in contrast to the late breakthrough of the injected N_2 without CO_2 at about 850 days for coal seam (I) (Fig. 11-I-a). This is because, for small cleat spacing, the injected CO_2 can be rapidly adsorbed into coal matrices instead of efficiently migrating toward the production well through cleat networks as predicted for coal seam (II). Consequently, a late breakthrough of injected gas develops for coal seam (I). Also because of the rapid adsorption and/or desorption of gas for the coal seam (I) with small cleat spacing, its sorption-dominated permeability reduction occurs earlier than for coal seam (II) although the absolute magnitude of permeability reduction is smaller (Fig. 11-I-b and II-b).

It is interesting to note that the cleat pressure gradient between the injection and production wells is generally steeper for coal seam (I) than for coal seam (II) throughout the simulation time (Fig. 12-I-a and II-a). Also much steeper free-gas concentration gradients in cleats and matrices are developed for coal seam (I) than for coal seam (II). Due to its low adsorption capacity and strength in coals, N_2 becomes markedly concentrated downstream in the free-gas mixture as CO_2 is preferentially and rapidly adsorbed into coal matrices (I) (Fig. 12-I-b), which retards the breakthrough of CO_2. On the contrary, relative smooth free-gas concentration fronts develop for the coal seam (II) due to its larger cleat spacing that develops relatively inefficient adsorption and diffusion of injected gas into coal matrices. Consequently, the injected gas penetrates through cleat networks more efficiently, resulting in an early breakthrough of the injected gas (Figs. 11-II-a and 12-II-b).

Coal seam permeability systematically evolves with injected gas concentration fronts. The portion of permeability reduction corresponds closely to high CO_2 concentrations, whereas the permeability enhancement corresponds to high N_2 concentration portions (Fig. 12-I-c and II-c). Thus, the permeability gradient between the injection well and production well also dynamically migrates with the gas concentration fronts. Overall, the coal fabrics strongly affect the dynamic permeability variations, acid gas sequestration efficiencies, and breakthrough characteristics.

6. Discussions

Possible permeability reduction during injection of CO_2, H_2S, N_2, or their mixture with CH_4 recovery has been investigated based on our experimental gas adsorption and coal swelling data of three Canadian coals (the Ardley, Wolf Mountain, and Quinsam coals) and a swelling-dependent permeability model for coal seams that we have developed. Recognizing the uncertainties of coal mechanical properties, we have considered a wide range of values for the Young's modulus E and the Poisson's ratio ν. Although only three coals are studied here, the results are instructive as to how cleat permeability changes during sequestration of CO_2 and H_2S into coal seams and CH_4 recovery.

Our analytical predictions of possible reduction or enhancement of coal permeability is based on the assumption that the injected gas is instantaneously adsorbed into coals and displaces the pre-adsorbed CH_4 out of coals without total pressure change. The analytic results generally agree with the permeability variations predicted by rigorous numerical modeling although detailed differences remain (Table 4). The mismatch between the numerical and analytical results may be mainly because of the different pressures at which the permeability values are compared. For example, for the primary recovery case, the pressure drawdown of the production well simulated numerically never reached 0.5 MPa. However, the analytic permeability change was evaluated at 0.5 MPa. The much higher numerical κ/κ_0 values than the analytic predictions for H_2S injection cases is mainly caused by the under-saturation of H_2S for the coal seam due to the nearly zero injection rates in numerical modeling. Overall, the analytical predictions catch the essence of dynamic permeability variation during acid gas sequestration or CH_4 recovery. Therefore, the analytical approach may be reliably applied to estimate the changes in coal permeability.

Generally, the virgin cleat porosity has the most significant influence on permeability changes during CO_2 and H_2S injection and CH_4 recovery. The smaller the initial cleat porosity, the more marked change in cleat permeability occurs with fluid pressure variation or the coal swelling upon gas adsorption or shrinking upon gas desorption. The cleat spacing of the three coals considered here are about 0.1 – 1 cm and initial cleat permeability are a few millidarcies (1 to 5 md). According to the match-stick model (eq. 12), cleat porosity for such permeability values is lower than 0.5%. With such low initial porosity, injection of CO_2 could reduce the cleat permeability by more than one order of magnitude assuming moderate Young's modulus and Poisson's ratio as represented by the reference curves in Figs. 3-5. Injection of pure H_2S into the three coals reduces the coal permeability by greater than five-orders of magnitude. Thus, it is impractical for pure H_2S injection into these coals, as illustrated by our numerical results (Table 4).

Due to the low adsorption strength and capacity of N_2 in coals, injection of pure N_2 into coals causes enhancement of cleat permeability by displacing the CH_4 out of coal seams. Therefore, injection of gas mixture of CO_2+N_2 into those coals can result in less reduction of cleat permeability and promote the sequestration efficiency. For example, by injecting a gas mixture of 50%CO_2+50%N_2, the sequestrated amount of CO_2 is about three-times that obtained by pumping pure CO_2 into the coal seam with an initial porosity of 0.27% (Table 4). However, injection of a gas mixture of N_2+H_2S does not promote noticeably the efficiency of H_2S sequestration into the coals (Table 4). Furthermore, the acid gas sequestration rates are far below the targeted sequestration amount (i.e.10,000 m^3 day^{-1}) for all cases even with flue gas injection, especially for H_2S sequestration (Table 4).

Coal fabric (e.g., cleat spacing) strongly affects the dynamics of permeability variation during CH_4 recovery and CO_2 and H_2S sequestration into coal seams. With similar cleat permeability for a coal seam, a large cleat spacing implies a smaller cleat porosity (ϕ) (see eq. 12). Hence strong permeability reduction may occur during injection of acid gases into the coal seam, which makes sequestration of acid gas into the coal seam difficult. Moreover, the larger cleat spacing likely causes the early breakthrough of injected gases because the injected gas is inefficiently adsorbed into the larger coal matrix and most gas flows through the cleat networks toward the production well (e.g., Fig. 12). The early injected-gas breakthrough may be also promoted by the early-stage enhancement of cleat permeability by elevated cleat pressure. Early-breakthrough of injected gas would result in failure of the sequestration. On the contrary, for a coal seam with dense cleat spacing, less permeability variation is incurred during CO_2 and H_2S sequestrations because of the larger initial cleat porosity (for the same permeability as a coal with less dense spacing). The rapid diffusive transport of injected gas into smaller coal matrices develops steeper concentration fronts, resulting in later breakthrough of the injected gas in the production gas (Fig. 12-Ib), and causes the permeability reduction at early stages, resulting in an early reduction of gas injection rates (compare Figs. 11-Ia and II-a). However, the overall injection rate for coal seam with large initial cleat porosity may be still much lager than that of coals with smaller porosity or larger cleat spacing. Thus higher sequestration efficiency is expected for coal seams with larger cleat porosity or smaller cleat spacing if their permeabilities are similar (Table. 4).

Gas adsorption properties also have important effects on the permeability variations. The smaller the difference of adsorption capacity for CH_4 and the acid gas to be sequestrated, the smaller net swelling of coal matrices will occur. This is mainly because the coal swelling is controlled by the net mass increase in adsorbed gas. The smaller difference between those gases, the smaller net mass increase will occur by displacing CH_4 from the coal seam. Thus, high-rank coal seams are more optimal for CO_2 and H_2S sequestration because they likely have denser cleat spacing and less differential adsorption capacities for different gas, even though coal seams with relative larger cleat spacing likely develop higher CH_4 primary recovery rates (Cui and Bustin, in preparation; also compare Fig. 11).

Different models have been proposed to describe the permeability change of coal seams during coalbed methane recovery (e.g., Sawyer et al., 1990; Shi and Durucan, 2004; Palmer and Mansoori, 1998). As pointed out by Palmer and Mansoori (1998), their model (i.e., eq. 19) is only applicable for small deformation or a few-fold change in porosity. For strong coal swelling induced by sorption of CO_2 or H_2S as in this study, their model predicts negative permeability (Fig. 13a). On the other hand, the model equation (20) as proposed by Shi and Durucan (2004) predicts much stronger reduction or rebound of permeability than Palmer and Mansoori's model (1998) (see Fig. 13a and b for example). Our newly derived model predicts permeability changes closer to the Palmer and Mansoori's model but does not produce negative values (Fig. 13a). Generally our model predicts permeability changes falling between those predicted by the other two models (e.g., Fig. 13b). Due to lack of constraining data and coal mechanical properties data, it is impossible to determine which model describes more accurately the permeability variations during gas production and acid gas injection. However, the stronger reduction of permeability predicted by eq. 20 or the model proposed by Shi and Durucan (2004) for acid gas sequestration (Fig. 13) would not change but underscore what we have learned by applying eq. 15 or our newly derived permeability model.

So far we have considered the likely change in cleat permeability assuming that the coal particles or coal matrix is incompressible ($K_s >> K$) or a constant Biot's coefficient $\zeta = 1 - K/K_s = 1$. With a heterogeneous dual-porosity structure, the cleat porosity (<<1%) contributed by fractures of a coal seam only accounts for a very small portion of its total porosity of few percents. The majority of porosity of coal seams is predominately distributed within the microporous coal matrices. However, the microporous coal matrices with variable sizes were presumably treated as the solid skeleton of a homogeneous poroelastic medium and were assumed to be incompressible in previous and present studies. Thus, the assumption of incompressibility of the coal matrices in a dual-porosity model may not hold because of its relatively large porosity even though relatively incompressible coal grains are also observed, such as the San Juan basins. Further, experimental measurements on different coals have suggested that the Biot's coefficient varies significantly from zero at relatively low pore pressures (low gas loadings) to one at high pressures (high gas loadings) (Zhao et al., 2003). The compressible coal matrix may consume some stress induced by fluid pressure variation and acid gas sorption, consequently resulting in less cleat pore deformation and less adsorption-induced permeability reduction. Indeed, if the coal matrix is quite compressible (e.g., $\zeta = 0.5$ or $K_s = 2K$), the predicted permeability reductions are nearly one-order of magnitude less than those for coal seams with incompressible coal matrix (Fig. 14). However, even with such quite compressible coal matrix (e.g., $\zeta = 0.5$), nearly one-order or two-order of magnitude of permeability reduction are predicted respectively for injection of 50%N_2+50% CO_2 or pure CO_2 into the Wolf Mountain coal (Fig. 14), which are still significant losses of permeability. Furthermore, for acid gas injection, the cleat pressure is most likely further elevated relatively by gas injections. Thus, the coal matrix likely behaves stiffer with the Biot's coefficient close to unit as suggested by the experimental data (Zhao et al., 2003) or as assumed in present study. However, the coal close to production wells may become more compressible with progressive drawdown of cleat pressure and gas production, and thus less variation of cleat porosity and permeability may occur.

With constant mechanical properties of coals, more than several orders of magnitude of cleat permeability loss during injection of CO_2 or H_2S is predicted for the three Canadian coals in this study. However, complete loss of cleat porosity or permeability may not happen in nature. The surfaces of cleats in coal seams include asperities, including minerals and coal fines deposited on cleat surfaces. Thus the cleat cannot close on asperities and likely become progressively stiffer with increasing stress induced by the coal swelling as a result of acid gas adsorption. Therefore, the swelling-induced permeability reduction may be less than predicted by our model although significant permeability reduction may still occur. Further, as the thermal stress may cause material failure by over-heating, the stress induced by sorption swelling can be large enough to induce the coal failure. With the uniaxial strain assumption, we estimated the likely horizontal effective stress change [$\Delta\sigma'_{xx} = (\sigma_{xx} - \sigma_{xx0}) - (p - p_0)$] induced by CO_2 or H_2S sorption, where σ_{xx} is given by eq. 13. As shown in Fig. 15, injection of ether pure CO_2 or its N_2-mixtures will cause more than a 10 MPa increase in compressive horizontal effective stress. The horizontal effective stress increase is more than 100 MPa for H_2S sequestration (Fig. 15). However, the over loading or vertical stress (σ_{zz}) is nearly constant and thus the effective vertical stress ($\sigma_{zz} - p$) is actually reduced by gas-injection-induced pressure elevation by a negative change of $\Delta\sigma'_{zz} = -(p - p_0)$. Thus the net maximum shear stress increase [$(\Delta\sigma'_{xx} - \Delta\sigma'_{zz})/2$] could be much larger than 5 MPa for CO_2 sequestration and 50 MPa for H_2S sequestration. The incurred large shear stress increase may cause the coal to yield or to slip along pre-existed cleats, possibly resulting in local conduits for the injected gas by permeability enhancement. Such local shearing-yield zones may be not limited to the coals near well bores as suggested for methane production (e.g., Vaziri et al., 1997), but propagate along with the acid gas infiltration front in coal seams. The local yield or bulking of coal seams induced by large shear stress may also trigger failure of over-lying confining strata of the sequestration coal seam, develop leakage pathways for the injected gas, and consequently make the acid gas sequestration environmentally unsafe. Also, when acid gas CO_2 or H_2S is injected into coal seams, it immediately comes in contact with cleat water and forms mild to strong acids (as they are highly soluble in water relative to CH_4), consequently causing some minerals to dissolve (leaching effect), making coal to become brittle, and resulting in coal failure coupled with the stress induced by sorption swelling. Overall, such impacts of acid-gas sorption-induced swelling on the mechanical behaviors of coal seams and ambient formations need to be further investigated in future studies.

Another assumption in our model and previous studies (e.g., Parmer and Mansoori, 1998; Shi and Durucan, 2004) is that a uniform fluid pressure field develops throughout the whole coal reservoir and deformation is restricted to only in vertical direction (uniaxial strain). However, our modeling results show that fluid pressure changes dynamically in coal seams during gas injection and CH_4 recovery. Large fluid pressure gradients develop between the injection and production wells, especially for areas close to the well bore (Fig. 12-Ia and II-a). The volumetric strain induced by adsorption of acid gas also changes dramatically in space and time as indicated by the steep gradient of gas composition and permeability changes (Fig. 12). Such dynamic changes in fluid pressure and adsorption-induced volumetric strain with time and space violate the conditions of uniform fluid pressures and uniaxial strains throughout a reservoir assumed in previous and present studies. The extent that these factors could change our understanding on hydro-mechanical behavior of coal-seam reservoirs during acid gas sequestration may be small but poorly-known and need further investigation although those assumptions have been widely applied in practical reservoir modeling.

7. Conclusions

Hydro-mechanical behavior of coal seams during coalbed methane recovery and proposed sequestration of CO_2 and H_2S into coals is complex. Many uncertainties in coal properties remain. However, with constraints from our experimental data of gas adsorption and volumetric strain induced by gas adsorption, as a first-order approximation, our model results provide insightful information on the likely variations of cleat permeability when gases (CO_2, H_2S, and N_2) are injected into coal seams and their impacts on efficiencies of CO_2 and H_2S sequestrations.

Volumetric strains induced by adsorption of gases into coals are linearly proportional to the volume of gas adsorbed. With unit volume of adsorbed gas, hydrogen sulphide causes the largest volumetric strain, nitrogen causes the least volumetric strain, and volumetric strain induced by sorption of unit volume of CO_2 is slightly higher than that of CH_4. However, because of much larger adsorption capacity and affinity of H_2S and CO_2 in coals, under the same pressure loading, H_2S and CO_2 cause much higher volumetric strains than CH_4, and N_2 causes the least strain due to its small adsorption capacity and affinity in coals. Therefore, sequestration of CO_2 and H_2S into unminable coal seams with simultaneous displacement of CH_4 from coal seams causes the net swelling of coal matrix and thus the reduction of cleat permeability and the sequestration efficiencies. Injection of pure CO_2 and H_2S into the three Canadian coals studied here is almost impractical due to more than two-orders of magnitude of permeability reduction. Injection of mixture of CO_2 and N_2 mixture can markedly promote the efficiency of CO_2 sequestration and CH_4 recovery. However, injection of mixture of H_2S and N_2 likely does not promote H_2S sequestration.

Coal fabric structure such as cleat spacing also influences the dynamic changes in coal permeability and sequestration features of CO_2 and H_2S into coals. A larger cleat spacing of a coal seam makes diffusion and adsorption of injected gas into microporous coal matrices inefficient. Hence, breakthrough of injected gas likely occurs at very early stages, which is facilitated by the early permeability enhancement due to elevated cleat pressures by initial gas injection. Moreover, coal seams with large cleat spacings likely have low initial cleat porosity and thus largest reduction in cleat permeability with adsorption of H_2S and CO_2. Therefore, an optimal coal seam for CO_2 and H_2S sequestration would be high-rank coals that likely have dense cleat spacing and less differential adsorption capacities between acid gas and CH_4, which likely develops a late breakthrough of injected gas and limited permeability reduction.

The possible maximum permeability reduction during acid gas injection and displacement of CH_4 can be estimated reliably by simply assuming that the pre-adsorbed CH_4 is displaced by equilibrium adsorption of the injected gases without reservoir pressure changes. Dynamic variations of cleat permeability during acid gas sequestration can be considered rigorously by numerical modeling of the whole process. However, the stress or pressure dependent mechanical properties of coal seams also need to be included, which remain poorly understood and require further studies.

References

Ahmed, T., 2000, Reservoir Engineering Handbook, 2ed, Gulf Professional Publishing, p.118-119.

Brill, J., and H. Beggs, 1978, Two-Phase Flow in Pipes, Tulsa, OK: The University of Tulsa.

Burden, R.L., J.D. Faires, 1997, Numerical Analysis, Brooks/Cole Publishing Company, p.599-606.

Chikatamarla, L., X. Cui, and R. M. Bustin, 2004, Implications of volumetric swelling/shrinkage of coal in sequestration of acid gases, No.0435, “The 2004 International Coalbed Methane Symposium”, May 3-7, 2004, Tuscaloosa, Alabama, USA.

Cui, X., R.M. Bustin, and G. Dipple, 2004, Selective transport of CO_2, CH_4, and N_2 in coals: insights from modeling of experimental gas adsorption data, Fuel, 83, 293-303.

Cui, X., and R.M. Bustin, Controls of coal fabric on coalbed gas production and compositional shift in both field production and canister desorption test, in preparation.

Do, D.D., 1998, Adsorption Analysis: Equilibrium and Kinetics, Series on Chemical Engineering, editor, R. T. Yang, Vol.2, Imperial College Press, pp.556-562.

Gash, B.W., 1991, Measurement of rock properties in coal foe coalbed methane production, Paper SPE 22909, presented at The 66th SPE annual Technical Conference and Exhibition, Dallas, Texas, USA.

Harpalani, C., and G. Chen, 1995, Influence of gas production induced volumetric strain on permeability of coal, Geotech. Geol. Engng., 15, 303-325.

Kümpel, H.J., 1991, Poroelasticity: Parameters reviewed, Geophysical Journal International, 105, 783-799.

Law, D. H.-S., L.G.H. Van der Meer, W.D. Gunter, 2002, Numerical simulator comparison study for enhanced coalbed methane recovery processes, Part I: Pure carbon dioxide injection, SPE 75669.

Law, D.H.-S., L.G.H. van der Meer and W.D. Gunter, 2003, Comparison simulators for greenhouse gas sequestration in coalbeds, Part III: More complex problems. Paper presented at NETL’s Second National Conference on Carbon Sequestration, Alexandria, Virginia, May 5–8, 2003.

Lewis, R.W., and B.A. Schrefler, 1998, The Finite Element Method in the Static and Dynamic Deformation and Consolidation of Porous Media (2ed), John Wiley & Sons, p.39-45.

Neuzil, C.E., 2003, Hydromechanical coupling in geologic processes, Hydrogeology Journal, 11, 41-83.

Palciauskas, V.V., and P.A. Domenico, 1982, Characterization of drained and undrained response of thermally loaded repository rocks, Water Resources Research, 18, 281-290.

Palmer, I., and J. Mansoori, 1998, How permeability depends on stress and pore pressure in coalbeds: A new model, SPE Reservoir Evaluation & Engineering, SPE 52607, 539-544.

Peaceman, D.W., 1983, Interpretation of well-block pressures in numerical reservoir simulation with non square grid blocks and anisotropic permeability, SPEJ, p.531-543.

Riazi, M.R., and C.H. Whitson, 1993, Estimating diffusion coefficients of dense fluids, Ind. Eng. Chem. Res., 32, 3081-3088.

Pekot, L.J., and S.R. Reeves, Modeling the effects of matrix shrinkage and differential swelling on coalbed methane recovery and carbon sequestration, SPE 0238??

Sawyer, W.K., G.W. Paul, R.A. Schraufnagel, 1990, Development and application of a 3D coalbed simulator, Petroleum Society of CIM/Society of Petroleum Engineers, Paper No. CIW/SPE 90-119.

Seidle, J.P., D.J. Jeansonns, and D.J. Erickson, 1992, Application of matchstick geometry to stress dependent permeability in coals, paper SPE 24361 presented at SPE Rocky Mountain Regional Meeting, Casper, Wyoming, 18-21 May, pp. 433-444.

Shi, J. Q., and S. Durucan, 2004, Drawdown induced changes in permeability of coalbeds: A new interpretation of the reservoir response to primary recovery, Transport in Porous Media, 56, 1-16.

Vaziri, H.H., X. Wang, I.D. Palmer, M. K hodaverdian, and J. McLennan, 1997, Back analysis of coalbed strength properties from field measurements of wellbore cavitation and methane production, Int. J. Rock Mech. Min. Sci., v.34, p.963-978.

Yang, R.T., 1997, Gas Separation by Adsorption Processes, Series on Chemical Engineering, vol. 1, Editor, R.T. Yang, Imperial College Press, pp.125-136.

Zhao, Y., Y. Hu, J. Wei, and D. Yang, 2003, The experimental approach to effective stress law of coal mass by effects methane, Transport in Porous Media, 53, 235-244.

Zimmerman, R.W., W.H. Somerton, M.S. King, 1986, Compressibility of porous rocks, Journal of Geophysical Research, 91, 12,765-12,777.

Zimmerman, R.W., 2000, Coupling in poroelasticity and thermoelasticity, International Journal of Rock Mechanics and Mining Sciences, 37, 79-87.

Table 1. Langmuir Isotherms of three coals (as received at 25 °C)

	Ardley		Wolf Mountain		Quinsam	
gas adsorption	V_L (cc/g)	P_L (MPa)	V_L (cc/g)	P_L (MPa)	V_L (cc/g)	P_L (MPa)
CH_4	5.09	5.12	13.42	2.39	8.80	0.93
CO_2	25.72	3.38	27.78	1.85	38.83	2.06
H_2S	23.6	0.19	49.55	0.26	65.19	0.67
N_2	3.07	8.59	10.34	9.06	6.17	11.57

Table 2. General properties of coal seams*

coal name	Ardley	Wolf Mountain	Quinsam
density ρ_c, g/cc	1.5	1.34	1.40
depth, m	200	300	300
initial pressure p_0, MPa	2	3	3
permeability κ_0, md	2	5	3
cleat spacing a, cm	0.1	0.5	0.5
initial cleat porosity ϕ_0, %	0.58	0.27	0.23
Young’s module E, GPa	3	3	3
Poisson’s ratio ν	0.3	0.3	0.3
vitrinite reflectance (R_{or} %)	0.46	0.62	062
moisture (%)	8.04	2.26	4.14
ash (%)	32.8	5.05	9.30

* The values in this table are applied to the reference curves in Figs. 3-5.

Table 3: Parameters for all simulation cases*

parameter	values
coal matrix porosity, ϕ_m, %	7
coal seam thickness, d, m	5
initial reservoir pressure, p_0, MPa	3
initial water saturation in cleats, $s_{w,}$ %	65
initial gas in cleats and coal matrix, y_{CH4}, %	100
maximum injection rate, Q^*d, full well, m^3/day @STD	10,000
maximum injection well pressure, p_{wim}, MPa	6
maximum injection rate, Q^*d, full well, m^3/day @STD	10,000
minimum production well pressure, p_{wpm}, MPa	0.05
well bore radius, r_w, cm	4

* All simulations are based on the properties of the Wolf Mountain coal. Thus, other coal properties are given in Tables 1 and 2 in the Wolf Mountain coal column unless explicitly specified. For H_2S injection simulations, the coal seam is assumed to have a larger initial cleat porosity of 1% and a small cleat spacing 1 mm.

Table 4: Summary of numerical results*

I-Gas Composition	a (mm)	ϕ_0 (%)	I-Acid (10^6 m^3)	P-CH_4 (10^6 m^3)	P-Acid (10^3 m^3)	κ/κ_0 (num)	κ/κ_0 (anl)**
100% CO_2	5	0.27	0.523	4.40	0.425	0.0023	0.0015
50%CO_2+50%N_2	5	0.27	1.37	5.44	1.26	0.022	0.027
50%CO_2+50%N_2	2	0.49	3.22	5.86	0.000	0.12	0.15
50%CO_2+50%N_2	10	0.17	1.43	5.22	101	0.0040	0.0026
99%H_2S+1%N_2	1	1.0	0.026	3.02	0.000	1×10^{-5}	9×10^{-7}
50%H_2S+50%N_2	1	1.0	0.028	3.05	0.000	6×10^{-5}	1.5×10^{-6}
20%H_2S+80%N_2	1	1.0	0.035	3.16	0.000	3×10^{-4}	1.8×10^{-5}
primary recovery	5	0.27	-	4.04	-	1.86	2.1
constant κ (=κ_0)	5	0.27	-	3.36	-	1	1

* Symbol I here represents the injected gas; Symbol P represents production of methane or breakthrough of H_2S or CO_2. All volume data are cumulative values for a 10-year period of injection and production of full wells.

** Only the minimum numerical value is chosen for comparison with the analytic one at 1.5 times the initial coal-seam pressure. However, for primary recovery case, the maximum numerical value is chosen to be compared with the analytical value predicted at 0.5 MPa.

Figure captions

Figure 1. Experimental volumetric strains induced by gas adsorption in coals. The symbols represent the experimental data, whereas the solid curves represent a fitted straight line passing through the origins.

Figure 2. Predicted volumetric strain under different pressures using eqs. 1 and 2 in text.

Figure 3. Permeability variation of the Ardley coal during CH_4 primary recovery (a) or enhanced CH_4 recovery by injection of CO_2 (b), H_2S (c), and N_2 (d). For gas injection to displace CH_4 (in panels b, c, and d), the pressure is the partial pressure (when $p < p_0$) or total pressure (when $p > p_0$) of the injected gas. Also instantaneous or equilibrium adsorption or desorption were assumed and thus the cleat and matrix pressures are always equal in value. The parameters for the reference curves are given in Table 2 except for the larger initial cleat porosity of 1.24% in panel (c). For comparison, only the parameter that is different from that of the reference curve is explicitly labeled. If two curves share the same shape symbol, then they have the same parameters except for the explicitly-labeled one. Flue gas composition is represented by the molar fraction of N_2.

Figure 4. Permeability variation of the Wolf Mountain coal during CH_4 primary recovery (a) or enhanced CH_4 recovery by injection of CO_2 (b), H_2S (c), and N_2 (d) (see Fig. 3 for caption). The parameters for the references curve are given in Table 2 except for the larger initial cleat porosity of 1% and smaller cleat spacing of 1 mm in panel (c).

Figure 5. Permeability variation of the Quinsam coal during CH_4 primary recovery (a) or enhanced CH_4 recovery by injection of CO_2 (b), H_2S (c), and N_2 (d) (see Fig. 3 for caption). The parameters for the reference curves are given in Table 2 except for the larger initial cleat porosity of 1% in panel (c).

Figure 6. Gas (κ_{rg}) and water (κ_{rw}) relative permeability as a function of water saturation (s_w).

Figure 7. Bulk diffusivity of gas in the Wolf Mountain coal particles. The symbols represent the values determined with the experimental adsorption-rate data on crushed coals. The fitted solid curves were applied in this study.

Figure 8. The five-spot well pattern and the finite difference grid. Symbols *I* and *P* represent respectively the injection and production wells. The numbers note the position of a grid block, e.g., block (1,1) is the injection-well block.

Figure 9. Modeling results for CO_2 sequestration into the Wolf Mountain coal (see Table 2 for coal seam properties): (a) gas injection and production rates and (b) permeability change with time for pure CO_2 injection, and (c) gas injection and production rates and (d) permeability change for 50%CO_2+50%N_2 injection. Symbols *I* and *P* in (a) and (c) represent the injected and produced gas, respectively. Each curve in (b) and (d) represents the permeability evolution with time for coals at different locations labeled by the bracketed numbers (see Fig. 8).

Figure 10. Simulation results for H_2S sequestration into the Wolf Mountain coal with a large initial cleat porosity of 1% and a cleat spacing of 1 mm (see Table 2 for other parameters): (a) injection rates of gas mixture with different compositions and (b) the corresponding permeability variations induced by gas sequestration.

Figure 11. Effects of coal fabric on CO_2 sequestration into two coal seams with different cleat spacings of 2 mm (coal seam I) and 1 cm (coal seam II), respectively. For both coal seams, their initial cleat porosities are determined with the match-stick model (eq. 12), and all other parameters are the same as the Wolf Mountain coal given in Table 2. For the coal seam I (left-side panels) and the coal seam II (right-side panels), (a) the gas injection or production rates evolve with time and (b) the permeability of coals at different locations (labeled by the grid block index, see Fig. 8) dynamically changes through time.

Figure 12. Effects of coal fabric on cleat pressure (a), free-gas composition (b), and cleat permeability (c) for the coal seam I (left-side panels) and the coal seam II (right-side panels). The horizontal axis represents the distance from the injection well (*I*) to the production well (*P*) along the diagonal line (I→P) in Fig. 8. The free-gas composition in cleats (y_c) and matrix (y_m) are nearly identical for coal seam I, and hence only the cleat gas compositions are shown here. For coal seam (II), the CO_2 concentration in coal matrix (y_m) is lagged behind its counterpart in cleats only at early

stages. The concentrations of N_2 in cleat and matrix are always similar and thus only its concentration in cleats is shown.

Figure 13. Comparison of different permeability models: (a) permeability reduction induced by CO_2-sorption and (b) permeability variation during primary CH_4 recovery. The coal seams in (a) and (b) have the same properties as the Wolf Mountain coal (Table 2).

Figure 14. Influence of a compressible coal matrix on permeability variations during injection of CO_2 and H_2S into the Wolf Mountain coal (see Table 2 for coal properties).

Figure 15. Horizontal effective stress increments induced by acid gas sorption. The coal seams have the same properties as the Wolf Mountain coal (see Table 2) or the reference curves in Fig. 4b and 4c for CO_2 and H_2S sorption respectively. The stress change is given as $[(\sigma_{xx} - \sigma_{xx0}) – (p - p_0)]$, where σ_{xx} is given by eq. 13 in text.

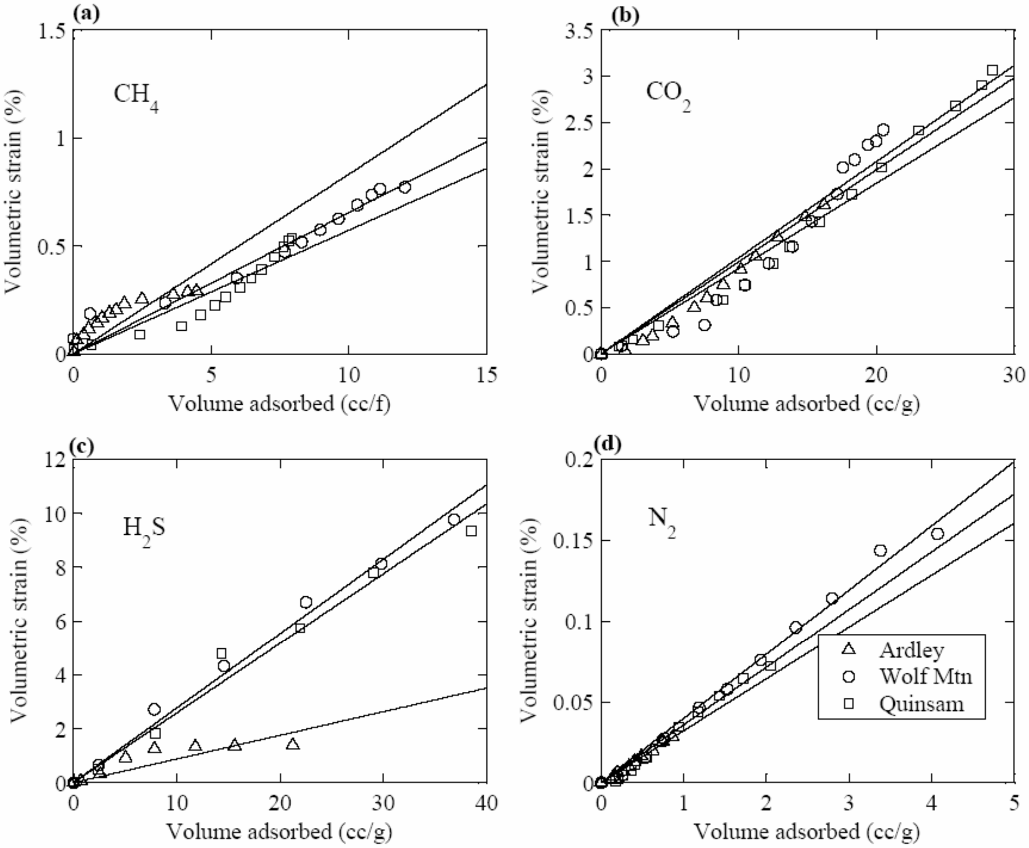
(a)
1.5
1
0.5
0
Volumetric strain (%)
CH_4
0
5
10
15
Volume adsorbed (cc/f)
(b)
3.5
3
2.5
2
1.5
1
0.5
0
Volumetric strain (%)
CO_2
0
10
20
30
Volume adsorbed (cc/g)
(c)
12
10
8
6
4
2
0
Volumetric strain (%)
H_2S
0
10
20
30
40
Volume adsorbed (cc/g)
(d)
0.2
0.15
0.1
0.05
0
Volumetric strain (%)
N_2
△ Ardley
○ Wolf Mtn
□ Quinsam
0
1
2
3
4
5
Volume adsorbed (cc/g)

Figure 1

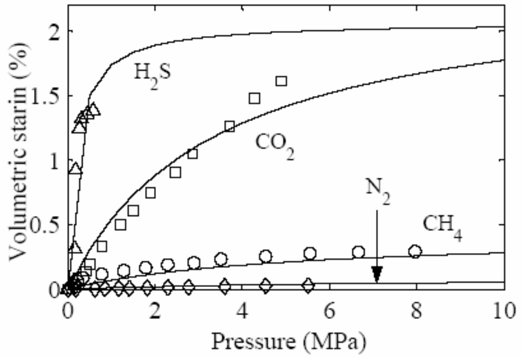

(a) Ardley coal

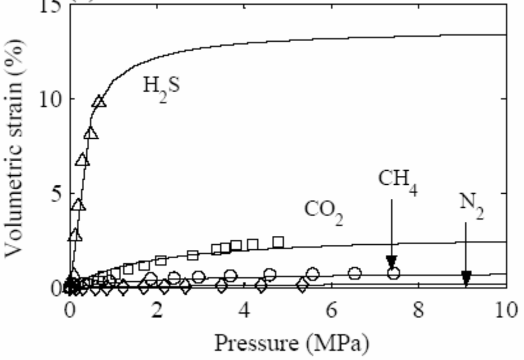

(b) Wolf Mtn coal

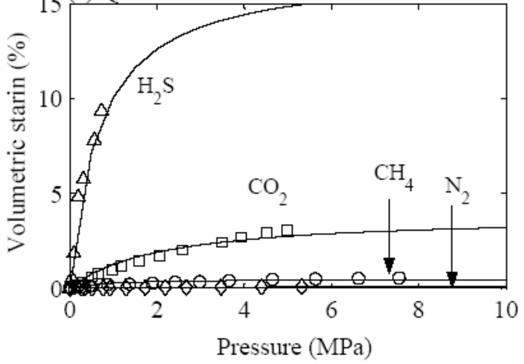

(c) Quinsam coal

Figure 2

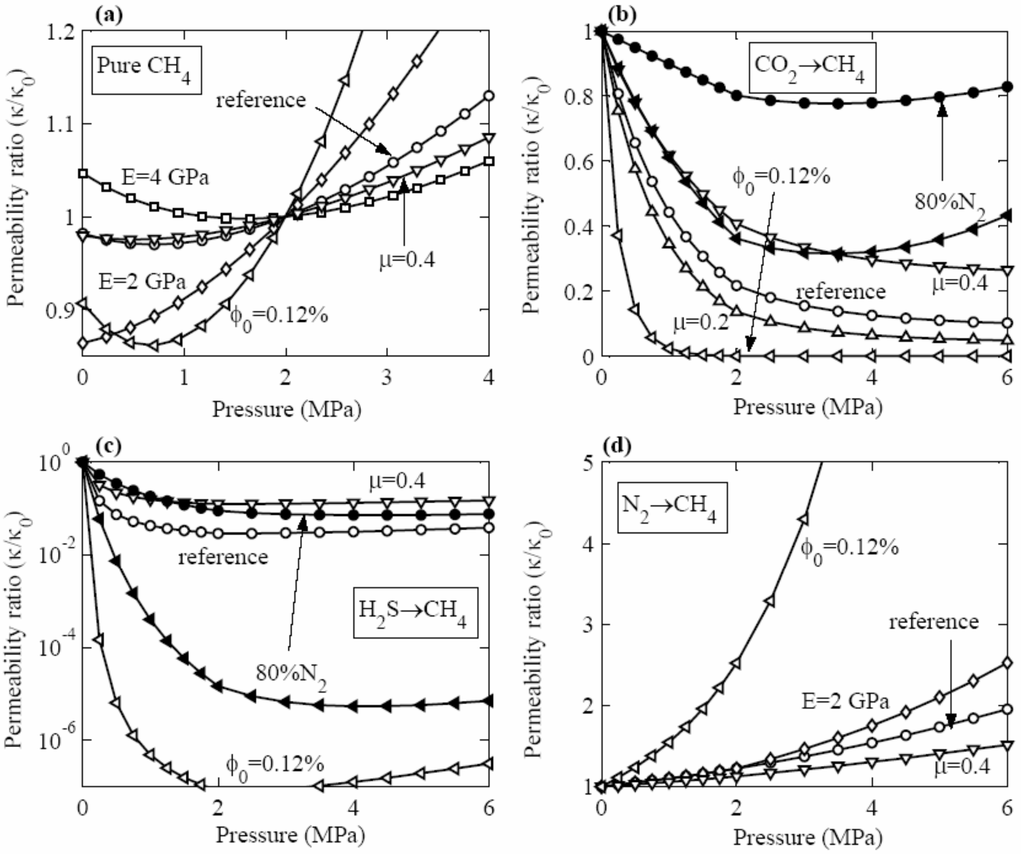(a)
Pure CH_4
Permeability ratio (κ/κ_0)
1.2
1.1
1
0.9
reference
E=4 GPa
E=2 GPa
μ=0.4
ϕ_0=0.12%
0
1
2
3
4
Pressure (MPa)
(b)
$CO_2 \rightarrow CH_4$
Permeability ratio (κ/κ_0)
1
0.8
0.6
0.4
0.2
0
ϕ_0=0.12%
80%N_2
reference
μ=0.4
μ=0.2
0
2
4
6
Pressure (MPa)
(c)
Permeability ratio (κ/κ_0)
10^0
10^{-2}
10^{-4}
10^{-6}
μ=0.4
reference
$H_2S \rightarrow CH_4$
80%N_2
ϕ_0=0.12%
0
2
4
6
Pressure (MPa)
(d)
$N_2 \rightarrow CH_4$
Permeability ratio (κ/κ_0)
5
4
3
2
1
ϕ_0=0.12%
reference
E=2 GPa
μ=0.4
0
2
4
6
Pressure (MPa)

Figure 3

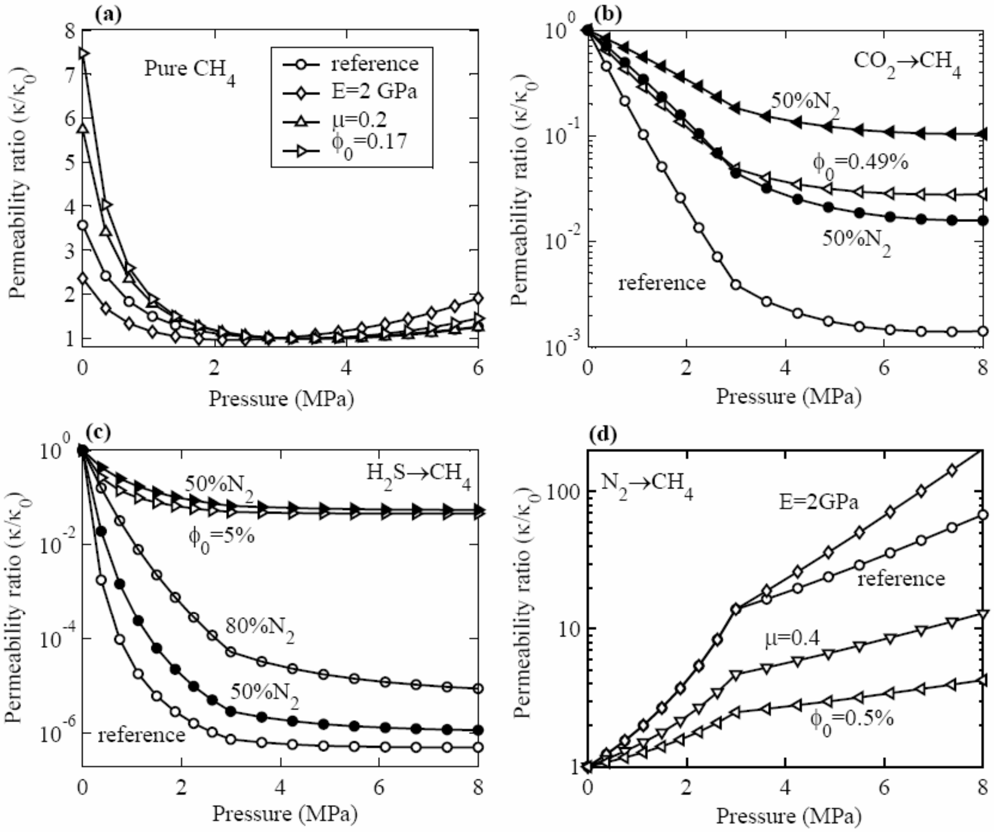(a)
Pure CH4
reference
E=2 GPa
μ=0.2
φ0=0.17
Permeability ratio (κ/κ0)
Pressure (MPa)
(b)
CO2→CH4
50%N2
φ0=0.49%
50%N2
reference
(c)
H2S→CH4
50%N2
φ0=5%
80%N2
50%N2
reference
(d)
N2→CH4
E=2GPa
reference
μ=0.4
φ0=0.5%

Figure 4

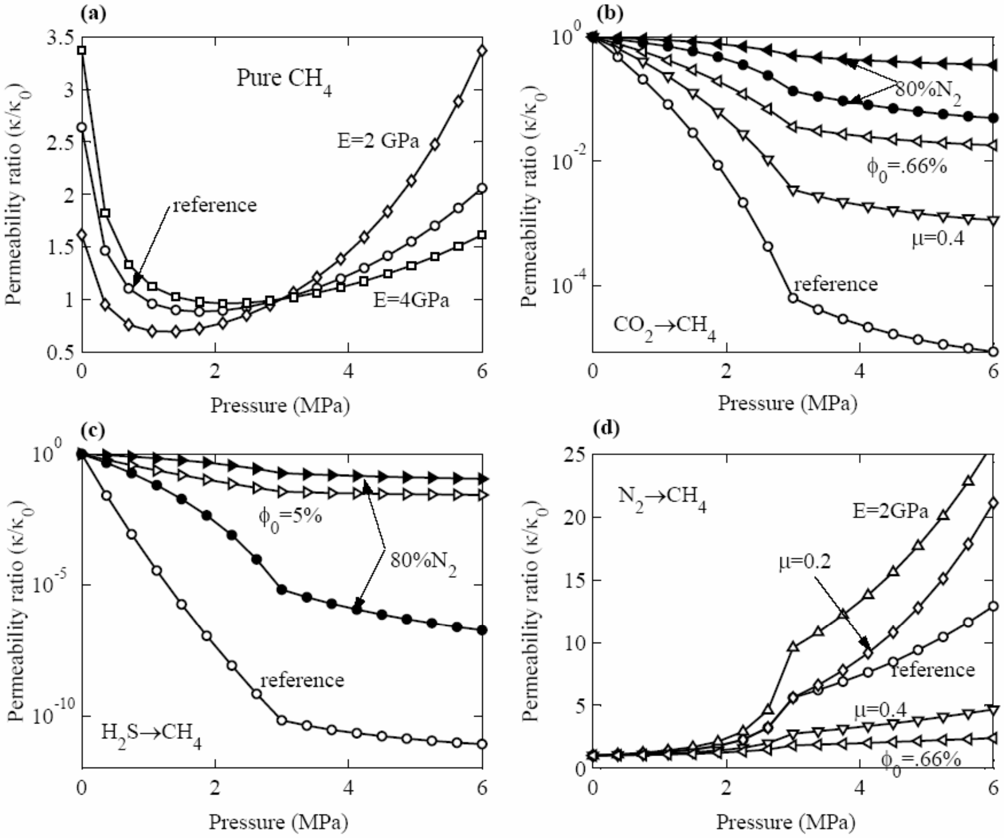
(a)
Pure CH4
E=2 GPa
reference
E=4GPa
Permeability ratio (κ/κ0)
Pressure (MPa)
(b)
80%N2
φ0=.66%
μ=0.4
reference
CO2→CH4
(c)
φ0=5%
80%N2
reference
H2S→CH4
(d)
N2→CH4
E=2GPa
μ=0.2
reference
μ=0.4
φ0=.66%

Figure 5

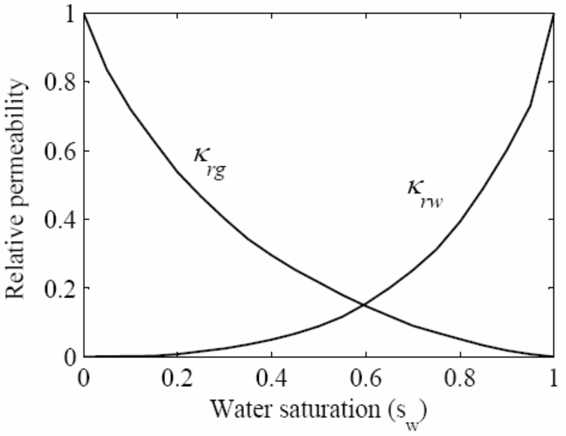
1
0.8
0.6
0.4
0.2
0
Relative permeability
0
0.2
0.4
0.6
0.8
1
Water saturation (s_w)
κ_{rg}
κ_{rw}

Figure 6

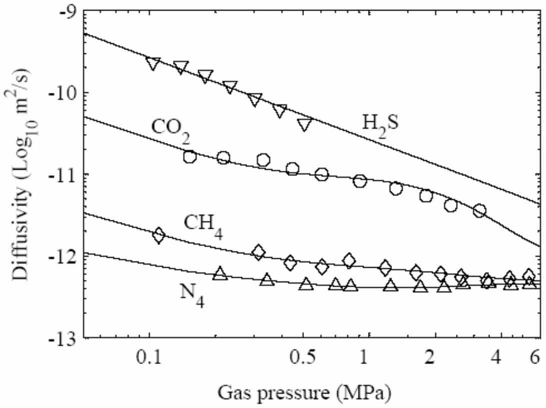
-9
-10
-11
-12
-13
Diffusivity (Log_{10} m^2/s)
0.1
0.5
1
2
4
6
Gas pressure (MPa)
H_2S
CO_2
CH_4
N_4

Figure 7

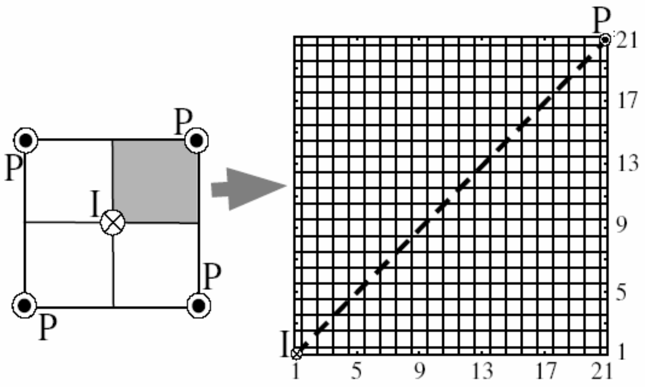

Figure 8

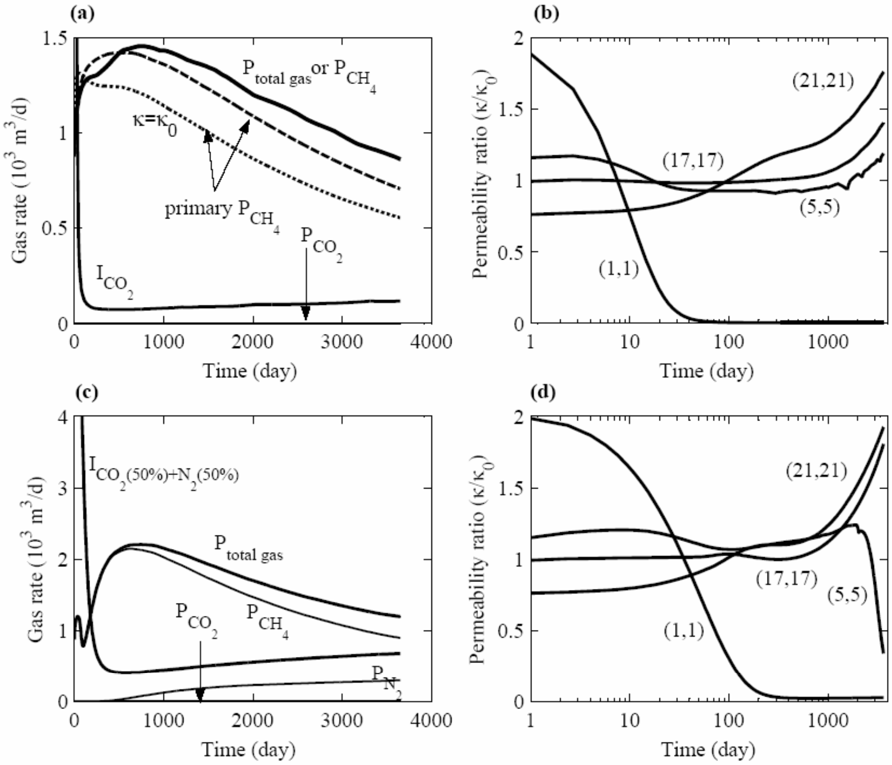
(a)
Gas rate (10^3 m^3/d)
Time (day)
$P_{total\ gas}$ or P_{CH_4}
κ=κ$_0$
primary P_{CH_4}
P_{CO_2}
I_{CO_2}
0
0.5
1
1.5
0
1000
2000
3000
4000
(b)
Permeability ratio (κ/κ$_0$)
Time (day)
(21,21)
(17,17)
(5,5)
(1,1)
0
0.5
1
1.5
2
1
10
100
1000
(c)
Gas rate (10^3 m^3/d)
Time (day)
$I_{CO_2(50\%)+N_2(50\%)}$
$P_{total\ gas}$
P_{CO_2}
P_{CH_4}
P_{N_2}
0
1
2
3
4
0
1000
2000
3000
4000
(d)
Permeability ratio (κ/κ$_0$)
Time (day)
(21,21)
(17,17)
(5,5)
(1,1)
0
0.5
1
1.5
2
1
10
100
1000

Figure 9

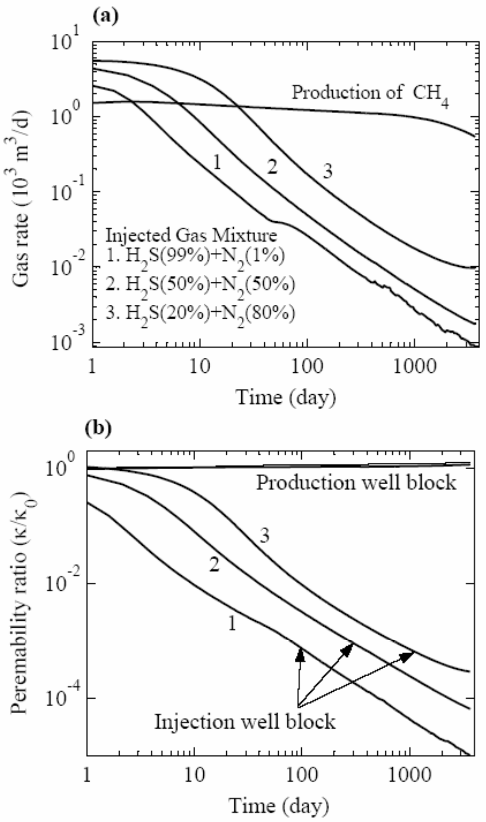
(a)
Gas rate (10^3 m^3/d)
10^1
10^0
10^{-1}
10^{-2}
10^{-3}
Production of CH_4
1
2
3
Injected Gas Mixture
1. H_2S(99%)+N_2(1%)
2. H_2S(50%)+N_2(50%)
3. H_2S(20%)+N_2(80%)
1
10
100
1000
Time (day)
(b)
Peremability ratio (κ/κ_0)
10^0
10^{-2}
10^{-4}
Production well block
3
2
1
Injection well block
1
10
100
1000
Time (day)

Figure 10

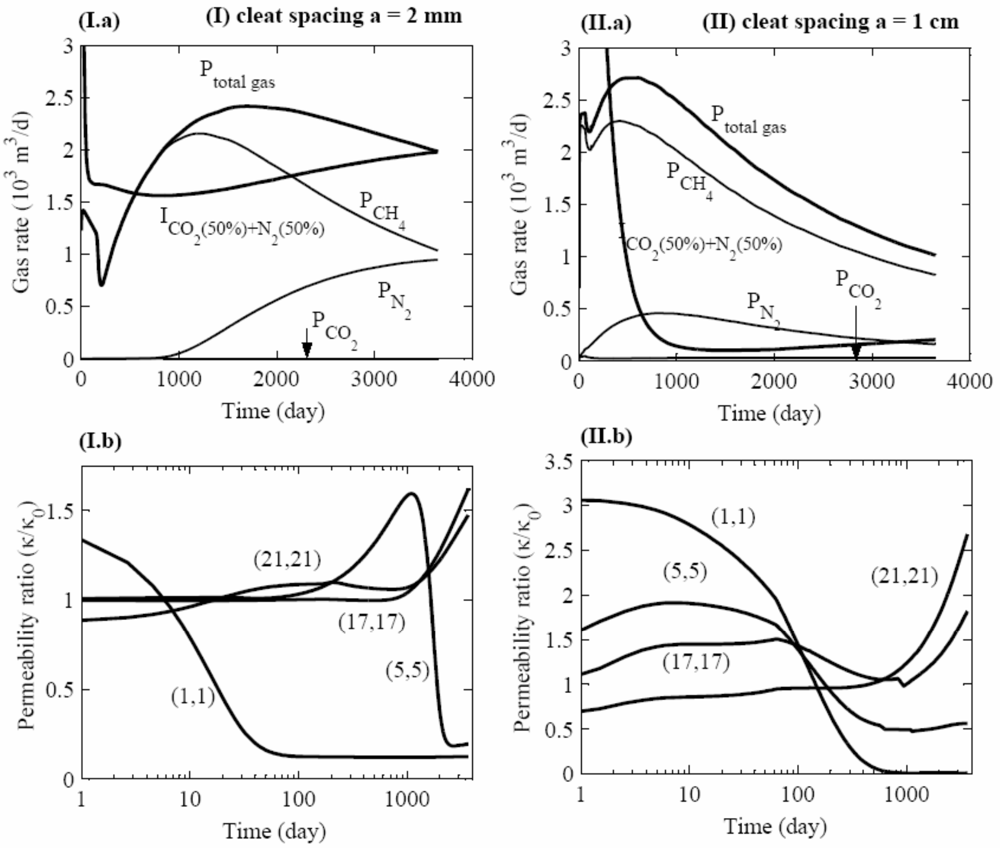
(I.a)
(I) cleat spacing a = 2 mm
P total gas
P CH4
I CO2(50%)+N2(50%)
P N2
P CO2
Gas rate (10^3 m^3/d)
Time (day)
0
0.5
1
1.5
2
2.5
3
0
1000
2000
3000
4000
(II.a)
(II) cleat spacing a = 1 cm
P total gas
P CH4
CO2(50%)+N2(50%)
P N2
P CO2
Gas rate (10^3 m^3/d)
Time (day)
0
0.5
1
1.5
2
2.5
3
0
1000
2000
3000
4000
(I.b)
(21,21)
(17,17)
(5,5)
(1,1)
Permeability ratio (κ/κ0)
Time (day)
0
0.5
1
1.5
1
10
100
1000
(II.b)
(1,1)
(5,5)
(21,21)
(17,17)
Permeability ratio (κ/κ0)
Time (day)
0
0.5
1
1.5
2
2.5
3
3.5
1
10
100
1000

Figure 11

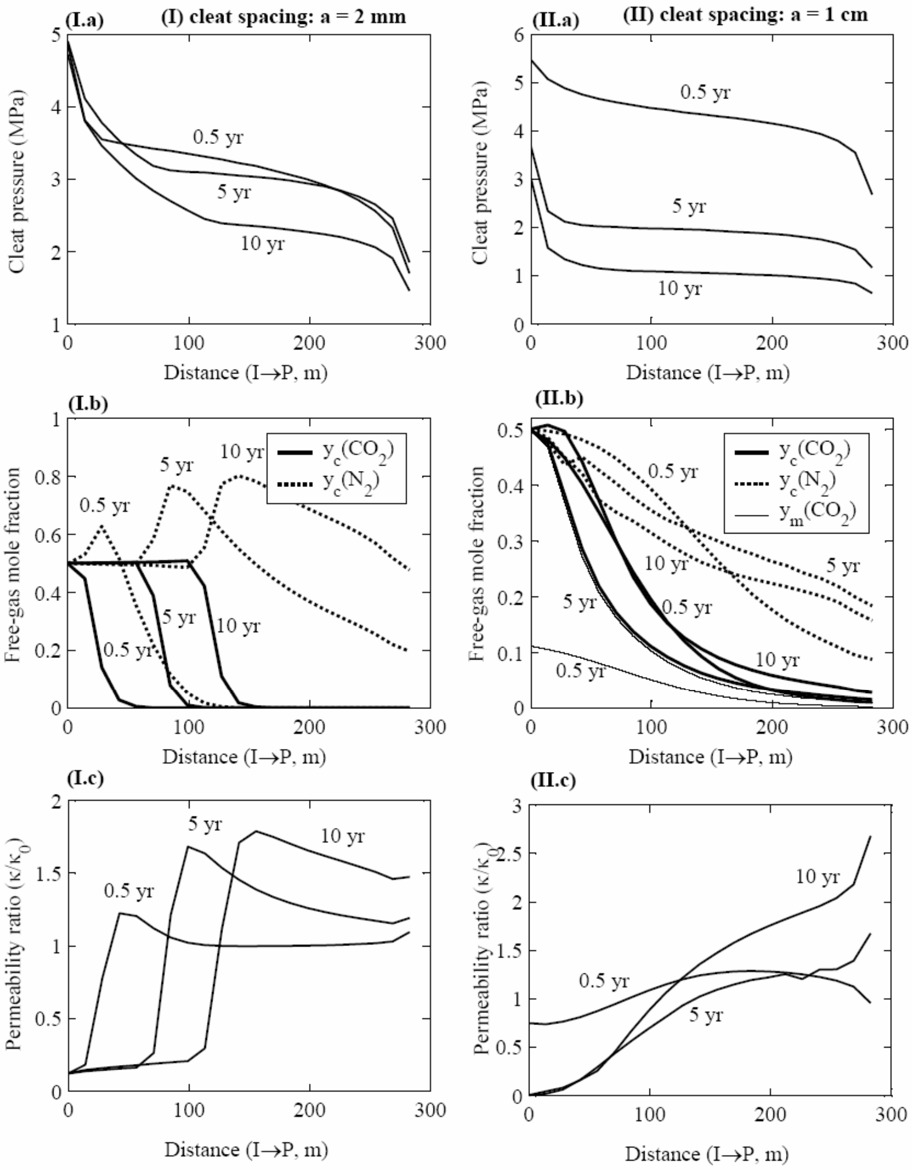
(I.a)
(I) cleat spacing: a = 2 mm
Cleat pressure (MPa)
0.5 yr
5 yr
10 yr
Distance (I→P, m)
(II.a)
(II) cleat spacing: a = 1 cm
Cleat pressure (MPa)
0.5 yr
5 yr
10 yr
Distance (I→P, m)
(I.b)
Free-gas mole fraction
$y_c(CO_2)$
$y_c(N_2)$
0.5 yr
5 yr
10 yr
0.5 yr
5 yr
10 yr
Distance (I→P, m)
(II.b)
Free-gas mole fraction
$y_c(CO_2)$
$y_c(N_2)$
$y_m(CO_2)$
0.5 yr
10 yr
5 yr
5 yr
0.5 yr
10 yr
0.5 yr
Distance (I→P, m)
(I.c)
Permeability ratio (κ/κ_0)
0.5 yr
5 yr
10 yr
Distance (I→P, m)
(II.c)
Permeability ratio (κ/κ_0)
10 yr
0.5 yr
5 yr
Distance (I→P, m)

Figure 12

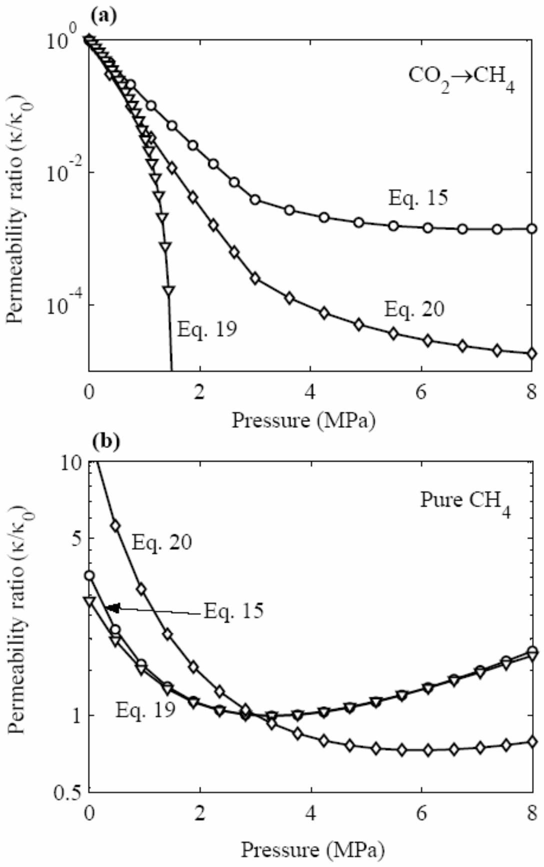
(a)
10^0
10^{-2}
10^{-4}
Permeability ratio (κ/κ_0)
$CO_2 \rightarrow CH_4$
Eq. 15
Eq. 20
Eq. 19
0
2
4
6
8
Pressure (MPa)
(b)
10
5
1
0.5
Permeability ratio (κ/κ_0)
Pure CH_4
Eq. 20
Eq. 15
Eq. 19
0
2
4
6
8
Pressure (MPa)

Figure 13

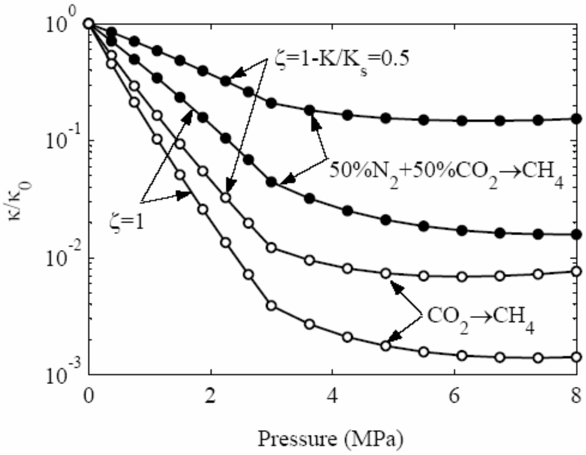

10^0
10^{-1}
10^{-2}
10^{-3}
κ/κ_0
0
2
4
6
8
Pressure (MPa)
$\zeta=1-K/K_s=0.5$
$50\%N_2+50\%CO_2\rightarrow CH_4$
$\zeta=1$
$CO_2\rightarrow CH_4$

Figure 14

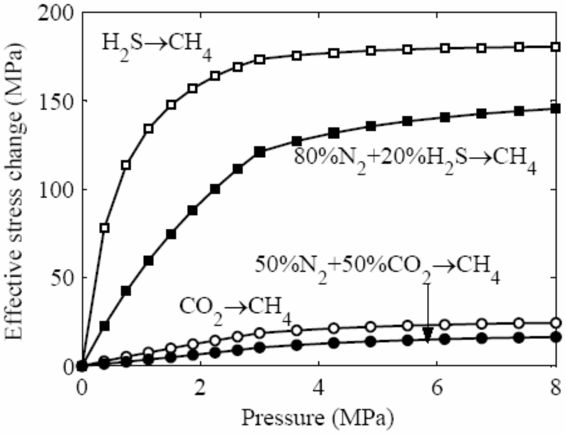
200
150
100
50
0
Effective stress change (MPa)
$H_2S \rightarrow CH_4$
$80\%N_2+20\%H_2S \rightarrow CH_4$
$50\%N_2+50\%CO_2 \rightarrow CH_4$
$CO_2 \rightarrow CH_4$
0
2
4
6
8
Pressure (MPa)

Figure 15